Novel Magnetic and Superconducting States in Spin-1/2 Kagome Lattice and its Doped Variant

by

Wing-Ho Ko

Submitted to the Department of Physics
in partial fulfillment of the requirements for the degree of

Doctor of Philosophy

at the

MASSACHUSETTS INSTITUTE OF TECHNOLOGY

September 2010

ARCHIVES
MASSACHUSETTS INSTITUTE OF TECHNOLOGY
OCT 3 1 2011
LIBRARIES

© Massachusetts Institute of Technology 2010. All rights reserved.

Author .....
Department of Physics
August 30, 2010

Certified by .....
Patrick A. Lee
William and Emma Rogers Professor
Thesis Supervisor

Accepted by .....
Krishna Rajagopal
Associate Department Head for Education

Novel Magnetic and Superconducting States in Spin-1/2 Kagome Lattice and its Doped Variant

by

Wing-Ho Ko

Submitted to the Department of Physics
on August 30, 2010, in partial fulfillment of the
requirements for the degree of
Doctor of Philosophy

Abstract

Quantum spin liquids, which are quantum ground states of interacting spin systems that break no symmetries, have long been a fascination among the theoretical condensed matter community. After years of experimental searches, several promising candidates finally emerged, including herbertsmithite $ZnCu_3(OH)_6Cl_2$, which can be modeled as a spin-1/2 kagome lattice. Theoretically, the $U(1)$ Dirac spin liquid ($U(1)$ DSL) state is shown to be a plausible description of the system, and previous works have indicate that this particular quantum spin liquid state may enjoy a host of interesting properties, such as the power-law decay of correlation functions, the existence of spin-1/2 excitations known as the spinon, and the existence of an emergent $U(1)$ gauge field.

In this thesis, after the relevant motivation and background information are discussed, I shall present my work on the spin-1/2 kagome lattice that built upon the $U(1)$ DSL state. First, I shall present the theoretical study of Raman scattering in the $U(1)$ DSL state, which shows that in all symmetry channels the Raman intensity profiles contain broad continua that display power-law behaviors at low energy, which can be attributed to the excitations of spinon-antispinon pairs. In addition, for the A_{2g} channel, the Raman profile also contains a characteristic $1/\omega$ singularity, which arise from an excitation of the emergent $U(1)$ gauge field. The possibility of more clearly observing the signature of this $U(1)$ emergent gauge field in resonant inelastic X-ray scattering (RIXS) is also discussed. Next, I shall consider the case when the spin-1/2 kagome lattice is subjected to an external magnetic field, in which a state with an additional uniform amount of gauge flux of top of the $U(1)$ DSL ansatz, which results in the formation of Landau levels in the spinon spectrum, is shown to be energetically favorable. Unlike the usual quantum Hall system, the Landau level state is shown to contain a gapless S_z density mode, which in turns indicate that system is XY ordered in the plane perpendicular to the applied magnetic field. Third, I shall consider the case in which the spin-1/2 kagome lattice is hole-doped. Similar to the B-field case, a Landau-level state is shown to be energetically favorable, in which a gapless charge density mode is shown to exists, and which through

the Anderson-Higgs mechanism causes the system to become a superconductor. This resulting superconductor is then shown to be exotic, in the sense that it contains minimal vortices having a flux of $hc/4e$, as well as bosonic quasiparticles that have semionic mutual statistics. The thesis concludes with a short summary and outlook.

Thesis Supervisor: Patrick A. Lee
Title: William and Emma Rogers Professor

Acknowledgments

While a doctoral thesis is really just a tiny drop in the sea of human knowledge, the task of producing one has always looked formidable to its author. Indeed, such a task would have never been attempted or completed without the encouragement, help, and support of many other people. And it is to these people that I now express my gratitudes.

First and foremost I would like to thank my thesis adviser, Prof. Patrick A. Lee, for his excellent mentorship in the past five years. Patrick has always been friendly, caring, and approachable to students, and has given me plenty of freedom in how I approach our research (which I, regrettably, abused occasionally). His broad knowledge about the field and his intuitive approach to physics problems have helped me a lot in developing my own skills in theoretical condensed matter physics.

Next I would like to thank Prof. Xiao-Gang Wen and Prof. Senthil Todadri, for their helpful and inspiring discussions, physics or otherwise, in both appointments and in casual chats. I have chosen MIT for my graduate studies partly because of the strong sense of community shared among faculty members in the theoretical condensed matter division, and my experience in the past five years suggest that I have made the right choice.

I have also enjoyed discussions and interactions with other graduate students and postdocs at MIT. These include Michael Hermele, Cody Nave, Ying Ran, Zheng-Cheng Gu, Kam-Tuen Law, Saeed Saremi, Maissam Barkeshli, Nan Gu, Jamal Rahi, Brian Swingle, Tarun Grover, Fa Wang, Tim Chen, Abolhassan Vaezi, Rahul Nandkishore, Juven Wang, Alejandro Rodriguez, Anjan Soumyanarayanan, and others. I would especially thank Saeed and Tim, whom I shared office with, and also Tarun, who have been a great companion to me in the past few years. It is my hope that I would continue to hear and learn from them in future.

I have enjoyed and greatly benefited from my collaborations with Cody, Ying and Xiao-Gang. I have also enjoyed and benefited from the somewhat unexpected and yet fruitful collaborations with Prof. Tai Kai Ng and his student Zheng-Xin Liu from

the Hong Kong University of Science and Technology.

I have learned a great deal from the classes I took here at MIT. For this I would like to thank Patrick, Senthil, Xiao-Gang, Prof. Robert Jaffe, Prof. Mehran Kardar, Prof. Wolfgang Ketterle, Prof. Issac Chuang, Prof. Leonid Levitov, Prof. Washington Taylor, Prof. Iain Stewart, Prof. John McGreevy, Prof. Edward Farhi, Prof. James Munkres, and Dr. Sanjoy Mahajan for their wonderful lectures.

In addition, I would like to thank Prof. John Joannopoulos for being my academic adviser in the past five years. I would also like to thank Senthil and Prof. Young Lee for sitting in my thesis committee.

I have benefited from many caring and inspiring teachers in my life, without whom I probably would not be able to land on MIT. From my primary education at the CCC Kei Wan Primary School (AM) I would like to especially thank Ms. Kong, whom helped me to launch from a rough start, and Ms. Lai, who have encouraged me to actively participate in class and pursue my own quest for knowledge. I am sure that Ms. Lai would be happy to learn that the boy who was nicknamed "Dr. Ko" has indeed made the title legitimate after fifteen years.

From my secondary education at the Diocesan Boys' School I would like to especially thank Mr. P. Y. Lam, whom taught me physics and advised the astronomy club that I chaired in Form six, and Ms. M. C. Tso, whom despite the somewhat authoritative style had been an excellent mathematics teacher and careers mistress.

From my undergraduate education at the University of Illinois at Urbana–Champaign I would like to thank Prof. Kevin Pitts, Prof. James Wiss, Prof. David Herzog, Prof. Michael Stone, and Ms. Celia Elliott in the physics department for their enthusiastic and inspiring lectures. I would especially thank my undergraduate research adviser, Prof. Richard Martin, for giving me a taste of what physics research is like. I would also thank Prof. Charles Henson and Prof. Bruce Reznick in the mathematics department, whom have forever raise my appreciation and appetite for higher mathematics. It is regretful that a choice have to be made between physics and mathematics when I decided to pursue a Ph. D.

On a more personal side, I would like to thank my friends in the Boston–Cambridge

area, especially Karen Lee, Amos Tai, Clement Chan, Chester Chu, James Lee, Albert Chow Jr., Danielle Chu, and Lawson Wong, whom have kept my life outside of the academia fulfilling and entertaining (perhaps too much so!) in the past five years.

In addition, I would like to thank my friends from Hong Kong whom have supported me at various points in my life. These include, among others, Matthew Chan, Raphael Hui, Edward Choi, and Henry Ng, all of whom I first met in secondary school. And I would especially thank Peter Chau, whom I have known for more than half of my (still young) life, and who have been a great companion to me for all these years. I wish him the best of luck in his own pursue of Ph. D. in philosophy.

No acknowledgment in a doctoral thesis is complete without mentioning one's parents. I would like to express my deepest gratitudes to my father and mother. Their hard efforts at work have afforded me the opportunity to pursue a career in physics, and they have been very supportive regarding my choice of career, despite the social pressure in Hong Kong for academically competent students to study in more conventional subjects such as medicine and civil engineering. My appetite for reading is also likely to be inherited from my father. I hope they would be happy about their son's achievement and would forgive him for his constant absence while studying abroad.

A great discovery solves a great problem but there is a grain of discovery in the solution of any problem.

George Pólya

Contents

List of Figures

List of Tables

Chapter 1

Introduction

Condensed matter physics concerns itself with the study of macroscopic properties of ordinary matters made out of electrons and ions, at energy scales that are low compared to the fundamental scale of its constituents. On the surface, the problem that confront a condensed matter theorist is much simpler than that of a high-energy theorist—there is no unknown particles to be discovered, no unidentified interactions to be pondered about, and no extra dimensions to be unveiled. The interactions between and among the electrons and ions are well-known and well-understood, and an undergraduate in physics could have easily written down *"the"* equation that governs all condensed matter systems. Thus, at first glance, there seems to be very little to be done in condensed matter theory.

Fortunately (but also unfortunately) for those of us who aspired to have a career in condensed matter theory, that deceptively simple-looking equation turns out to be intractable as it stands. In the early days of condensed matter physics, much progress has been made by treating the electron-electron interaction perturbatively (after making the Born-Oppenheimer approximation of separating the slow ionic motion from the fast electronic motion). Such "weak-coupling" approach has been successful in explaining the physical properties of simple metals and superconductors, and its modern descendants, in the form of, e.g., density functional theory [1, 2, 3], have been applied to increasing sophisticated physical systems and still manage to produce decent results.

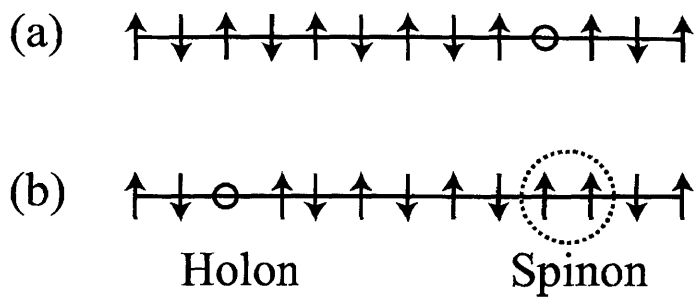

Figure 1-1: Physical picture of spin-charge separation in a one-dimensional spin-1/2 chain. (a) A physical electron removed from the chain; (b) the resulting spin and charge excitations. Taken from Ref. [4]

Nonetheless, there remains a large class of materials in which this perturbative approach fails. Such systems are generally referred to as being "strongly correlated." A particularly instructive class of examples are the one-dimensional systems [4]. Because of the strong phase-space restriction, perturbation theory fails no matter how small the interaction appears to be. To understand these one-dimensional systems, a host of analytical and numerical techniques, e.g., bosonization [5, 6, 7] and density matrix renormalization group (DMRG) [8, 9], have been developed. Using these techniques, it has been shown that one-dimensional systems possess a variety of unusual behaviors. In particular, it has been shown that the spin and charge excitations in these systems are completely decoupled and in general propagates at different velocities, a phenomena known as "spin-charge separation." Intuitively, one may understood such behavior by visioning a physical electron splitting into a chargeless spin 1/2 excitation (spinon) and a charge e spinless excitation (holon). See Fig. 1-1 for illustration.

Motivated by the one-dimensional cases, various proposals have been made in higher dimensional systems in which a similarly exotic phase of matter may be realized. One such proposal is the so-called quantum spin liquid (QSL) states, which is a strongly correlated state of matter that is insulating but which has no spin ordering. More drastically, it contains fermionic spin-1/2 excitations as well as bosonic excitations that resembles photons in certain ways. Recently, experiments have re-

veal several materials in which the spin liquid states may be realized, among them herbertsmithite $ZnCu_3(OH)_6Cl_2$, which can be modeled as a spin-1/2 kagome lattice.

In this thesis I will present my theoretical works on the spin-1/2 kagome system, which are built upon the assumption that the system is well-described by a particular quantum spin liquid state called $U(1)$ Dirac spin liquid ($U(1)$ DSL) state. In the first part I will discuss theoretical prediction on how the spin-liquid state will response under Raman scattering and Resonant inelastic X-ray scattering (RIXS), which may provides evidence for the existence of the fermionic spin-1/2 excitations and the "fictitious" gauge boson excitation as mentioned above. In the second part I will discuss what may happens to the system when an external magnetic field is applied or when it is hole-doped, and show that an exotic superconducting phase, in which fractionalized quasiparticles exists, may appear in the latter case.

1.1 Anti-ferromagnetic Heisenberg model and the quantum spin liquid

As mentioned above, a quantum spin liquid is a strongly correlated insulator. Specifically, it is a Mott insulator [10], in which charge fluctuation is suppressed because the strong on-site Coulomb repulsion incur a large energy cost when extra electrons occupy a lattice site. For most Mott insulator, effective spin-spin interaction between neighboring sites resulting from the virtual hopping of electrons leads to a magnetic ordering when temperature is sufficiently low. The quantum spin liquid thus represents an exceptional case in which no ordering exists despite the existence of interactions.

To be more precise, consider for simplicity a system in which each lattice site consists of a single orbital. In such case, the system can be described by the Hubbard model:

$$H_{\mathrm{Hb}} = \sum_{i,j}\sum_{\sigma} t_{ij} c^{\dagger}_{i\sigma} c_{j\sigma} + U \sum_{i} n_{i\uparrow} n_{i\downarrow} \ , \tag{1.1}$$

where $c_{i\sigma}$ ($c^{\dagger}_{i\sigma}$) is the electron destruction (creation) operator, with i, j labeling lattice

sites and $\sigma = \uparrow, \downarrow$ label spins, and which $n_{i\sigma} = c^{\dagger}_{i\sigma} c_{i\sigma}$ is the number operator for spin σ on site i.

When $U \gg t$ and when the average occupation on each lattice site is less than or equal to one, the lowest-energy states of the systems are those in which none of the site is doubly occupied. Using perturbation theory, the effective Hamiltonian restricted to this nearly-degenerate ground-state manifold is found to be [11]:

$$H_{tJ} = \sum_{i,j} \mathcal{P}_S \left(\frac{J_{ij}}{2} \left(\boldsymbol{S}_i \cdot \boldsymbol{S}_j - \frac{1}{4} n_i n_j \right) - \sum_{\sigma} t_{ij} \left(c^{\dagger}_{i\sigma} c_{j\sigma} + h.c. \right) \right) \mathcal{P}_S \quad , \tag{1.2}$$

where $\mathcal{P}$ is the projection operator onto the states with zero double occupancy, $n_i = n_{i\uparrow} + n_{i\downarrow}$, $\boldsymbol{S} = \frac{1}{2} \sum_{\alpha,\beta} c^{\dagger}_{i\alpha} \boldsymbol{\tau}_{\alpha\beta} c_{i\beta}$ (with $\boldsymbol{\tau}$ being the usual Pauli matrices) is the spin-1/2 operators constructed from electron operators, and $J_{ij} = 4t^2_{ij}/U$. Observe that J_{ij} is positive and hence corresponds to an antiferromagnetic (AF) interaction. The model given by Eq. (1.2) is often referred to as the t-J model.

When the average occupation equals to one, the t-J model reduces to the Heisenberg model:

$$H_{Hsb} = \frac{1}{2} \sum_{i,j} J_{ij} \boldsymbol{S}_i \cdot \boldsymbol{S}_j \quad , \tag{1.3}$$

where the constant term $\frac{1}{4} n_i n_j$ has been dropped. Note that in this case there is no charge degree of freedom remaining, thus the system is an insulator as claimed. It should also be remarked that while the derivation of the Heisenberg model sketched above is specific to the one-band Hubbard model, similar derivation can also be done in more complicated case, with the spin-1/2 operator $\boldsymbol{S}_i$ by spin operators of appropriate total spin S determined by a combination of Hund's rule and crystal field considerations, and the value of J_{ij} determined according to the precise scenario [12].

For the nearest-neighbor AF Heisenberg model (which for the rest of this chapter will be assumed to be the model under consideration, unless otherwise stated), the classical ground state (commonly referred to as the Néel order) on a bipartite lattice (i.e., a lattice that can be subdivided into two sublattices A and B, such that the nearest neighbors of a site in sublattice A all belong to sublattice B, and vice versa)

is easily seen to be an alternating pattern of anti-parallel spins (c.f. Fig. 1-2(a)). While such state cannot be the exact quantum ground state, quantum fluctuation in general does not destroy this order, as can be checked from, e.g., a spin-wave expansion [13]. Indeed, there have numerous observations of antiferromagnetic ordering in real materials [14], using techniques such as neutron scattering [15].

However, the magnetically ordered Néel state is not the only plausible ground state. An early example is the spin-Peierl state [16, 17], in which spin-lattice coupling causes the lattice spins on quasi-one-dimensional spin chains to spontaneously dimerize and deform the lattice. More generally, a spin system may form what is known as the valence bond solid (VBS) state. In a VBS state, lattice spins form singlet pairs in which certain singlet bonds are preferred to others, thus breaking the translation and/or the rotation symmetry of the lattice.

Perhaps more interesting is Anderson's proposal [18] in 1973 of a new possible ground state for the $S = 1/2$ triangular lattice. The state, which he termed the resonating-valence-bond (RVB) state, can be visualized as a linear superposition of configurations each formed by pairing spins into singlets. The RVB state has no static magnetic ordering and breaks no spin or lattice symmetry. Moreover, elementary excitations in this state will be spin-1/2 quasiparticles obtained from breaking a bond [19], which are now referred to as spinons. The RVB state is thus a quantum spin liquid, and a first proposal of such beyond one dimension.

While numerical evidence now suggests that the ground state of the nearest-neighbor AF Heisenberg model on the triangular lattice is ordered [20], the quantum spin liquid state may still be realized in other situations. One influential proposal, for example, is that the pseudo-gap phase in the cuprates superconductor is well-described as a quantum spin liquid [21]. Moreover, recent experiments have found several materials (whose effective interactions may be more complicated than being merely nearest-neighbor AF Heisenberg) in which the quantum spin liquid state may be realized. These include: (1) the organic salts κ-$(ET)_2X$ [22, 23] and $EtMe_3Sb[Pd(dmit)_2]_2$ [24], whose spins form triangular lattices; (2) the spinel related oxide $Na_4Ir_3O_8$ [25], whose spins form the so-called "hyper-kagome" lattice;

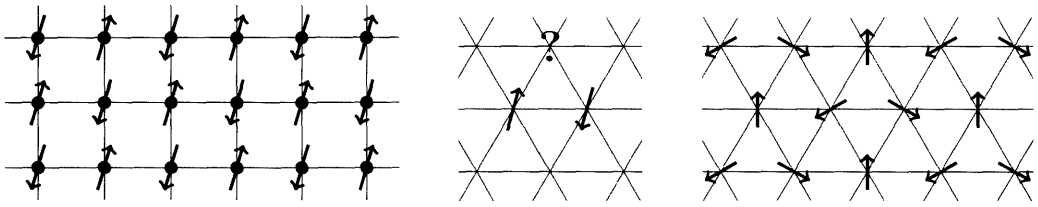

Figure 1-2: (a) Néel order on the square lattice; (b) Geometric frustration in the triangular lattice; (c) compromised Néel state on the triangular lattice.

and (3) herbertsmithite $ZnCu_3(OH)_6Cl_2$ [26, 27] and Vesignieite $BaCu_3V_2O_8(OH)_2$ [28], whose spins form kagome lattices.

1.1.1 Factors that favor spin liquid state

Under what circumstances will the spin liquid state be favorable? Anderson's proposal of the RVB state in the triangular lattice is partly motivated by the *geometric frustration* that is present in the triangular lattice. In general, geometric frustration occurs when the geometry of the lattice make it impossible for a classical spin configuration to simultaneously minimize the energy of all interactions. In the case of the triangular lattice, once two sites on a triangular plaquette is chosen to be anti-parallel, there is no way for the third spin in the plaquette to be simultaneously anti-parallel to these two spins (c.f. Fig. 1-2(b)). Hence the lattice is geometrically frustrated. Because of this geometric frustration, the Néel order in the triangular lattice is one in which each spin is at an angle of 120° with its neighboring spins, such that $\sum_i \boldsymbol{S}_i = \boldsymbol{0}$ on each triangle (Fig. 1-2(c)) [18]. Compared with the Néel order on a bipartite lattice, the Néel order on the triangular lattice is less energetically favorable, thus making the spin-liquid state a more attractive alternative.

It should be noted that frustration can also arise when additional interactions between the lattice spins, such as next-nearest neighbor Heisenberg interactions, are taken into account. For example, a square lattice can become frustrated when J_{ij} is antiferromagnetic for both nearest and next-nearest neighbors. Frustration introduced by additional interactions are particularly relevant for the so-called weak Mott

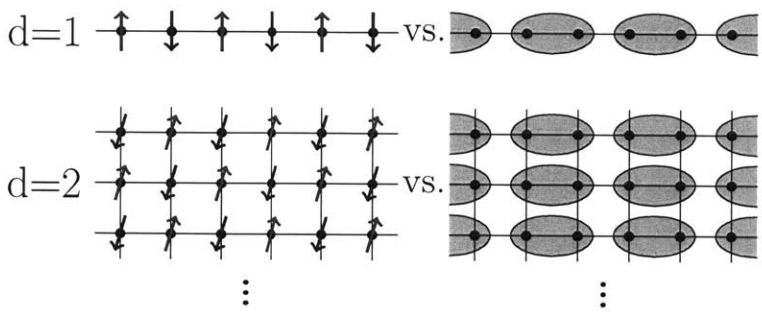

Figure 1-3: Néel state vs. singlet state on d-dimensional square lattices.

insulator, in which strong virtual charge fluctuations requires the inclusion of additional ring-exchange terms in the effective spin Hamiltonian[29]. Indeed, while the nearest-neighbor AF Heisenberg model on the triangular lattice is likely to be ordered, there are numerical evidence that the inclusion of ring-exchange interactions may favor spin liquid states [30, 31], which may explain the spin-liquid behavior in the organic salts organic salts κ-$(ET)_2X$ mentioned above.

In addition to frustration, low dimensionality and small total spin on each site also play important roles. For an intuitive picture, it suffices to consider a simple energy comparison between a classical Néel state and a singlet-pairing state of spin-S in a d-dimensions square lattice (Fig. 1-3), treating both as trial wavefunction to the nearest-neighbor Heisenberg Hamiltonian Eq. (1.3) (with $J_{ij} = J$ if i,j are nearest neighbor and 0 otherwise). The per-site energy expectation for the Néel state and the singlet-pairing state are, respectively:

$$\langle E_{\text{Néel}} \rangle = -dJS^2 \ , \tag{1.4}$$

$$\langle E_{\text{singlet}} \rangle = -\frac{J}{2} S(S+1) \ . \tag{1.5}$$

From this we see that as the singlet state becomes less and less energetically favorable when d and S increases.

The above criteria still leave us plenty of choices, since there are plenty of two-dimensional lattices that are geometrically frustrated. Is there any way to see which one may be more favorable to the quantum spin liquid state? Intuitively, we can

think of the quantum spin liquid as a state in which the classical ground states are mixed because of quantum fluctuation. With this picture in mind, one loose way to judge whether a lattice is more favorable to the quantum spin liquid state than the other is to compare the number of classical ground states that the system has. For example, while the triangular lattice is frustrated, once the orientation of two adjacent spins are determined, the Néel ordering pattern is uniquely specified. In contrast, in the kagome lattice the ground state cannot be uniquely specified by a local spin configuration, as will be discussed below.

1.2 The Schwinger fermion and slave boson formulation of spin liquid

While Anderson's picture of the quantum spin liquid state as a superposition of singlet pairs an inspiring one, it is not very convenient for analytic treatments of the theory. It would be desirable to have a mean-field theory for spin liquid, so that different types of spin liquid can be specified by choosing different mean-field parameters, and such that elementary excitations can be expressed in terms of the appropriate operators in the theory.

For the Heisenberg model, an obvious choice for mean-field parameter is the spin operator $\boldsymbol{S}$. However, this choice does not work for a spin liquid, in which $\langle \boldsymbol{S} \rangle = \mathbf{0}$. One way to circumvent this difficulty is to employ a slave-particle formulation, in which the spin operator is re-expressed in terms of fermion or boson operators. A famous example for this is the Schwinger boson decomposition [32], in which the spin-S operator $\boldsymbol{S}$ is expressed in terms of two species of bosons a and b, subjected to the constraint $a^\dagger a + b^\dagger b = 2S$ (the constraint ensures that all states are in the physical spin-S sector).

For a spin liquid state on a spin-1/2 lattice, it is useful to adopt instead a fermionic representation of the spin operators, in which two species of fermions $f_\uparrow$ and $f_\downarrow$ are

introduced, such that:

$$S^+ = S^x + iS^y = f_\uparrow^\dagger f_\downarrow \ , \tag{1.6}$$

$$S^- = S^x + iS^y = f_\downarrow^\dagger f_\uparrow \ , \tag{1.7}$$

$$S^z = \frac{1}{2}(f_\uparrow^\dagger f_\uparrow - f_\downarrow^\dagger f_\downarrow) \ . \tag{1.8}$$

Note that the above equations can be more compactly expressed as $\boldsymbol{S} = \frac{1}{2} f_\alpha^\dagger \boldsymbol{\tau}_{\alpha\beta} f_\beta$, where $\boldsymbol{\tau}$ are the usual Pauli matrices. From this we see that $f_\uparrow$ and $f_\downarrow$ together form a spin doublet. As in the Schwinger boson case, the Hilbert space is enlarged. Of the four possible states, only $|\uparrow\rangle = f_\uparrow^\dagger|\emptyset\rangle$ and $|\downarrow\rangle = f_\downarrow^\dagger|\emptyset\rangle$ are physical. The appropriate constraint in this case reads:

$$f_\uparrow^\dagger f_\uparrow + f_\downarrow^\dagger f_\downarrow = 1 \ . \tag{1.9}$$

In this representation, the Heisenberg Hamiltonian can be rewritten as [33]:

$$H_{\text{Hsb}} = -\sum_{ij} \frac{J_{ij}}{2} \left(f_{i\alpha}^\dagger f_{j\alpha} f_{j\beta}^\dagger f_{i\beta} \right) \ , \tag{1.10}$$

where an inconsequential constant has been dropped.

Observe that Eq. (1.10) resembles the Hamiltonians that arise from two-body interactions. As in that case, we can introduce mean-field parameters to decouple the four-fermion terms. Furthermore, at the mean-field level the constraint Eq. (1.9) can be imposed on average by adding a Lagrange multiplier $\lambda_i(\sum_\alpha f_{i\alpha}^\dagger f_{i\alpha} - 1)$ to the Hamiltonian. In particular, letting χ_{ij} to be our mean-field parameter, determined self-consistently through $\chi_{ij} = \langle \sum_\alpha f_{i\alpha}^\dagger f_{j\alpha} \rangle$, Eq. (1.10) becomes:

$$H_{MF} = -\sum_{ij} \frac{J_{ij}}{2} \left((\chi_{ij} f_{i\alpha}^\dagger f_{j\alpha} + h.c.) - |\chi_{ij}|^2 \right) + \sum_i \lambda_i \left(\sum\nolimits_\alpha f_{i\alpha}^\dagger f_{j\alpha} - 1 \right) \ . \tag{1.11}$$

Intuitively, χ_{ij} can be thought of as parameterizing the bond strength of the singlet bond that connects site i and j. Moreover, we see that f_σ plays the role of elementary excitation in Eq. (1.11). We can thus identify f_σ as the spinons as discussed above. In this way, different spin liquid ansatzes can be specified by different choices of χ_{ij}.

Note however that not all choices of χ_{ij} give rises to a legitimate spin liquid state, since a spin liquid must by definition be invariant under lattice symmetries, which imposes additional requirements on χ_{ij}. In particular, an ansatz in which $|\chi_{ij}|$ varies among different bonds that are related by lattice symmetry cannot be describe a spin liquid state, but will instead describe what called a valence bond solid (VBS) state. Intuitively, in a valence bond solid state the lattice spins also form singlet pairs, but unlike a quantum spin liquid, certain singlet bonds are preferred to others, thus breaking the translation and/or the rotation symmetry of the lattice.

Since Eq. (1.11) is a quadratic Hamiltonian of fermionic variables, at the mean-field level the ground state can be understood as spinons filling up the respective band structure. Different ansatzes will result in different band structures, which in turn dictates the physical properties of the resulting state.

1.2.1 Gauge field and deconfinement

The simple mean-field theory presented above missed a crucial feature of the spin liquid, namely the existence of an emergent gauge field [34]. To uncover this emergent gauge field, it is advantageous to adopt a path integral formulation. In the path integral formulation, both α_i^0 and χ_{ij} are to be treated as auxiliary variables, each to be integrated over in the respective functional integral. The full partition function thus reads [33]:

$$Z = \int \mathcal{D}\alpha_i^0 \int \mathcal{D}\chi_{ij} \int \mathcal{D}f e^{-\int dt \mathcal{L}} , \tag{1.12}$$

where the Lagrangian $\mathcal{L}$ is given by:

$$\mathcal{L} = \sum_{i,\alpha} f_{i\alpha}^\dagger \partial_t f_{i\alpha} + \sum_{ij} \frac{J_{ij}}{2} \left((\chi_{ij} f_{i\alpha}^\dagger f_{j\alpha} + h.c.) - |\chi_{ij}|^2 \right) - i \sum_i \lambda_i \left(\sum\nolimits_\alpha f_{i\alpha}^\dagger f_{j\alpha} - 1 \right) . \tag{1.13}$$

It should be remarked that while the constraint Eq. (1.9) is enforced only on average in the mean-field Hamiltonian, it is enforced exactly in the path integral formulation Eqs. (1.12)–(1.13), as long as the fluctuations of λ_i are included. Similarly, the decoupling of four-fermion terms are exact as long as the the fluctuations of χ_{ij}

are included (in this context the χ_{ij} is often referred to as a Hubbard-Stratonovich variable, and the transformation that decouples the four-operator terms is referred to as the Hubbard-Stratonovich transformation). The mean-field Hamiltonian can thus be thought of as being derived from the path integral formulation by neglecting the fluctuations of χ_{ij} and λ_i.

Because of the $|\chi_{ij}|^2$ term in Eq. (1.11), the magnitude fluctuation of χ_{ij} is in general gapped and thus it is legitimate to ignore it. The same cannot be said about λ_i and the phase of χ_{ij}. Letting $\chi_{ij} = |\chi_{ij}|e^{i\alpha_{ij}}$ and rewriting λ_i as α_i^0, with the understanding that these are fluctuating quantities, Eq. (1.11) becomes:

$$H_{MF} = -\sum_{ij} \frac{J_{ij}}{2} \left((|\chi_{ij}|e^{i\alpha_{ij}} f_{i\alpha}^\dagger f_{j\alpha} + h.c.) - |\chi_{ij}|^2 \right) + \sum_i \alpha_i^0 \left(\sum\nolimits_\alpha f_{i\alpha}^\dagger f_{j\alpha} - 1 \right) , \tag{1.14}$$

from which we see that α_i^0 and the phase of χ_{ij} naturally form the components of a $U(1)$ lattice gauge field. Indeed, this gauge field is associated with the gauge redundancy in the definition of $f_{i\sigma}$, since the Lagrangian is invariant under the following set of transformation:

$$f_{i\sigma} \mapsto e^{i\theta} f_{i\sigma} \; ; \qquad \alpha_{ij} \mapsto \alpha_{ij} + \theta_i - \theta_j \; ; \qquad \alpha_i^0 \mapsto \alpha_i^0 + \frac{\partial \theta_i}{\partial \tau} \; . \tag{1.15}$$

Observe that the gauge field thus defined is a *compact* gauge field, since α_{ij} is identified modulo 2π. Consequently, monopoles of this gauge fields are allowed, and from the argument by Polyakov [35], the existence of monopole will lead to the confined phase, in which the gauge field forces the spinons to bind together into an object neutral with respect to the gauge charge (this is analogous to the case in QCD, in which quarks are forced to bind into gauge-neutral baryons). In such case, the elementary excitations of the system will no longer be spin-1/2 spinons but rather spin-1 magnons.

Fortunately, Hermele *et. al.*[36] have shown that when the low-energy spinon spectrum consists of N Dirac cones and when N is sufficiently large, the system will flow to the deconfined phase under renormalization group flow, under which the monopole

becomes irrelevant. While the spinons will still be interacting strongly with the gauge field, it is at least sensible to talk about these spin-1/2 excitations as separate entity in the system.

1.2.2 Projected wavefunction

While mean-field theory is a convenient way to parameterize different spin liquid (and VBS) ansatzes and a useful way to consider their low-energy excitations, it often fails to give accurate estimate as to which mean-field state is most energetically favorable. One way to think about this issue is to realize that an mean-field ansatz can be thought of as defining a mean-field trial-wavefunction $|\psi_{\text{mean}}\rangle$, which has the problem of including configurations that are *unphysical*, i.e., configurations for which the constraint Eq. (1.9) is not satisfied. Then, a natural way to circumvent this difficulty would be to instead identify the mean-field ansatz with a *projected* trial wavefunction, in which the unphysical states are removed. More precisely, given a mean-field ansatz that corresponds to the mean-field trial wavefunction $|\psi_{\text{mean}}\rangle$, we identify:

$$|\psi\rangle = \mathcal{P}|\psi_{\text{mean}}\rangle \tag{1.16}$$

as the projected trial wavefunction that represent the ansatz, in which $\mathcal{P} = \prod_i (1 - n_{i\uparrow}n_{i\downarrow})$ is the projection operator. The idea of incorporating projection in evaluating the energy of mean-field states is pioneered by Gutzwiller [37], and its application to the RVB state has been pointed out by Anderson [21]. Once the above identification is made, numerical techniques, such as the variational Monte Carlo (VMC) method [38], can be applied to compare the energetics of different mean-field states.

1.2.3 Extension to the doped case

The forgoing discussion can be readily extended to the hole-doped case, described by the t-J model Eq. (1.2), and for brevity I shall only list the major results here.

In the doped case, the *projected* electron operator $\mathcal{P}c^\dagger\mathcal{P}$ can be expressed as a composite of a spinless charge-e bosonic particle h (called holon) and a chargeless

spin-1/2 fermionic spinon f [39]:

$$\mathcal{P}c^\dagger_{i\sigma}\mathcal{P} = f^\dagger_{i\sigma}h_i \ . \tag{1.17}$$

The constraint that need to be enforced is now:

$$f^\dagger_{i\uparrow}f_{i\uparrow} + f^\dagger_{i\downarrow}f_{i\downarrow} + h^\dagger_i h_i = 1 \ , \tag{1.18}$$

which intuitively corresponds to the statement that each site is either empty, or is occupied by an up-spin or a down-spin. Because a bosonic particle is introduced to keep track of the charge degree of freedom, the transformation Eq. (eq:c=fh) (and by extension Eqs. (1.6)–(1.8)) is often termed the slave-boson transformation.

Substituting Eq. (1.17) into the t-J model Eq. (1.2) will again lead to four-operators interactions, which can again be decoupled by introducing Hubbard-Stratonovich variables. This yields the mean-field Hamiltonian [40]:

$$\begin{aligned} H_{\rm MF} = &\sum_{i\sigma} f^\dagger_{i\sigma}(\alpha^0_i - \mu_F)f_{i\sigma} - \sum_{\langle ij\rangle,\sigma} |\chi_{ij}|(J_{ij}e^{i\alpha_{ij}}f_{i\sigma}f_{j\sigma} + h.c.) \\ &+ \sum_i h^\dagger_i(\alpha^0_i - \mu_B)h_i - \sum_{\langle ij\rangle} |\chi_{ij}|(t_{ij}e^{i\alpha_{ij}}h^\dagger_i h_j + h.c.) \ , \end{aligned} \tag{1.19}$$

where $\chi_{ij} = |\chi_{ij}|e^{i\alpha_{ij}}$ is the Hubbard-Stratonovich variable to be determined at mean-field by the self-consistency condition $\chi_{ij} = \langle \sum_\alpha f^\dagger_{i\alpha}f_{j\alpha}\rangle$, and that α^0_i arises from enforcing the constraint Eq. (1.18). Observe that the spinons and holons are decoupled and interact only through a common gauge field. Note also that the spinons and holons are governed to the *same* band structure.

As before, α^i_0 and $e^{i\alpha_{ij}}$ together form a compact $U(1)$ gauge field and should be treated as fluctuating quantities. This gauge field is associated with a gauge redundancy:

$$f_{i\sigma} \mapsto e^{i\theta}f_{i\sigma} \ ; \qquad h_i \mapsto e^{i\theta}h_i \ ; \qquad \alpha_{ij} \mapsto \alpha_{ij} + \theta_i - \theta_j \ ; \qquad \alpha^0_i \mapsto \alpha^0_i + \frac{\partial\theta_i}{\partial\tau} \ . \tag{1.20}$$

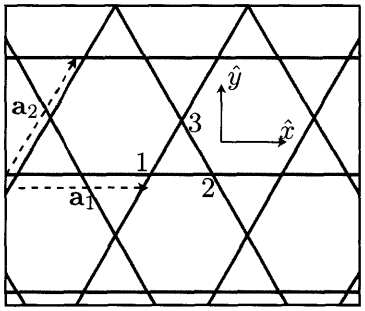

Figure 1-4: The kagome lattice.

It should be noted that the slave-boson formulation is among one of the favorite tools for understanding the microscopic physics of the cuprates [40].

1.3 The spin-1/2 kagome lattice

The name kagome comes from a Japanese word meaning "eye of cage." Geometrically, it can be described as a lattice of corner-sharing triangles (Fig. 1-4). As in the triangular lattice, the classical ground states of the lattice is characterized by the condition that $\sum_i \boldsymbol{S}_i = \mathbf{0}$ on each triangle. However, unlike the triangular lattice, the spin configuration on one triangle does not uniquely determine the spin configuration of the other triangles. In fact, for planar spins, the problem of enumerating all classical ground states can be mapped to the problem of enumerating the ways to color a honeycomb lattice with three colors, such that no adjacent sites share the same color [41], which yields an extensive entropy of approximately 0.126 k_B per site [42]. Moreover, ground states whose spins are non-planar can be obtained from planar ones by continuously rotating all spins on a closed path in which all their adjacent spins are of the same orientation [43] (However, this degeneracy in the classical case may be lifted by the order-by-disorder mechanism [44], which picks out in a particular planar configuration known as the $\sqrt{3} \times \sqrt{3}$ order[45, 46]). From the forgoing discussions, the kagome lattice is thus an attractive candidate on which the quantum spin liquid state may be realized.

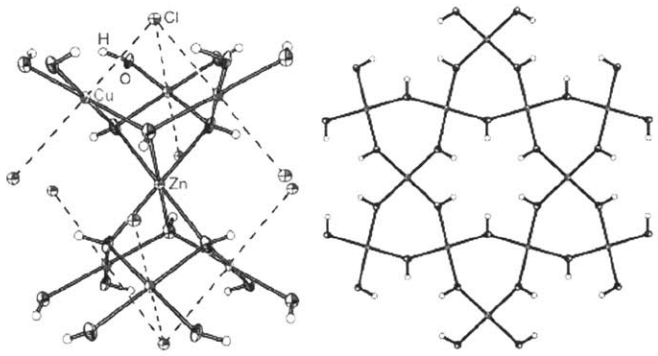

Figure 1-5: Crystal structure of herbertsmithite in (a) three-dimension; and (b) when projected onto the kagome plane. Adopted from Ref. [26].

1.3.1 Material realization of the spin-1/2 kagome lattice

Previously, kagome lattices of antiferromagnetically interacting magnetic ions have been realized in the garnet compound $SrCr_{9-x}Ga_{3+x}O_{19}$ [47, 48] and the jarosite materials $KFe_3(OH)_6(SO_4)_2$ [49, 50, 51] and $KCr_3(OH)_6(SO_4)_2$ [51, 52]. However, in these cases the magnetic ions are either spin-3/2 (for chromium ion Cr^{3+}) or spin-5/2 (for iron ion Fe^{3+}), and the materials are found to possess spin-glass or Néel ordering behavior at low temperatures.

The first material realization of spin-1/2 kagome lattice comes in the form of Volborthite $Cu_3V_2O_7(OH)_2 \cdot 2H_2O$ [53, 54, 55], in which the Cu^{2+} serve as the magnetic ions. Unfortunately, the AF interaction in Volborthite is latter shown to be anisotropic, and the material is found to have a transition to a (weakly) ordered phase at low temperature.

Finally, in 2005, reliable method was found to synthesize herbertsmithite [26] $ZnCu_3(OH)_6Cl_2$, which appears to be a "perfect" spin-1/2 kagome system with isotropic AF Heisenberg interaction (however, Dzyaloshinskii-Moriya (DM) interactions may not be negligible in the material [56], and defects on the copper sites resulting from zinc and copper ions interchanging may be as high as 5% [57]). So far, experimental data are consistent with the picture that the material is magnetically disordered: while fitting the high-temperature susceptibility indicates that the nearest-neighbor

AF interaction is about 190 K, neutron scattering suggests that the material is disordered down to the lowest measured temperature of 1.8 K [27]; and μSR shows no signature of spin freezing down to the lowest measured temperature of 50 mK [58, 59]. Moreover, thermodynamic measurements also show interesting behaviors of the material: the heat capacity follows a power law behavior for a wide intermediate range of temperature (approximately from 0.5 to 25 K) [27]; and while the spin susceptibility increases as temperature decreases towards zero [27, 60], NMR study [61] suggests that the susceptibility increase is caused by impurities, and that intrinsic susceptibility actually follow a power law. Taken together, the thermodynamic measurements seem to favor a state with gapless excitations, even though the evidences are far from conclusive.

It should be remarked that spin-liquid behavior has also been reported in another material that realizes the spin-1/2 kagome system, namely the Vesignieite $BaCu_3V_2O_8(OH)_2$. Existing data suggests that it also shows lack any magnetic ordering or spin freezing [28]. However, given the rarity of data on this material, it has yet to provide as much insight into the spin-1/2 kagome lattice as herbertsmithite.

1.3.2 Theoretical studies of the spin-1/2 kagome lattice

Partly motivated by the experimental results, and partly motivated numerical evidences from spin-wave theory [62], series expansion [63], and exact diagonalization [64] from early theoretical studies, the (nearest-neighbor AF Heisenberg) spin-1/2 kagome lattice is widely believed to be magnetically disordered. However, the nature of ground state is still under active debate. Specifically, the 36-site valence bond solid (VBS) state, first proposed by Marston and Zeng [65] and later by Nikolic and Senthil [66], have shown itself to be a resilient alternative to the spin liquid proposals. Among recent numerical studies, entanglement renormalization [67] and series expansion [68] found the VBS state more favorable than spin liquid state, while DMRG [69] found the spin liquid state more favorable.

An important aspect of this debate is the question of whether a singlet-triplet gap exists. In general, because a VBS state breaks the rotation and translation symmetry

of the lattice, an excitation from a VBS state is in general gapped. In contrast, depending on the details of the spinon band structure, a spin liquid may be gapped or gapless. In an exact diagonalization study by Waldtmann *et. al.*[70], it was suggested that a small gap of $J/20$ exists, thus supporting a gapped scenario. However, a more recent study from the same group [71] now suggests that this small gap is consistent with the finite size effect of other known gapless systems, thus suggesting that the state may be a gapless spin liquid.

Part of the debate also concerns the question of which particular spin liquid state among the various proposals will be most energetically favorable (many of these proposed state states can be constructed from a common parent state by perturbing the parameters [72]). In a projected wavefunction study Ran *et. al.*[73] shows that the $U(1)$ Dirac spin liquid state, so named because the low-energy spinon excitation of the system are described by Dirac nodes, stands out in energetics when compared with other plausible spin liquid candidates, and that the state is locally stable. Moreover, the energy estimate for the $U(1)$ DSL state is very close to the ground state energy estimate from exact diagonalization, despite the lack of any tunable variational parameters. Taken together, this make the $U(1)$ DSL state an attractive proposal for the spin-1/2 kagome lattice.

1.3.3 The $U(1)$ Dirac spin liquid state

Recall that a spin liquid state is uniquely specified once the set of mean-field parameters $\{\chi_{ij}\}$ are specified. Since our underlying model is the nearest-neighbor Heisenberg model, it suffices to specify χ_{ij} for all nearest-neighbor bonds. Moreover, since we are considering a spin liquid state, all χ_{ij} must have the same magnitude, so we may set $\chi_{ij} = \chi e^{i\alpha_{ij}}$. A spin liquid state is then uniquely determined once the phases $e^{i\alpha_{ij}}$ are specified.

Moreover, since the slave-boson representation has gauge redundancy as described by Eq. (1.15), configurations of α_{ij} that are related to each other by Eq. (1.15) must be physically equivalent, and it is desirable to describe the mean-field ansatzes in a more gauge invariant way, which can be achieved by specifying the amount of flux

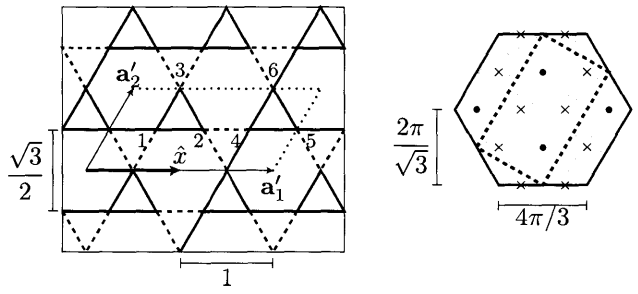

(a) (b)

Figure 1-6: (a) The kagome lattice with the $U(1)$ DSL ansatz. The (red) dashed lines correspond to bonds with effective hopping $\tilde{t} = -\chi J$ while the (blue) unbroken lines correspond to bonds with effective hopping $\tilde{t} = \chi J$. $\boldsymbol{a}'_1$ and $\boldsymbol{a}'_2$ are the primitive vectors of the doubled unit cell. (b) The original Brillouin zone (bounded by unbroken lines) and the reduced Brillouin zone (bounded by broken lines) of the $U(1)$ DSL ansatz. The dots indicate locations of the Dirac nodes at half-filling, the crosses indicate locations of the Dirac nodes crossing the second and the third band, and the thin (gray) lines indicate saddle regions at which the band energies are the same as that at $\boldsymbol{k} = 0$.

through each other triangular and hexagonal plaquettes of kagome lattice (the flux through an oriented plaquette P is defined by the product $\prod_{ij \in P} e^{i\alpha_{ij}}$).

With this prerequisite the $U(1)$ DSL state can be concisely described as the mean-field ansatz with a π flux through every hexagon and 0 flux through every triangle. [72, 73, 74]. Note that since the π and $-\pi$ are identified, the $U(1)$ DSL state is symmetric under time-reversal symmetry, which invert the signs of fluxes.

In order to compute the spinon band structure a particular gauge must be chosen. Moreover, observe that the total amount of gauge flux through a unit cell of the kagome lattice is π. Consequently, let T_{a_1} and T_{a_2} be the translation operators that corresponds to translation along lattice vectors $\boldsymbol{a}_1$ and $\boldsymbol{a}_2$, respectively (the convention for lattice vector and unit cell is shown in Fig. 1-4), it follows that:

$$T_{a_1}^{-1} T_{a_2}^{-1} T_{a_1} T_{a_2} = -1 \tag{1.21}$$

on the single spinon sector. Consequently, it is not possible to simultaneously diago-

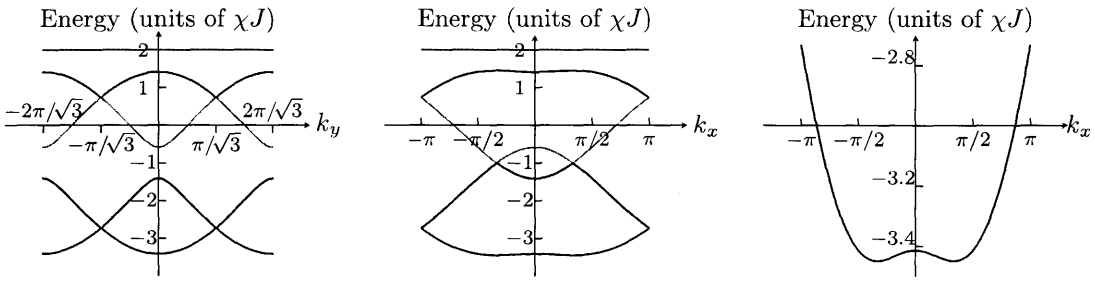

(a) (b) (c)

Figure 1-7: The band structure of the kagome lattice with the $U(1)$ DSL ansatz plotted along (a) $k_x = 0$ and (b) $k_y = 0$, with (c) a magnification of the bottom band in (b). Note that the top band is twofold degenerate.

nalize the Hamiltonian Eq. (1.11) and the two translation operators T_{a_1}, T_{a_2}. Because of this, the unit cell must necessarily be doubled when a gauge is fixed. The gauge convention that will be taken for the rest of this thesis is shown on Fig. 1-6(a), in which the blue unbroken bond corresponds to $a_{ij} = 0$ while the red broken bond corresponds to $\alpha_{ij} = \pi$.

It may appears that the rotation and translation symmetry of the system is broken by this gauge choice. This, however, is purely an artifact of our description. Specifically, the bond pattern shown in Fig. 1-6(a) is invariant under all lattice symmetry as long as one follows the physical transformation by an appropriate gauge transformation. Formally speaking, the symmetry of the $U(1)$ DSL state is manifested in the so-called projective symmetry group [75].

It is easy to check that, in units where $\chi J = 1$, this effective tight-binding Hamiltonian produces the following bands:

$$E_{\text{top}} = 2 \qquad \text{(doubly degenerate)} \,, \tag{1.22}$$

$$E_{\pm,\mp} = -1 \pm \sqrt{3 \mp \sqrt{2}\sqrt{3 - \cos 2k_x + 2\cos k_x \cos\sqrt{3}k_y}} \,. \tag{1.23}$$

At any $\boldsymbol{k}$-point, $E_{-,+} \leq E_{-,-} \leq E_{+,-} \leq E_{+,+} < E_{\text{top}}$. For plots of this band structure, see Fig. 1-7.

At low energy, the spinon spectrum is well-described by four (two spins times two $\boldsymbol{k}$-points) Dirac nodes, located at momentum $\pm\boldsymbol{Q} = \pm\pi/\sqrt{3}\,\hat{y}$ [c.f. Figs. 1-6(b) and 1-7(a)]. More specifically, at low-energy we may expand the mean-field Hamiltonian Eq. (1.11) around the Dirac points, which result in the Dirac Hamiltonian:

$$H_{\text{Dirac}} = \nu_F \sum_{\sigma,\alpha,\boldsymbol{q}} \psi^\dagger_{\sigma,\alpha,\boldsymbol{q}}(q_x\tau_x + q_y\tau_y)\psi_{\sigma,\alpha,\boldsymbol{q}} \ , \tag{1.24}$$

where $\sigma = \uparrow, \downarrow$ index spins, $\alpha = \pm$ index the location of the Dirac node, and $\boldsymbol{q}$ denotes the momentum as measured from the Dirac node (note that the component index of theψ, $\psi^\dagger$ and the Pauli matrices τ_i have been omitted for brevity). The relation between the two-component fermionic operators $\psi, \psi^\dagger$ and the spinon operators $f, f^\dagger$ defined on the lattice sites can be found in [74].

At low temperature and at the mean-field level the thermodynamics of the $U(1)$ DSL state will be dominated by the spinon Dirac node. Specifically, it magnetic susceptibility is predicted to be linear in temperature while the heat capacity is predicted to be quadratic in temperature [73].

Recall that the spinons are interacting with a $U(1)$ gauge field (which we shall taken as being non-compact, following the argument given in Sec. 1.2.1). Consequently, the low-energy effective theory of the $U(1)$ DSL state is essentially the same as the theory quantum electrodynamics in (2+1) dimensions (often abbreviated as QED_3). Specifically, in the continuum limit, the low-energy physics of the $U(1)$ DSL state can be described by the following action [73]:

$$S = \int dt d^2\boldsymbol{x} \left(\frac{1}{g^2}(\epsilon_{\lambda\mu\nu}\partial_\mu\alpha_\nu)^2 + \sum_{\sigma,\alpha} \psi^\dagger_{\sigma,\alpha}(\partial_\mu - i\alpha_\mu)\tau_\mu\psi_{\sigma,\alpha} + \right) \cdots \ . \tag{1.25}$$

here g is the effective coupling constant of the $U(1)$ gauge field, which is renormalized from infinity via renormalization. Using this mapping from the $U(1)$ DSL to QED_3, many correlations in the $U(1)$ DSL state can be inferred, and are shown to be obeying power laws [74]. Moreover, as the low-energy action Eq. (1.25) possess an emergent $SU(4)$ symmetry under which the four species of Dirac fermions are rotated into each

other, many different correlation functions turn out to have the same scaling behavior and are thus "competing" with each other. Because of this, the $U(1)$ DSL state is said to be a quantum critical phase.

As we have already seen, the Dirac node structure and the emergent gauge field have far reaching consequences on the properties on the $U(1)$ DSL state, many of which are novel and interesting. In the remainder of the thesis I will present my own study on the $U(1)$ DSL state, and we shall again see these features of the $U(1)$ DSL state playing prominent roles.

Chapter 2

Raman signature of the $U(1)$ DSL state

Raman spectroscopy is a "photon-in, photon-out" experimental technique in which photons at optical frequencies are scattered from a target material. While most of the incident photons are scattered elastically, some interact with the target material, resulting in frequency shifts in the scattered photons. By plotting the intensity of the scattered light as a function of frequency shift, various excitations of the target material can be probed [76]. Compared to other spectroscopic method such as angle-resolved photoemission spectroscopy (ARPES), Raman spectroscopy is particularly useful in probing the collective excitations of the target material. Moreover, since interaction between the photons and the target material can be affected by the photon polarization, additional information about the excitations can be inferred from the polarization mode of the incident and scattered photon.

Because the momentum of an optical photon is in general much smaller than the inverse lattice scale of the target material, Raman spectroscopy has the disadvantage that only excitations with small momenta can be detected. This problem can be resolved by replacing optical light by x-ray, and the resulting technique is referred to as the resonant inelastic x-ray scattering (RIXS) [77].

Recently, Cepas *et. al.*[78] considered Raman scattering on the spin-1/2 kagome system and concluded that a generic spin-liquid state can be distinguished from a

generic valence-bond-solid state by the polarization dependence of the signal. They also obtained a more detailed prediction of the Raman intensity using a random phase approximation, which may be too crude given the subtle orders[74] that may be present in the system.

In this chapter, I will discuss my work on deriving the Raman signature of the $U(1)$ DSL state, which shows that spinons will produce a broad continuum with power-law behavior at low energy, while the emergent gauge field will produce a $1/\omega$ singularity near $k = 0$. The possibility and challenges of obtaining finite-momentum characteristic of this emergent gauge boson in RIXS will also be discussed.

2.1 Shastry–Shraiman formulation of Raman scattering in Mott system

A formulation of Raman scattering in a Mott insulator can be made starting with the Hubbard Hamiltonian Eq. (1.1). While Eq. (1.1) does not include coupling to external photon, it can be incorporated by the replacement $c^\dagger_{i\sigma}c_{j\sigma} \mapsto c^\dagger_{i\sigma}c_{j\sigma}\exp(\frac{ie}{\hbar c}\int_j^i \boldsymbol{A}\cdot d\boldsymbol{x})$. Expanding this exponential and including also the free photon Hamiltonian H_γ, the Hamiltonian now reads:

$$H = H_{\mathrm{Hb}} + H_\gamma + H_C \ , \tag{2.1}$$

where H_{Hb} denotes the original Hubbard Hamiltonian as written in Eq. (1.1), and:

$$H_C = -\sum_{ij,\sigma} t_{ij}c^\dagger_{i\sigma}c_{j\sigma}\left(\frac{ie}{\hbar c}\boldsymbol{A}(\tfrac{\boldsymbol{x}_i+\boldsymbol{x}_j}{2})\cdot(\boldsymbol{x}_i-\boldsymbol{x}_j) - \frac{e^2}{\hbar^2c^2}\Big(\boldsymbol{A}(\tfrac{\boldsymbol{x}_i+\boldsymbol{x}_j}{2})\cdot(\boldsymbol{x}_i-\boldsymbol{x}_j)\Big)^2+\cdots\right) , \tag{2.2}$$

$$H_\gamma = \sum_{\boldsymbol{q}} \omega_{\boldsymbol{q}} a^{\alpha\dagger}_{\boldsymbol{q}} a^{\alpha}_{\boldsymbol{q}} \ , \tag{2.3}$$

in which $a^{\alpha\dagger}_{\boldsymbol{q}}$ ($a^{\alpha}_{\boldsymbol{q}}$) denotes the photon creation (annihilation) operator at momentum $\boldsymbol{q}$ and polarization α, and $\boldsymbol{A}(\boldsymbol{x})$ denotes the photon operator in real space. The $\cdots$ are terms at higher order in $\boldsymbol{A}$.

By treating H_C as a time-dependent perturbation, the transition rate from an initial state $|i\rangle$ to a final state $|f\rangle$ is given by:

$$\Gamma_{fi} = 2\pi |\langle f|T|i\rangle|^2 \delta(\mathcal{E}_f - \mathcal{E}_i) \ , \tag{2.4}$$

where $\mathcal{E}_i$ ($\mathcal{E}_f$) is the energy of the initial (final) state and $T = H_C + H_C(\mathcal{E}_i - H_{\rm Hb} - H_\gamma + i\eta)^{-1} H_C + \cdots$ is the T-matrix.

Since the fine-structure constant $e^2/\hbar c \approx 1/137$ is small and since we are interested in Raman processes (one photon in, one photon out), only terms second order in $\boldsymbol{A}$ need to be retained. At this order, the T-matrix reads:

$$T = H_C^{(2)} + H_C^{(1)} \frac{1}{\mathcal{E}_i - (H_{\rm Hb} + H_\gamma) + i\eta} H_C^{(1)} = T_{\rm NR} + T_{\rm R} \ , \tag{2.5}$$

where $H_C^{(n)}$ denotes the part of H_C that is n-th order in $\boldsymbol{A}$. The subscript R and NR on the last equality stands for resonant and non-resonant, respectively.

We are interested in a half-filled system ($\langle \sum_\sigma n_{i\sigma} \rangle = 1$) in the localized regime ($U \gg t$), in which both the initial and the final state belongs to the near-degenerate ground-state manifold $n_{i\uparrow} n_{i\downarrow} = 0$. In such case, $T_{\rm NR}$ has no matrix element that directly connects between the initial and the final states. Hence, only $T_{\rm R}$ is relevant for our purpose.

Let ω_i (ω_f), $\boldsymbol{k}_i$ ($\boldsymbol{k}_f$), and $\boldsymbol{e}_i$ ($\boldsymbol{e}_f$) be the frequency, momentum, and polarization of the incoming (outgoing) photon, respectively. Then, $\mathcal{E}_i = \omega_i + \mathcal{E}_i^{(\rm Hb)} = \omega_i + \mathcal{O}(t^2/U)$, where $H_{Hb}|i\rangle = \mathcal{E}_i^{(\rm Hb)}|i\rangle$; and $\boldsymbol{A}(\boldsymbol{x}) \mapsto g_i \boldsymbol{e}_i a_{\boldsymbol{k}_i}^{e_i} e^{i\boldsymbol{k}_i\cdot\boldsymbol{x}} + g_f \bar{\boldsymbol{e}}_f a_{\boldsymbol{k}_f}^{e_f\dagger} e^{-i\boldsymbol{k}_f\cdot\boldsymbol{x}}$, where $g_i = \sqrt{hc^2/\omega_{\boldsymbol{k}_i}\Omega}$ and $g_f = \sqrt{hc^2/\omega_{\boldsymbol{k}_f}\Omega}$, with Ω being the appropriate volume determined by the size of the sample and/or the size of the laser spot. In much of the following I will assume as typical that the momenta carried by the photons are much smaller than the inverse lattice spacing, and hence $e^{-i\boldsymbol{k}_i\cdot\boldsymbol{x}} \approx e^{-i\boldsymbol{k}_f\cdot\boldsymbol{x}} \approx 1$. I will also assume that the system is near resonance, so that $U \gg |\omega_i - U| \gtrsim |t|$. Consequently, henceforth I will keep only terms that are zeroth order in t/U and expand in powers of $t/(\omega_i - U)$.

Since the initial and final states both belong to the near-degenerate ground-state

manifold, it should be possible to re-express T_{R} in terms of spin operators. A procedure for doing so was developed by Shastry and Shraiman.[79, 80] A first step in the derivation is to expand the denominator of T_{R}:

$$\begin{aligned} T_{\mathrm{R}} &= H_C^{(1)} \frac{1}{\mathcal{E}_i - (H_{\mathrm{Hb}} + H_\gamma) + i\eta} H_C^{(1)} \\ &= H_C^{(1)} \frac{1}{\mathcal{E}_i - H_U - H_\gamma + i\eta} \sum_{n=0}^{\infty} \left(H_t \frac{1}{\mathcal{E}_i - H_U - H_\gamma + i\eta} \right)^n H_C^{(1)} \, . \end{aligned} \tag{2.6}$$

Next, a spin quantization axis is fixed and the initial states $|i\rangle = |\{\sigma\}\rangle \otimes |\boldsymbol{k}_i, \boldsymbol{e}_i\rangle$ and final states $|f\rangle = |\{\sigma'\}\rangle \otimes |\boldsymbol{k}_f, \boldsymbol{e}_f\rangle$ are taken to be a direct product of a definite spin state in position basis with a photon energy eigenstate.[1] Then, a complete set of states is inserted in between the operators in Eq. (2.6). By the assumption $U \gg |\omega_i - U| \gtrsim |t|$, the intermediate states are dominated by those having no photons and exactly one holon and one doublon. Thus, they take the generic form $|r_d; r_h; \{\tau\}\rangle \otimes |\emptyset\rangle$, where $|r_d; r_h; \{\tau\}\rangle = (\sum_\sigma c^\dagger_{r_d,\sigma} c_{r_h,\sigma})|\{\tau\}\rangle$ is obtained from the spin state $|\{\tau\}\rangle$ by removing an electron at r_h and putting it at r_d, and $|\emptyset\rangle$ denotes the photon vacuum state. Henceforth I will adopt the abbreviation that spins are summed implicitly within pairs of electron operators enclosed by parentheses, so that, e.g., $(c_i^\dagger c_j) = \sum_\sigma c^\dagger_{i\sigma} c_{j\sigma}$.

Under this insertion, $(\mathcal{E}_i - H_U - H_\gamma)^{-1} = (\omega_i - U)^{-1}$ becomes a c-number. Moreover, recall that H_t and (neglecting the photon part) H_C are sums of operators of the form $(c_i^\dagger c_j)$. Once a particular term is picked for each of these sums, and given an initial spin state $|\{\sigma\}\rangle$, the resulting chain of operators automatically and uniquely determines the intermediate states (which may be 0). Thus the intermediate states can be trivially re-summed, and Eq. (2.6) becomes, in schematic form:

[1] This introduces a small nuance that $\mathcal{E}_i$ can no-longer be treated as a scaler but must be considered as a matrix that depends on the initial and final spin states (but independent of the intermediate states). However, the off-diagonal terms of this matrix is of order t/U and hence negligible.

$$\langle\{\sigma'\}|T_{\rm R}|\{\sigma\}\rangle = \sum_{i_1 j_1, i_2 j_2, \ldots} \Big(C_{i_1 j_1, i_2 j_2, \{\sigma\}} \langle\{\sigma'\}|(c^\dagger_{i_2} c_{j_2})(c^\dagger_{i_1} c_{j_1})|\{\sigma\}\rangle + C_{i_1 j_1, \ldots, i_3 j_3, \{\sigma\}} \langle\{\sigma'\}|(c^\dagger_{i_3} c_{j_3})(c^\dagger_{i_2} c_{j_2})(c^\dagger_{i_1} c_{j_1})|\{\sigma\}\rangle + \ldots \Big) . \tag{2.7}$$

The sum in Eq. (2.7) is formidable. However, if H_C and H_t connects only between sites that are a few lattice constants away, then at low order in $t/(\omega_i - U)$, except for the choice of the initial site (j_1 in Eq. (2.7)) the number of non-zero terms is finite and does not scale with the lattice size. Thus, Eq. (2.7) provides a systematic way of analyzing the contributions to the Raman intensity.

The final step in the Shastry–Shraiman formulation is to convert the chain of electron operators $(c^\dagger_{i_n} c_{j_n}) \cdots (c^\dagger_{i_1} c_{j_1})$ into spin operators using the anti-commutation relation and the following spin identities:

$$\begin{aligned} c^\dagger_\sigma c_{\sigma'} &= \tilde{\chi}_{\sigma'\sigma} = \frac{1}{2}\delta_{\sigma',\sigma} + \boldsymbol{S}\cdot\boldsymbol{\tau}_{\sigma'\sigma} , \\ c_\sigma c^\dagger_{\sigma'} &= \chi_{\sigma\sigma'} = \frac{1}{2}\delta_{\sigma,\sigma'} - \boldsymbol{S}\cdot\boldsymbol{\tau}_{\sigma\sigma'} , \end{aligned} \tag{2.8}$$

where $\boldsymbol{S} = c^\dagger_\sigma(\boldsymbol{\tau}_{\sigma\sigma'}/2)c_{\sigma'}$ is the spin operator for spin-1/2 and $\boldsymbol{\tau}$ is the usual Pauli matrices.

To the lowest non-vanishing order in $t/(\omega_i - U)$, the Shastry–Shraiman formulation reproduces the Fleury–London Hamiltonian,[81] i.e.:

$$\begin{aligned} \langle f|T_{\rm R}|i\rangle &= \langle\{\sigma'\}|H_{\rm FL}|\{\sigma\}\rangle + \mathcal{O}\left(\frac{t^3}{(\omega_i - U)^2}\right) , \\ H_{\rm FL} &= \sum_{\boldsymbol{r},\boldsymbol{r}'} \frac{2t^2_{\boldsymbol{r}\boldsymbol{r}'}}{U - \omega_i} (\boldsymbol{e}_i\cdot\boldsymbol{\mu})(\bar{\boldsymbol{e}}_f\cdot\boldsymbol{\mu})\left(\frac{1}{4} - \boldsymbol{S}_{\boldsymbol{r}}\cdot\boldsymbol{S}_{\boldsymbol{r}'}\right) , \end{aligned} \tag{2.9}$$

where $\boldsymbol{\mu} = \boldsymbol{r}' - \boldsymbol{r}$ is the vector that connects lattice site $\boldsymbol{r}$ to lattice site $\boldsymbol{r}'$.

For theoretical calculations, it is convenient to decompose the polarization dependence of the Raman intensity into the irreducible representations (irreps) of the lattice point group, since operators belonging to different irreps do not interfere with each other (note however that subtractions between various experimental setups are

often required to extract the signal that corresponds to a particular channel[80]). It is known[61] that herbertsmithite belongs to the space group $R\bar{3}m$ and hence to the point group D_{3d}. In D_{3d}, the polarization tensor $\sum_{\alpha,\beta=x,y} C_{\alpha,\beta}\bar{e}_f^{\alpha}e_i^{\beta}$ in the kagome plane decomposes into two one-dimensional irreps A_{1g} and A_{2g}, and one two-dimensional irrep E_g:

$$\begin{aligned} A_{1g} &: \bar{e}_f^x e_i^x + \bar{e}_f^y e_i^y \ , \\ A_{2g} &: \bar{e}_f^x e_i^y - \bar{e}_f^y e_i^x \ , \\ E_g \begin{cases} E_g^{(1)} & : \bar{e}_f^x e_i^x - \bar{e}_f^y e_i^y \\ E_g^{(2)} & : \bar{e}_f^x e_i^y + \bar{e}_f^y e_i^x \end{cases} & . \end{aligned} \tag{2.10}$$

To the lowest non-vanishing order in $t/(\omega_i - U)$, the A_{1g} and the E_g component of the T-matrix are derived from the Fleury–London Hamiltonian Eq. (2.9). However, the resulting expression for the A_{1g} channel is the sum of a constant and a term proportional to the Heisenberg Hamiltonian and thus at zeroth order in t/U does not induce any inelastic transitions. For inelastic transitions in the A_{1g} channel, the leading-order contribution appears at the $t^4/(\omega_i - U)^3$ order instead. The leading-order contribution to the A_{2g} channel also appears at the $t^4/(\omega_i - U)^3$ order. The detailed calculations will be present in the next two subsections, but I will collect the final results here. To leading order and neglecting the elastic part, the operators that corresponds to the different channels are, for the kagome lattice:

$$\begin{aligned} O_{E_g^{(1)}} = \frac{4t^2}{\omega_i - U} \sum_R \Big(& \frac{1}{4} \boldsymbol{S}_{R,3} \cdot (\boldsymbol{S}_{R,1} + \boldsymbol{S}_{R+\boldsymbol{a}_2,1} + \boldsymbol{S}_{R,2} + \boldsymbol{S}_{R+\boldsymbol{a}_2-\boldsymbol{a}_1,2}) \\ & - \frac{1}{2} \boldsymbol{S}_{R,2} \cdot (\boldsymbol{S}_{R,1} + \boldsymbol{S}_{R+\boldsymbol{a}_1,1}) \Big) \ , \end{aligned} \tag{2.11}$$

$$O_{E_g^{(2)}} = \frac{4t^2}{\omega_i - U} \sum_R \frac{\sqrt{3}}{4} \Big(\boldsymbol{S}_{R,3} \cdot (\boldsymbol{S}_{R,1} + \boldsymbol{S}_{R+\boldsymbol{a}_2,1}) - \boldsymbol{S}_{R,3} \cdot (\boldsymbol{S}_{R,2} + \boldsymbol{S}_{R+\boldsymbol{a}_2-\boldsymbol{a}_1,2}) \Big) \ , \tag{2.12}$$

$$\begin{aligned} O_{A_{1g}} = \frac{-t^4}{(\omega_i - U)^3} \sum_R \Big(& 2\boldsymbol{S}_{R,1} \cdot (\boldsymbol{S}_{R+\boldsymbol{a}_1,1} + \boldsymbol{S}_{R+\boldsymbol{a}_2,1}) + 2\boldsymbol{S}_{R,2} \cdot (\boldsymbol{S}_{R-\boldsymbol{a}_1,2} + \boldsymbol{S}_{R+\boldsymbol{a}_2-\boldsymbol{a}_1,2}) \\ & + 2\boldsymbol{S}_{R,3} \cdot (\boldsymbol{S}_{R-\boldsymbol{a}_2,3} + \boldsymbol{S}_{R-\boldsymbol{a}_2+\boldsymbol{a}_1,3}) + \boldsymbol{S}_{R,1} \cdot (\boldsymbol{S}_{R+\boldsymbol{a}_2-\boldsymbol{a}_1,2} + \boldsymbol{S}_{R+\boldsymbol{a}_1-\boldsymbol{a}_2,3}) \\ & + \boldsymbol{S}_{R,2} \cdot (\boldsymbol{S}_{R-\boldsymbol{a}_2,3} + \boldsymbol{S}_{R+\boldsymbol{a}_2,1}) + \boldsymbol{S}_{R,3} \cdot (\boldsymbol{S}_{R+\boldsymbol{a}_1,1} + \boldsymbol{S}_{R-\boldsymbol{a}_1,2}) \Big) \ , \end{aligned} \tag{2.13}$$

$$O_{A_{2g}} = \frac{2\sqrt{3}it^4}{(\omega_i - U)^3} \sum_R \Big(3\,\mathcal{S}_{R,1;R,2;R,3} + 3\,\mathcal{S}_{R,1;R-\boldsymbol{a}_1,2;R-\boldsymbol{a}_2,3}$$
$$+ \mathcal{S}_{R,1;R,3;R+\boldsymbol{a}_2-\boldsymbol{a}_1,2} + \mathcal{S}_{R+\boldsymbol{a}_2,1;R,3;R,2} + \mathcal{S}_{R,3;R,2;R+\boldsymbol{a}_1,1}$$
$$+ \mathcal{S}_{R-\boldsymbol{a}_2+\boldsymbol{a}_1,3;R,2;R,1} + \mathcal{S}_{R,2;R,1;R-\boldsymbol{a}_2,3} + \mathcal{S}_{R-\boldsymbol{a}_1,2;R,1;R,3} \Big)$$
$$= \frac{2\sqrt{3}it^4}{(\omega_i - U)^3} \sum_R \Big(3 \; + 3 \; + \; + \; + \;$$
$$+ \; + \; + \; \Big) \,, \tag{2.14}$$

where $\mathcal{S}_{i;j;k}$ denotes $\boldsymbol{S}_i \cdot (\boldsymbol{S}_j \times \boldsymbol{S}_k)$, and which a graphical representation has been adopted on the final line.

2.1.1 Derivation of the Raman transition in the A_{2g} channel

In this subsection I shall consider the derivation of Raman transition rate in the $\bar{e}_f^x e_i^y - \bar{e}_f^y e_i^x$ channel. For completeness, I will present derivations not only for the kagome lattice, but also for the square, the triangular, and the honeycomb ones. Although the irreducible representation that corresponds to the polarization $\bar{e}_f^x e_i^y - \bar{e}_f^y e_i^x$ may be named differently in these lattices, I shall abuse notation and continue to refer to them as the "A_{2g}" channel.

For the square lattice with only nearest-neighbor hopping, Shastry and Shraiman claimed that spin-chirality term $\boldsymbol{S}_i \cdot (\boldsymbol{S}_j \times \boldsymbol{S}_k)$ appears in this channel at the $t^4/(\omega_i - U)^3$ order. However, our re-derivation does not confirm this result and instead concludes that the spin-chirality term vanishes to this order. While it is hard to pin down

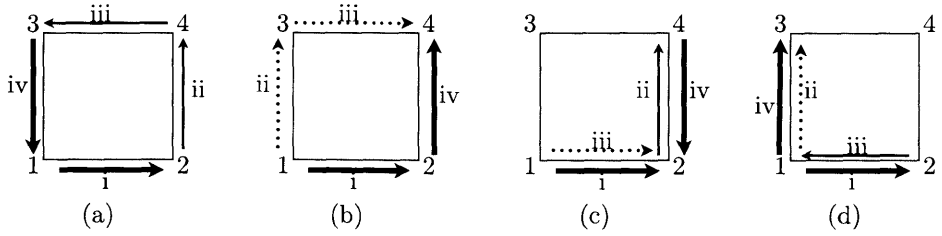

Figure 2-1: Pathways with two internal hops in a square lattice, with the initial holon fixed at site 1 and initial doublon fixed at site 2.

the source of this discrepancy, two possibilities are plausible. First, the pathways that contribute to the spin-chirality term includes not only those in which a doublon or holon hops through a loop [Figs. 2-1(a) and 2-1(b)], but also those in which a holon "chases" a doublon or vice versa without involving a fourth site [Figs. 2-1(c) and 2-1(d)]. These chasing pathways are non-intuitive and could be easily missed. Second, observe that for $c_\sigma^\dagger c_{\sigma'}$, the spin indices are flipped in Eq. (2.8) when going from electron operators to spin operators. This, together with the applications of the anti-commutation relation, can easily produce minus sign errors.

Our conclusion that the spin-chirality term vanishes to the $t^4/(\omega_i - U)^3$ order in the one-band Hubbard model need not contradict with the experimental claim that the spin-chirality term has been observed in the cuprates,[82] for in the cuprates—with the holon being delocalized as Zhang-Rice singlet while the doublon being localized at the copper site—the holon and doublon hopping magnitude need not be equal. In that case, the crucial cancellation between the four pathways in Fig. 2-1 no longer occurs. Furthermore, in the Shastry–Shraiman formalism the spin-chirality term may also be present at higher order in $t/(\omega_i - U)$ and/or when further neighbor hoppings are included. Since the ratio $t/(\omega_i - U)$ need not be small near resonance, these higher-order effects can manifest in experiments.

To extract the A_{2g} channel from the general polarization matrix, note that given any particular hopping pathway, a "reversed pathway" can be constructed, in which all electron operators are conjugated and their order reversed [for example, $(c_1^\dagger c_2)$ $(c_2^\dagger c_3)$ $(c_3^\dagger c_1)$ is the reversed pathway of $(c_1^\dagger c_3)$ $(c_3^\dagger c_2)$ $(c_2^\dagger c_1)$]. Then, $\bar{e}_f^x e_i^y \mapsto \bar{e}_f^y e_i^x$ and the order the spin operators thus obtained are inverted. Hence, to the $t^4/(\omega_i - U)^3$ order, which corresponds to at most four spin operators, the only terms that survive in the A_{2g} channel are the spin-chirality operators $\boldsymbol{S}_i \cdot (\boldsymbol{S}_j \times \boldsymbol{S}_k)$. Thus, in our derivation it suffices to extract the spin-chirality contributions from pathways whose initial and final currents are not co-linear.

To depict the hopping pathways efficiently, the following abbreviations are introduced in the diagrams. A thick (blue) arrow is used to indicate the initial or the final hop in which a holon–doublon pair is created or destroyed. For the internal hops,

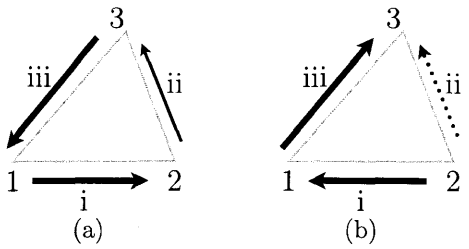

Figure 2-2: Two types of one-internal-hop pathways. Thick (blue) arrows denote initial or final hops in which a holon–doublon pair is created or destroyed, thin (magenta) unbroken arrows denote the movement of doublons, and thin (magenta) broken arrows denote the movement of holons. Lower case roman letters are used to indicate the order of hops. In (a) the internal hop is performed by the doublon while in (b) the internal hop is performed by the holon.

the movement of a doublon is indicated by a thin (magenta) unbroken arrow and the movement of a holon is indicated by a thin (magenta) broken arrow. Lower case roman letters are used to indicate the ordering of hops. Note that in this scheme, a solid magenta arrow from i to j corresponds to the electron operators $(c_j^\dagger c_i)$, while a broken magenta arrow from i to j corresponds to the electron operators $(c_i^\dagger c_j)$.

The lowest order at which the spin-chirality term can show up is $t^3/(\omega_i - U)^2$, which corresponds to pathways with one internal hop. Such pathway can be found in the triangular or the kagome lattice, or when next-nearest hopping is included. I will show that the contributions to the A_{2g} channel by these pathways cancel in pairs at this order.

It is easy to see that there are two types one-internal-hop pathways in general, both involving three lattice sites. In a pathway of the first type, a holon-doublon pair is created across a bond by an incident photon. Then, the doublon moves to a third site before recombining with the holon to emit a Raman-shifted photon [Fig. 2-2(a)]. A pathway of the second type is similar, except that it is the *holon* that moves to a third site before recombining [Fig. 2-2(b)].

Applying the procedures as explained in Sec. 2.1, the operator that corresponds

to the pathway in Fig. 2-2(a) is given by:

$$\begin{aligned} T_{1,e} &= (\bar{\boldsymbol{e}}_f \cdot \boldsymbol{x}_{13})(\boldsymbol{e}_i \cdot \boldsymbol{x}_{21}) \frac{(-it_{13})(-t_{32})(-it_{21})}{(\omega_i - U)^2} (c_1^\dagger c_3)(c_3^\dagger c_2)(c_2^\dagger c_1) \\ &= (\bar{\boldsymbol{e}}_f \cdot \boldsymbol{x}_{13})(\boldsymbol{e}_i \cdot \boldsymbol{x}_{21}) \frac{t_{13}t_{32}t_{21}}{(\omega_i - U)^2} \operatorname{tr}\{\chi_3 \chi_2 \tilde{\chi}_1\} \\ &\doteq (\bar{\boldsymbol{e}}_f \cdot \boldsymbol{x}_{13})(\boldsymbol{e}_i \cdot \boldsymbol{x}_{21}) \frac{t_{13}t_{32}t_{21}}{(\omega_i - U)^2} 2i\, \boldsymbol{S}_3 \cdot \boldsymbol{S}_2 \times \boldsymbol{S}_1 \ , \end{aligned} \tag{2.15}$$

where $\boldsymbol{x}_{ij} = \boldsymbol{x}_i - \boldsymbol{x}_j$ is the vector from site j to site i, and "$\doteq$" denotes equality upon neglecting terms that do not contribute to the A_{2g} channel.

Similarly, the operator that corresponds to the pathway in Fig. 2-2(b) is given by:

$$\begin{aligned} T_{1,h} &= (\bar{\boldsymbol{e}}_f \cdot \boldsymbol{x}_{31})(\boldsymbol{e}_i \cdot \boldsymbol{x}_{12}) \frac{(-it_{31})(-t_{23})(-it_{12})}{(\omega_i - U)^2} (c_3^\dagger c_1)(c_2^\dagger c_3)(c_1^\dagger c_2) \\ &= (\bar{\boldsymbol{e}}_f \cdot \boldsymbol{x}_{31})(\boldsymbol{e}_i \cdot \boldsymbol{x}_{12}) \frac{t_{31}t_{23}t_{12}}{(\omega_i - U)^2} (-1) \operatorname{tr}\{\chi_1 \tilde{\chi}_2 \tilde{\chi}_3\} \\ &\doteq (\bar{\boldsymbol{e}}_f \cdot \boldsymbol{x}_{31})(\boldsymbol{e}_i \cdot \boldsymbol{x}_{12}) \frac{t_{31}t_{23}t_{12}}{(\omega_i - U)^2} 2i\, \boldsymbol{S}_1 \cdot \boldsymbol{S}_2 \times \boldsymbol{S}_3 \\ &\doteq -T_{1,e} \ , \end{aligned} \tag{2.16}$$

where t_{ij} are assumed to be real in the last step.

Since the two pathways depicted in Fig. 2-2 always come in pair, the contribution to the A_{2g} channel by one-internal-hop pathways vanishes upon summing as claimed.

Now consider pathways that involve two internal hops, starting with the square lattice. Henceforth I shall assume that hopping is between nearest neighbors only, uniform, and real. The abbreviations $C_2 = t^4/(\omega_i - U)^3$ and $\mathcal{S}_{i;j;k} = \boldsymbol{S}_i \cdot (\boldsymbol{S}_j \times \boldsymbol{S}_k)$ will also be used.

To count the two-internal-hop pathways in the square lattice systemically, first fix the initial holon at site 1 and the initial doublon at site 2, and align the coordinates so that $y = 0$ for site 1 and 2 and that $\boldsymbol{x}_{21} = \hat{x}$. All other pathways are clearly related to the ones satisfying the above conditions via symmetries. For the final hop and the initial hop to be non-collinear, a third site not collinear with site 1 and 2 must be involved, and we may further restrict our attention to pathways in which the third site lies in the $y > 0$ half-plane, since the remaining pathways are related to these via

the mirror reflection $y \to -y$.

There are four pathways that satisfy the above restrictions, which are precisely the ones depicted in in Fig. 2-1. Applying the procedures as explained Sec. 2.1, the contributions by these pathways are given by:

$$\begin{aligned} T_{2,a} &= C_2 e_i^x (-\bar{e}_f^y)(c_1^\dagger c_3)(c_3^\dagger c_4)(c_4^\dagger c_2)(c_2^\dagger c_1) \\ &= -C_2 e_i^x \bar{e}_f^y \,\mathrm{tr}\{\chi_3\chi_4\chi_2\tilde{\chi}_1\} \\ &\doteq -iC_2 e_i^x \bar{e}_f^y (\mathcal{S}_{3;4;1} + \mathcal{S}_{3;2;1} + \mathcal{S}_{4;2;1} - \mathcal{S}_{3;4;2}) \ , \end{aligned} \tag{2.17}$$

$$\begin{aligned} T_{2,b} &= C_2 e_i^x \bar{e}_f^y (c_4^\dagger c_2)(c_3^\dagger c_4)(c_1^\dagger c_3)(c_2^\dagger c_1) \\ &= C_2 e_i^x \bar{e}_f^y \,\mathrm{tr}\{\chi_2\tilde{\chi}_1\tilde{\chi}_3\tilde{\chi}_4\} \\ &\doteq iC_2 e_i^x \bar{e}_f^y (\mathcal{S}_{1;3;4} - \mathcal{S}_{2;3;4} - \mathcal{S}_{4;2;1} - \mathcal{S}_{2;1;3}) \ , \end{aligned} \tag{2.18}$$

$$\begin{aligned} T_{2,c} &= C_2 e_i^x (-\bar{e}_f^y)(c_2^\dagger c_4)(c_1^\dagger c_2)(c_4^\dagger c_2)(c_2^\dagger c_1) \\ &= -C_2 e_i^x \bar{e}_f^y \Big((c_4 c_1^\dagger)(c_4^\dagger c_2)(c_2^\dagger c_1) + (c_4 c_4^\dagger)(c_1^\dagger c_2)(c_2^\dagger c_1) \Big) \\ &= -C_2 e_i^x \bar{e}_f^y \Big(\mathrm{tr}\{(-1)\chi_4\chi_2\tilde{\chi}_1\} + \mathrm{tr}\{\chi_4\}\,\mathrm{tr}\{\chi_2\tilde{\chi}_1\} \Big) \\ &\doteq -2iC_2 i e_i^x \bar{e}_f^y \mathcal{S}_{4;2;1} \ , \end{aligned} \tag{2.19}$$

$$\begin{aligned} T_{2,d} &= C_2 e_i^x \bar{e}_f^y (c_3^\dagger c_1)(c_1^\dagger c_2)(c_1^\dagger c_3)(c_2^\dagger c_1) \\ &= C_2 e_i^x \bar{e}_f^y \Big((c_3^\dagger c_2)(c_1^\dagger c_3)(c_2^\dagger c_1) + (c_3^\dagger c_3)(c_1^\dagger c_2)(c_2^\dagger c_1) \Big) \\ &= C_2 e_i^x \bar{e}_f^y \Big(\mathrm{tr}\{(-1)\tilde{\chi}_3\chi_2\tilde{\chi}_1\} + \mathrm{tr}\{\tilde{\chi}_3\}\,\mathrm{tr}\{\chi_2\tilde{\chi}_1\} \Big) \\ &\doteq 2iC_2 i e_i^x \bar{e}_f^y \mathcal{S}_{3;2;1} \ . \end{aligned} \tag{2.20}$$

Summing all four terms, it is found that $T_{2,a} + T_{2,b} + T_{2,c} + T_{2,d} \doteq 0$. Hence, for the square lattice with only nearest-neighbor hopping, the operator that corresponds to the Raman transition in the A_{2g} channel, $O_{A_{2g}}$, vanishes to the $t^4/(\omega_i - U)^3$ order.

Notice that the orthogonality between the $\hat{x}$ and $\hat{y}$ has not been invoked in the above derivation. Consequently, the above derivation carries to the triangular lattice upon mapping $\hat{x}$ and $\hat{y}$ in the square lattice to any two of bond directions in the triangular lattice. See Fig. 2-3 for illustration. It can be checked that all two-internal-

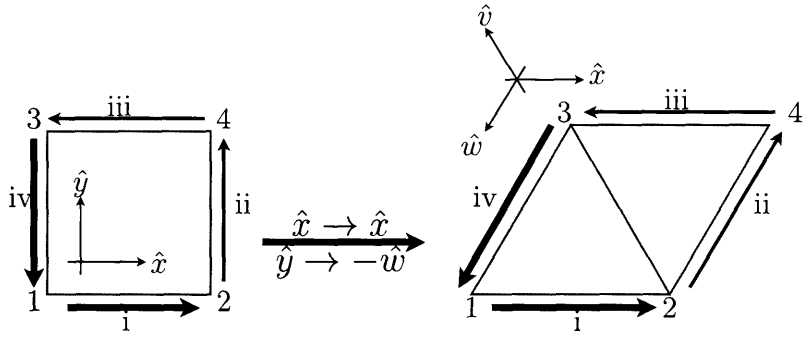

Figure 2-3: Mapping between the pathways in the square lattice and the pathways in the triangular lattice.

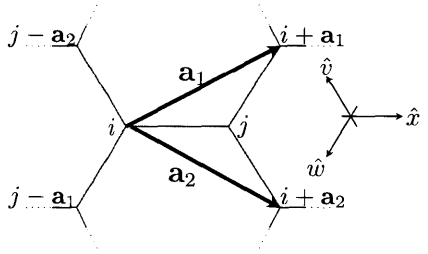

Figure 2-4: The honeycomb lattice (thin gray lines), wherein the site label i, j, the unit vectors $\hat{x}$, $\hat{v}$, $\hat{w}$ (thin black arrows), and the primitive lattice vector (thick black arrows), are defined.

hop pathways with non-collinear initial and final hops in the triangular lattice can be obtained from such mappings and that there is no issue of double-counting. Hence, it can be concluded that $O_{A_{2g}}$ vanishes up to the $t^4/(\omega_i - U)^3$ order in the triangular lattice also.

Evidently, the criterion that any three non-collinear nearest-neighbor sites belong to a four-site loop is a crucial ingredient for the cancellations of the two-internal-hop contributions as seen above. This criterion is not met in the honeycomb lattice or in the kagome lattice. Hence, $O_{A_{2g}}$ may not vanish in these lattices at the $t^4/(\omega_i - U)^3$ order.

First consider the honeycomb lattice, which is shown in Fig. 2-4, wherein the site labels i, j, the unit vectors $\hat{x}$, $\hat{v}$, $\hat{w}$ along bond directions, and the primitive lattice vectors $\boldsymbol{a}_1$, $\boldsymbol{a}_2$, are defined. For an initial holon at i and an initial doublon

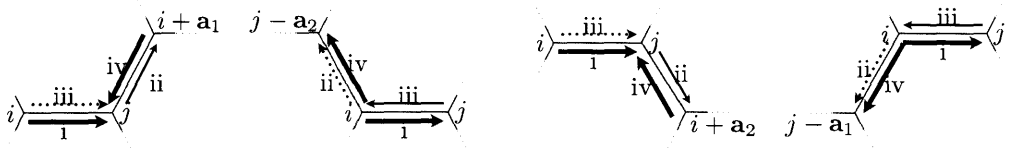

Figure 2-5: Pathways with two internal hops that contribute to the A_{2g} channel in the honeycomb lattice, with the initial holon fixed at site i and initial doublon fixed at site j.

at j, there are four two-internal-hop pathways, listed in Fig. 2-5. Summing up their contributions, we get:

$$T_{2,i,j} \doteq 2iC_2\Big(- e_i^x \bar{e}_f^w \mathcal{S}_{i+\boldsymbol{a}_1;j;i} + e_i^x \bar{e}_f^v \mathcal{S}_{j-\boldsymbol{a}_2;j;i} - e_i^x \bar{e}_f^v \mathcal{S}_{i+\boldsymbol{a}_2;j;i} + e_i^x \bar{e}_f^w \mathcal{S}_{j-\boldsymbol{a}_1;j;i}\Big) \ . \tag{2.21}$$

If the initial doublon is fixed at $j - \boldsymbol{a}_2$ or $j - \boldsymbol{a}_1$ instead, the contributions are, respectively,

$$T_{2,i,j-\boldsymbol{a}_2} \doteq 2iC_2\Big(e_i^v \bar{e}_f^x (\mathcal{S}_{j;j-\boldsymbol{a}_2;i} - \mathcal{S}_{i-\boldsymbol{a}_2;j-\boldsymbol{a}_2;i}) + e_i^v \bar{e}_f^w (\mathcal{S}_{j-\boldsymbol{a}_1;j-\boldsymbol{a}_2;i} - \mathcal{S}_{i+\boldsymbol{a}_1-\boldsymbol{a}_2;j-\boldsymbol{a}_2;i})\Big) \ , \tag{2.22}$$

$$T_{2,i,j-\boldsymbol{a}_1} \doteq 2iC_2\Big(e_i^w \bar{e}_f^v (\mathcal{S}_{j-\boldsymbol{a}_2;j-\boldsymbol{a}_1;i} - \mathcal{S}_{i+\boldsymbol{a}_2-\boldsymbol{a}_1;j-\boldsymbol{a}_1;i}) + e_i^w \bar{e}_f^x (\mathcal{S}_{j;j-\boldsymbol{a}_1;i} - \mathcal{S}_{i-\boldsymbol{a}_1;j-\boldsymbol{a}_1;i})\Big) \ . \tag{2.23}$$

And the analog of Eqs. 2.21–2.23, when the holon is fixed at j, are given by:

$$T_{2,j,i} \doteq 2iC_2\Big(e_i^x \bar{e}_f^w (\mathcal{S}_{i+\boldsymbol{a}_1;j;i} - \mathcal{S}_{j-\boldsymbol{a}_1;j;i}) + e_i^x \bar{e}_f^v (\mathcal{S}_{i+\boldsymbol{a}_2;j;i} - \mathcal{S}_{j-\boldsymbol{a}_2;j;i})\Big) \ , \tag{2.24}$$

$$T_{2,j,i+\boldsymbol{a}_2} \doteq 2iC_2\Big(e_i^v \bar{e}_f^x (\mathcal{S}_{i;i+\boldsymbol{a}_2;j} - \mathcal{S}_{j+\boldsymbol{a}_2;i+\boldsymbol{a}_2;j}) + e_i^v \bar{e}_f^w (\mathcal{S}_{i+\boldsymbol{a}_1;i+\boldsymbol{a}_2;j} - \mathcal{S}_{j+\boldsymbol{a}_2-\boldsymbol{a}_1;i+\boldsymbol{a}_2;j})\Big) \ , \tag{2.25}$$

$$T_{2,j,i+\boldsymbol{a}_1} \doteq 2iC_2\Big(e_i^w \bar{e}_f^v (\mathcal{S}_{i+\boldsymbol{a}_2;i+\boldsymbol{a}_1;j} - \mathcal{S}_{j+\boldsymbol{a}_1-\boldsymbol{a}_2;i+\boldsymbol{a}_1;j}) + e_i^w \bar{e}_f^x (\mathcal{S}_{i;i+\boldsymbol{a}_1;j} - \mathcal{S}_{j+\boldsymbol{a}_1;i+\boldsymbol{a}_1;j})\Big) \ . \tag{2.26}$$

Summing Eqs. 2.21–2.26 over all lattice vectors $\{\boldsymbol{R}\}$, and reorganize slightly, we

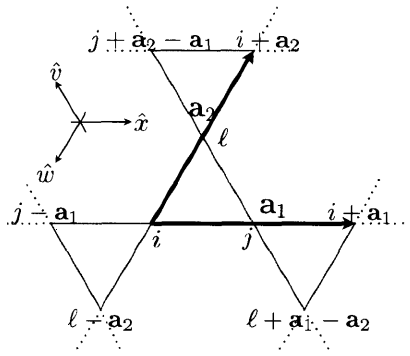

Figure 2-6: The kagome lattice (thin gray lines), wherein the site label i, j, the unit vectors $\hat{x}$, $\hat{v}$, $\hat{w}$ (thin black arrows), and the primitive lattice vector (thick black arrows), are defined.

finally obtain:

$$
\begin{aligned}
T_{2,\mathrm{hex}} \doteq 4iC_2 \sum_R \Big(& (\mathcal{S}_{j;i;i-\boldsymbol{a}_1} + \mathcal{S}_{i;j;i+\boldsymbol{a}_1})(e_i^x \bar{e}_f^w - e_i^w \bar{e}_f^x) \\
& + (\mathcal{S}_{i-\boldsymbol{a}_2;i;j} + \mathcal{S}_{i+\boldsymbol{a}_2;j;i})(e_i^v \bar{e}_f^x - e_i^x \bar{e}_f^v) + (\mathcal{S}_{j-\boldsymbol{a}_1;i;i-\boldsymbol{a}_2} + \mathcal{S}_{i+\boldsymbol{a}_1;j;i+\boldsymbol{a}_2})(e_i^w \bar{e}_f^v - e_i^v \bar{e}_f^w) \Big) \\
= 4iC_2 \sum_R \Bigg(& \Big(\quad + \quad \Big)(e_i^x \bar{e}_f^w - e_i^w \bar{e}_f^x) \\
& + \Big(\quad + \quad \Big)(e_i^v \bar{e}_f^x - e_i^x \bar{e}_f^v) + \Big(\quad + \quad \Big)(e_i^w \bar{e}_f^v - e_i^v \bar{e}_f^w) \Bigg) ,
\end{aligned}
\tag{2.27}
$$

where graphical symbols are introduced on the second equality to denote the spin-chirality operators. Note that even though the site labels are omitted in the symbols, upon the summation over lattice vectors $\{\boldsymbol{R}\}$ there is no ambiguity as to which spin-chirality operator a particular symbol is referring to.

Using $e^v = -\frac{1}{2}e^x + \frac{\sqrt{3}}{2}e^y$ and $e^w = -\frac{1}{2}e^x - \frac{\sqrt{3}}{2}e^y$, Eq. (2.27) can be converted back to the Cartesian coordinates, which yields:

$$
T_{2,\mathrm{hex}} \doteq 2\sqrt{3}iC_2(e_i^y \bar{e}_f^x - e_i^x \bar{e}_f^y) \sum_R \Big(\quad + \quad + \quad + \quad + \quad + \quad \Big) .
\tag{2.28}
$$

Finally consider the kagome lattice, which is shown in Fig. 2-6, wherein the site

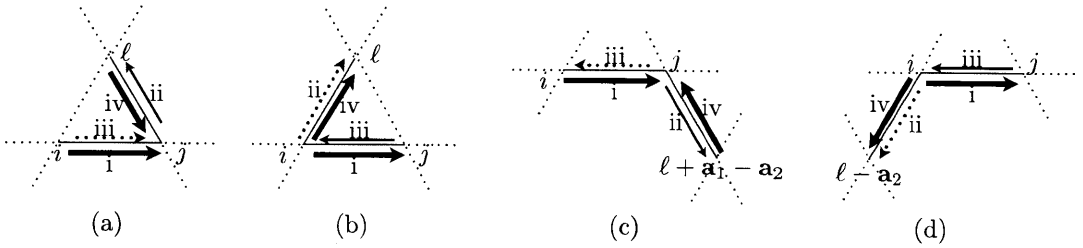

Figure 2-7: Pathways with two internal hops that contribute to the A_{2g} channel in the kagome lattice, with the initial holon fixed at site i and initial doublon fixed at site j.

labels i, j, ℓ, unit vectors $\hat{x}$, $\hat{v}$, $\hat{w}$, and primitive lattice vectors $\boldsymbol{a}_1$, $\boldsymbol{a}_2$, are defined. Fixing the initial holon at site i and the initial doublon at site j, four two-internal-hop pathways contribute to the A_{2g} channel (Fig. 2-7). The sum of their contributions is:

$$T_{2,i,j} \doteq 2iC_2\Big(+ e_i^x \bar{e}_f^v \mathcal{S}_{\ell;j;i} - e_i^x \bar{e}_f^w \mathcal{S}_{\ell;j;i} - e_i^x \bar{e}_f^v \mathcal{S}_{\ell+\boldsymbol{a}_1-\boldsymbol{a}_2;j;i} + e_i^x \bar{e}_f^w \mathcal{S}_{\ell-\boldsymbol{a}_2;j;i}\Big)$$
$$= 2iC_2\Big(e_i^x \bar{e}_f^w \Big(\quad + \quad \Big) - e_i^x \bar{e}_f^v \Big(\quad + \quad \Big)\Big) \,, \tag{2.29}$$

where graphical symbols are again introduced on the second equality. Note again that upon summing over all lattice vectors $\{\boldsymbol{R}\}$ there is no ambiguity as to which spin-chirality operator a particular symbol refers to.

By changing the site where the initial doublon is located, we get, upon summation, the following contribution to $O_{A_{2g}}$ by two-internal-hop pathways whose initial holon is located at site i:

$$T_{2,i} \doteq 2iC_2\Big(e_i^w \bar{e}_f^v \Big(\quad + \quad + \quad + \quad \Big) - e_i^x \bar{e}_f^v \Big(\quad + \quad + \quad + \quad \Big)$$
$$+ (e_i^x \bar{e}_f^w - e_i^w \bar{e}_f^x) \Big(\quad + \quad + \quad + \quad \Big)\Big) \,. \tag{2.30}$$

Obtaining the contributions to $O_{A_{2g}}$ by two-internal-hop pathways whose initial holon is located at site j or ℓ in an analogous manner, we finally get, upon summing

over all lattice vectors and basis sites,

$$T_{2,\mathrm{kag}} \doteq 4iC_2 \sum_{\boldsymbol{R}} \Big((e_i^x \bar{e}_f^w - e_i^w \bar{e}_f^x) \Big(\quad + \quad + \quad + \quad \Big)$$
$$+ (e_i^v \bar{e}_f^x - e_i^x \bar{e}_f^v) \Big(\quad + \quad + \quad + \quad \Big) \tag{2.31}$$
$$+ (e_i^w \bar{e}_f^v - e_i^v \bar{e}_f^w) \Big(\quad + \quad + \quad + \quad \Big) \Big) \,.$$

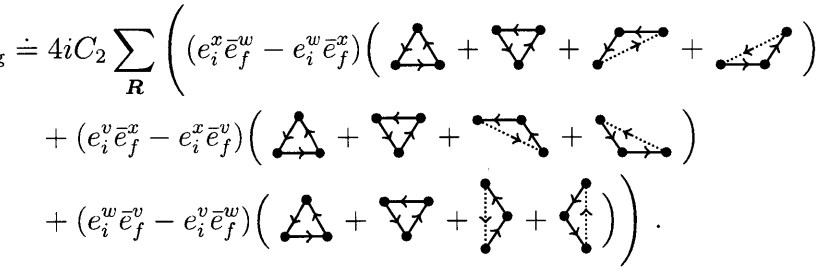

Or, converting back to the Cartesian coordinates:

$$T_{2,\mathrm{kag}} \doteq 2\sqrt{3}iC_2 (e_i^y \bar{e}_f^x - e_i^x \bar{e}_f^y) \sum_{\boldsymbol{R}} \Big(3 \quad + 3 \quad$$
$$+ \quad + \quad + \quad + \quad + \quad \Big) \,, \tag{2.32}$$

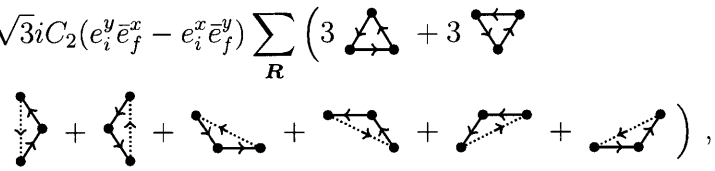

which is what being quoted in Eq. (2.14).

In summary, it is found that, with only nearest-neighbor hopping, the A_{2g} channel Raman T-matrix does not vanish in the honeycomb lattice or the kagome lattice at the $t^4/(U-\omega_i)^3$ order, but does so to this order in the square lattice and the triangular lattice.

2.1.2 Derivation of $O_{A_{1g}}$ and O_{E_g} to the $t^4/(\omega_i - U)^3$ order.

In this subsection I shall derive $O_{A_{1g}}$ and O_{E_g} to the $t^4/(\omega_i - U)^3$ order for the kagome lattice. As already noted in Sec. 2.1, at the $t^2/(\omega_i - U)$ order the Shastry–Shraiman formulation reproduces the Fleury–London Hamiltonian. In the A_{1g} channel this gives rise to an operator proportional to the Heisenberg Hamiltonian, and in the E_g channel it gives rise to the operators $O_{E_g^{(1)}}$ and $O_{E_g^{(2)}}$ as shown in Eqs. 2.11–2.12.

At the $t^3/(\omega_i - U)^2$ order, it can be checked that the two types of pathways depicted in Fig. 2-2 cancel each other not only in the A_{2g} channel but also in the E_g and A_{1g} channels. Thus, it remains to consider pathways having two internal hops, which contributes at the $t^4/(\omega_i - U)^3$ order.

By considering pathways and their "reserved" counterparts, in which all electron

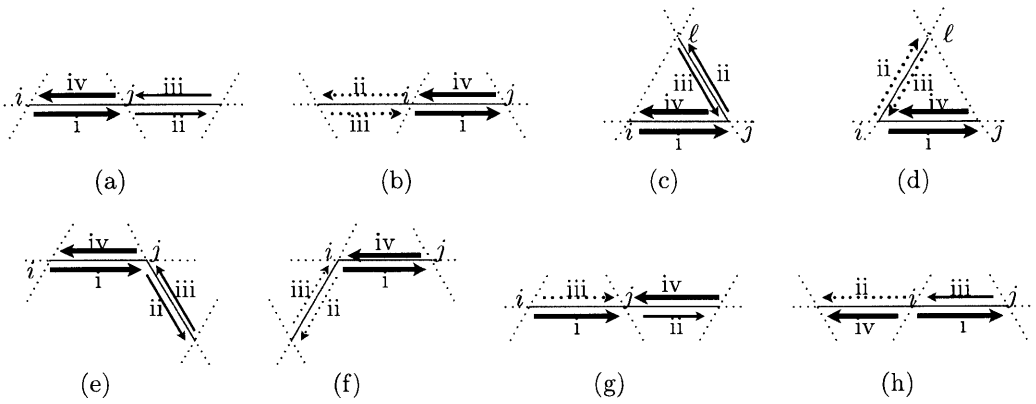

Figure 2-8: Pathways with two internal hops in a kagome lattice, with the initial holon fixed at site i and initial doublon fixed at site j.

operators are conjugated and their order inverted, it is shown in subsection 2.1.1 that only spin-chirality operators contribute to the A_{2g} channel. From the same construction, it can be seen that the spin-chirality operators *do not* contribute to the E_g and A_{1g} channels. Moreover, we are interested in the inelastic, and hence non-constant, part of the Raman transition operators. Therefore, to determine the $t^4/(\omega_i - U)^3$ order terms in O_{E_g} and $O_{A_{2g}}$, it suffices to extract the spin dot product terms for each process.

Fixing the initial holon at site i and the initial doublon at site j, there are eight more two-internal-hop pathways that contribute to the A_{1g} and E_g channels in addition to the four depicted in Fig. 2-7. These are listed in Fig. 2-8.

Applying the procedures as explained in Sec. 2.1, the spin dot products resulting from Figs. 2-7(a), 2-7(b), 2-8(c), and 2-8(d) are, respectively:

$$\begin{aligned} T_{\text{kag},a} &= C_2 e_i^x (-\bar{e}_f^v) \Big(\operatorname{tr}\{(-1)\chi_\ell \chi_j \tilde{\chi}_i\} + \operatorname{tr}\{\chi_\ell\} \operatorname{tr}\{\chi_j \tilde{\chi}_i\} \Big) \\ &\doteq C_2 e_i^x (-\bar{e}_f^v) (\boldsymbol{S}_\ell \cdot \boldsymbol{S}_i - \boldsymbol{S}_i \cdot \boldsymbol{S}_j - \boldsymbol{S}_j \cdot \boldsymbol{S}_\ell) \ , \end{aligned} \tag{2.33}$$

$$\begin{aligned} T_{\text{kag},b} &= C_2 e_i^x (-\bar{e}_f^w) \Big(\operatorname{tr}\{(-1)\chi_\ell \chi_j \tilde{\chi}_i\} + \operatorname{tr}\{\chi_\ell\} \operatorname{tr}\{\chi_j \tilde{\chi}_i\} \Big) \\ &\doteq C_2 e_i^x (-\bar{e}_f^w) (\boldsymbol{S}_j \cdot \boldsymbol{S}_\ell - \boldsymbol{S}_i \cdot \boldsymbol{S}_j - \boldsymbol{S}_\ell \cdot \boldsymbol{S}_i) \ , \end{aligned} \tag{2.34}$$

$$T_{\mathrm{kag},c} = C_2 e_i^x(-\bar{e}_f^x)(c_i^\dagger c_j)(c_j^\dagger c_\ell)(c_\ell^\dagger c_j)(c_j^\dagger c_i) = C_2 e_i^x(-\bar{e}_f^x)\,\mathrm{tr}\{\tilde{\chi}_\ell\}\,\mathrm{tr}\{\chi_j\tilde{\chi}_i\}$$
$$\doteq\ -2C_2 e_i^x(-\bar{e}_f^x)\boldsymbol{S}_i\cdot\boldsymbol{S}_j\ , \tag{2.35}$$

$$T_{\mathrm{kag},d} = C_2 e_i^x(-\bar{e}_f^x)(c_i^\dagger c_j)(c_\ell^\dagger c_i)(c_i^\dagger c_\ell)(c_j^\dagger c_i) = C_2 e_i^x(-\bar{e}_f^x)\,\mathrm{tr}\{\chi_\ell\}\,\mathrm{tr}\{\chi_j\tilde{\chi}_i\}$$
$$\doteq\ -2C_2 e_i^x(-\bar{e}_f^x)\boldsymbol{S}_i\cdot\boldsymbol{S}_j\ , \tag{2.36}$$

where $\doteq$ denotes equality upon neglecting additive constants and spin-chirality terms. The contributions of other pathways in Figs. 2-7 and 2-8 can be obtained by relabeling sites and vectors that appear in Eqs. 2.33–2.36.

The sum over all pathways in Figs. 2-7 and 2-8 gives:

$$\begin{aligned}T_{\mathrm{kag},i,j} \doteq C_2\Big(&e_i^x\bar{e}_f^x\big(\boldsymbol{S}_i\cdot\boldsymbol{S}_{j-\boldsymbol{a}_1}+\boldsymbol{S}_j\cdot\boldsymbol{S}_{i+\boldsymbol{a}_1}+14\boldsymbol{S}_i\cdot\boldsymbol{S}_j-\boldsymbol{S}_i\cdot\boldsymbol{S}_{i+\boldsymbol{a}_1}-\boldsymbol{S}_j\cdot\boldsymbol{S}_{j-\boldsymbol{a}_1}\big)\\&+e_i^x\bar{e}_f^v\big(\boldsymbol{S}_i\cdot\boldsymbol{S}_{\ell+\boldsymbol{a}_1-\boldsymbol{a}_2}+\boldsymbol{S}_j\cdot\boldsymbol{S}_\ell-\boldsymbol{S}_i\cdot\boldsymbol{S}_\ell-\boldsymbol{S}_j\cdot\boldsymbol{S}_{\ell+\boldsymbol{a}_1-\boldsymbol{a}_2}\big)\\&+e_i^x\bar{e}_f^w\big(\boldsymbol{S}_j\cdot\boldsymbol{S}_{\ell-\boldsymbol{a}_2}+\boldsymbol{S}_i\cdot\boldsymbol{S}_\ell-\boldsymbol{S}_j\cdot\boldsymbol{S}_\ell-\boldsymbol{S}_i\cdot\boldsymbol{S}_{\ell-\boldsymbol{a}_2}\big)\Big)\ .\end{aligned} \tag{2.37}$$

The contributions when the initial holon and/or the initial doublon are located at other sites can be obtained by relabeling. The sum over the locations of the initial holon and the initial doublon yields:

$$\begin{aligned}T_{\mathrm{kag}} \doteq 2C_2\sum_{\{\boldsymbol{R}\}}\Big(&e_i^x\bar{e}_f^x\big(16\boldsymbol{S}_i\cdot\boldsymbol{S}_j+16\boldsymbol{S}_j\cdot\boldsymbol{S}_{i+\boldsymbol{a}_1}-2\boldsymbol{S}_i\cdot\boldsymbol{S}_{i+\boldsymbol{a}_1}-2\boldsymbol{S}_j\cdot\boldsymbol{S}_{j-\boldsymbol{a}_1}\big)\\&+e_i^v\bar{e}_f^v\big(16\boldsymbol{S}_j\cdot\boldsymbol{S}_\ell+16\boldsymbol{S}_\ell\cdot\boldsymbol{S}_{j+\boldsymbol{a}_2-\boldsymbol{a}_1}-2\boldsymbol{S}_j\cdot\boldsymbol{S}_{j+\boldsymbol{a}_2-\boldsymbol{a}_1}-2\boldsymbol{S}_\ell\cdot\boldsymbol{S}_{\ell+\boldsymbol{a}_2-\boldsymbol{a}_1}\big)\\&+e_i^w\bar{e}_f^w\big(16\boldsymbol{S}_i\cdot\boldsymbol{S}_\ell+16\boldsymbol{S}_\ell\cdot\boldsymbol{S}_{i+\boldsymbol{a}_2}-2\boldsymbol{S}_i\cdot\boldsymbol{S}_{i+\boldsymbol{a}_2}-2\boldsymbol{S}_\ell\cdot\boldsymbol{S}_{\ell+\boldsymbol{a}_2}\big)\\&+(e_i^x\bar{e}_f^w+e_i^w\bar{e}_f^x)\big(\boldsymbol{S}_j\cdot\boldsymbol{S}_{\ell-\boldsymbol{a}_2}+\boldsymbol{S}_\ell\cdot\boldsymbol{S}_{j-\boldsymbol{a}_1}-\boldsymbol{S}_j\cdot\boldsymbol{S}_\ell-\boldsymbol{S}_{\ell-\boldsymbol{a}_2}\cdot\boldsymbol{S}_{j-\boldsymbol{a}_1}\big)\\&+(e_i^x\bar{e}_f^v+e_i^v\bar{e}_f^x)\big(\boldsymbol{S}_i\cdot\boldsymbol{S}_{\ell+\boldsymbol{a}_1-\boldsymbol{a}_2}+\boldsymbol{S}_\ell\cdot\boldsymbol{S}_{j+\boldsymbol{a}_1}-\boldsymbol{S}_i\cdot\boldsymbol{S}_\ell-\boldsymbol{S}_{\ell+\boldsymbol{a}_1-\boldsymbol{a}_2}\cdot\boldsymbol{S}_{j+\boldsymbol{a}_1}\big)\\&+(e_i^v\bar{e}_f^w+e_i^w\bar{e}_f^v)\big(\boldsymbol{S}_i\cdot\boldsymbol{S}_{j+\boldsymbol{a}_2-\boldsymbol{a}_1}+\boldsymbol{S}_j\cdot\boldsymbol{S}_{i+\boldsymbol{a}_2}-\boldsymbol{S}_i\cdot\boldsymbol{S}_j-\boldsymbol{S}_{j+\boldsymbol{a}_2-\boldsymbol{a}_1}\cdot\boldsymbol{S}_{i+\boldsymbol{a}_2}\big)\Big)\ .\end{aligned} \tag{2.38}$$

Projecting onto the A_{1g} channel and neglecting a piece proportional to the Heisenberg Hamiltonian yields Eq. (2.13), while projecting into the E_g channels yields the

following contributions to $O_{E_g^{(1)}}$ and $O_{E_g^{(2)}}$ at the $t^4/(\omega_i - U)^3$ order, respectively:

$$\begin{aligned}\delta O_{E_g^{(1)}} = C_2\Big((&-\boldsymbol{S}_j \cdot \boldsymbol{S}_{\ell-\boldsymbol{a}_2} - \boldsymbol{S}_\ell \cdot \boldsymbol{S}_{j-\boldsymbol{a}_1} - \boldsymbol{S}_i \cdot \boldsymbol{S}_{\ell+\boldsymbol{a}_1-\boldsymbol{a}_2} - \boldsymbol{S}_\ell \cdot \boldsymbol{S}_{j+\boldsymbol{a}_1} \\ &2\boldsymbol{S}_i \cdot \boldsymbol{S}_{j+\boldsymbol{a}_2-\boldsymbol{a}_1} + 2\boldsymbol{S}_j \cdot \boldsymbol{S}_{i+\boldsymbol{a}_2}) - (2\boldsymbol{S}_i \cdot \boldsymbol{S}_{i+\boldsymbol{a}_1} + 2\boldsymbol{S}_j \cdot \boldsymbol{S}_{j-\boldsymbol{a}_1} \\ &- \boldsymbol{S}_i \cdot \boldsymbol{S}_{i+\boldsymbol{a}_2} - \boldsymbol{S}_\ell \cdot \boldsymbol{S}_{\ell+\boldsymbol{a}_2} - \boldsymbol{S}_j \cdot \boldsymbol{S}_{j+\boldsymbol{a}_2-\boldsymbol{a}_1} - \boldsymbol{S}_\ell \cdot \boldsymbol{S}_{\ell+\boldsymbol{a}_2-\boldsymbol{a}_1}) \\ &+ 7(2\boldsymbol{S}_i \cdot \boldsymbol{S}_j + 2\boldsymbol{S}_j \cdot \boldsymbol{S}_{i+\boldsymbol{a}_1} - \boldsymbol{S}_i \cdot \boldsymbol{S}_\ell - \boldsymbol{S}_\ell \cdot \boldsymbol{S}_{i+\boldsymbol{a}_2} - \boldsymbol{S}_j \cdot \boldsymbol{S}_\ell - \boldsymbol{S}_\ell \cdot \boldsymbol{S}_{j+\boldsymbol{a}_2-\boldsymbol{a}_1})\Big)\,,\end{aligned} \tag{2.39}$$

$$\begin{aligned}\delta O_{E_g^{(2)}} = \sqrt{3}C_2\Big((&\boldsymbol{S}_j \cdot \boldsymbol{S}_{\ell-\boldsymbol{a}_2} + \boldsymbol{S}_\ell \cdot \boldsymbol{S}_{j-\boldsymbol{a}_1} - \boldsymbol{S}_i \cdot \boldsymbol{S}_{\ell+\boldsymbol{a}_1-\boldsymbol{a}_2} - \boldsymbol{S}_\ell \cdot \boldsymbol{S}_{j+\boldsymbol{a}_1}) \\ &- (\boldsymbol{S}_i \cdot \boldsymbol{S}_{i+\boldsymbol{a}_2} + \boldsymbol{S}_\ell \cdot \boldsymbol{S}_{\ell+\boldsymbol{a}_2} - \boldsymbol{S}_j \cdot \boldsymbol{S}_{j+\boldsymbol{a}_2-\boldsymbol{a}_1} - \boldsymbol{S}_\ell \cdot \boldsymbol{S}_{\ell+\boldsymbol{a}_2-\boldsymbol{a}_1}) \\ &+ 7(\boldsymbol{S}_i \cdot \boldsymbol{S}_\ell + \boldsymbol{S}_\ell \cdot \boldsymbol{S}_{i+\boldsymbol{a}_2} - \boldsymbol{S}_j \cdot \boldsymbol{S}_\ell - \boldsymbol{S}_\ell \cdot \boldsymbol{S}_{j+\boldsymbol{a}_2-\boldsymbol{a}_1})\Big)\,.\end{aligned} \tag{2.40}$$

2.2 Results for the $U(1)$ DSL state

Under the $U(1)$ DSL ansatz, we may take $|i\rangle = |i^{(\mathrm{Hb})}\rangle \otimes |\boldsymbol{k}_i, \boldsymbol{e}_i\rangle$ and $|f\rangle = |f^{(\mathrm{Hb})}\rangle \otimes |\boldsymbol{k}_f, \boldsymbol{e}_f\rangle$ in the transition rate Eq. (2.4), where $|i^{(\mathrm{Hb})}\rangle$ and $|f^{(\mathrm{Hb})}\rangle$ are states obtained from filling the spinon bands. In particular, at zero temperature (which will be assumed henceforth), $|i^{(\mathrm{Hb})}\rangle$ is simply a state with spinons filled up to the Dirac nodes at the top of $E_{+,-}$, and $|f^{(\mathrm{Hb})}\rangle$ are states with a few spinon-antispinon pairs excited from $|i^{(\mathrm{Hb})}\rangle$.

Moreover, the spin operators that appear in Eqs. 2.11–2.14 can be converted to spinon operators using Eqs. (1.6)–(1.8), which allows the matrix elements between $|i^{(\mathrm{Hb})}\rangle$ and $|f^{(\mathrm{Hb})}\rangle$ to be calculated at mean field using Wick's theorem.

At zero temperature, to obtain the overall Raman intensity I_α for channel α at a given Raman shift $\Delta\omega = \omega_i - \omega_f$, all final states that satisfies the energy constraint $\mathcal{E}_f^{(\mathrm{Hb})} - \mathcal{E}_i^{(\mathrm{Hb})} = \Delta\omega$ must be summed over. Strictly enforcing this constraint is difficult in a numerical computation. Instead, the final states are sampled $|f^{(\mathrm{Hb})}\rangle$ without imposing the energy constraint, but sort them into bins of energy. The overall intensity is then obtained by summing all states whose energy fall within the same bin. The summation is performed numerically using a simple Monte Carlo

sampling of the momenta and band indices of the spinon and antispinon excitations in $|f^{(\mathrm{Hb})}\rangle$.

Some calculations are also performed in a slightly different way, by first converting the summed squared amplitude into a correlation function:

$$\begin{aligned} I_\alpha(\Delta\omega) &= \sum_f \left|\langle f^{(\mathrm{Hb})}|O_\alpha|i^{(\mathrm{Hb})}\rangle\right|^2 \delta(\mathcal{E}_f^{(\mathrm{Hb})} - \mathcal{E}_i^{(\mathrm{Hb})} - \Delta\omega) \\ &= \int dt\, e^{i\Delta\omega t}\langle i^{(\mathrm{Hb})}|O_\alpha(t)O_\alpha(0)|i^{(\mathrm{Hb})}\rangle \ . \end{aligned} \tag{2.41}$$

To calculate this correlation function, the spinon operators that appears in O_α (c.f. Eqs. 2.11–2.14) are converted from real space to momentum space, which introduces sums over momenta and band indices. Such sums are again computed by simple Monte Carlo samplings in the manner explained above.

To simplify notations, in the following I shall abuse notation and write $|i\rangle$ in place of $|i^{(\mathrm{Hb})}\rangle$ and similarly write $|f\rangle$ for $|f^{(\mathrm{Hb})}\rangle$ whenever the context is clear.

2.2.1 E_g channel

First consider the Raman intensity in the E_g channel, $I_{E_g} \equiv I_{E_g^{(1)}} + I_{E_g^{(2)}}$. By computing the correlation function Eq. (2.41) (with $\alpha = E_g^{(1)}$ and $E_g^{(2)}$), we obtain the Raman intensity profile as shown in Fig. 2-9.

From Fig. 2-9, it can be seen that the Raman response take the form of a broad continuum ranging from approximately $1.5\chi J$ to approximately $11\chi J$, with occasional sharp spikes. The existence of a continuum is not a surprise, since the operators $O_{E_g^{(1)}}$ and $O_{E_g^{(2)}}$ in Eqs. 2.11–2.12 corresponds to two-spinon-two-antispinon operators in the $U(1)$ DSL ansatz, and hence the final states $|f\rangle$ are spinon-antispinon pairs and thus there is a continuum of phase space for excitations. The cutoff near $11\chi J$ is also natural, since the total band-width in the $U(1)$ DSL ansatz is approximately 6 χJ, and hence with two spinons and two antispinons the excitation energy is at most 12 χJ. The sharp peaks and the low-energy suppression, however, require further investigations.

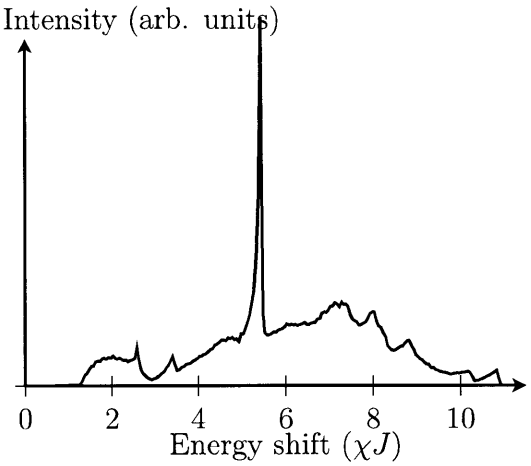

Figure 2-9: Raman intensity in the E_g channel, computed using the correlation Eq. (2.41), with a bin size of $0.05\chi J$ in energy.

To gain more insight into how the various features in Fig. 2-9 comes about, it is useful to consider the sum over final states explicitly. Given the form of $O_{E_g^{(1)}}$ and $O_{E_g^{(2)}}$ in Eqs. 2.11–2.12, there are two types of final states: the first consists of two spinon-antispinon pairs excited from the ground state $|i\rangle$ while the second consists of *one* spinon-antispinon pair excited from $|i\rangle$. Schematically, these take the form:

$$|f_{\text{2pairs}}\rangle = f^\dagger_{k_1,n_1,\sigma} f_{k_2,n_2,\sigma} f^\dagger_{k_3,n_3,\sigma'} f_{k_4,n_4,\sigma'} |i\rangle \ , \tag{2.42}$$

$$|f_{\text{1pair}}\rangle = f^\dagger_{k_1,n_1,\sigma} f_{k_2,n_2,\sigma} |i\rangle \ . \tag{2.43}$$

In both cases the momentum conservation $\sum_{i \text{ odd}} \boldsymbol{k}_i = \sum_{i \text{ even}} \boldsymbol{k}_i$ holds, and that the band index n_i denotes one of the top three (empty) bands when i is odd and one of the bottom three (occupied) bands when i is even.

For the one-pair final state to have a non-zero matrix element with the initial state, a pair of spinon-antispinon operator must self-contract within $O_{E_g^{(1)}}$ and $O_{E_g^{(2)}}$, e.g.,

$$\begin{aligned} f^\dagger_{i\sigma} f_{j\sigma} f^\dagger_{j\sigma'} f_{i\sigma'} &\mapsto \langle f^\dagger_{i\sigma} f_{j\sigma} \rangle f^\dagger_{j\sigma'} f_{i\sigma'} + f^\dagger_{i\sigma} f_{j\sigma} \langle f^\dagger_{j\sigma'} f_{i\sigma'} \rangle - \langle f^\dagger_{i\sigma} f_{i\sigma'} \rangle f^\dagger_{j\sigma'} f_{j\sigma} - \langle f^\dagger_{j\sigma'} f_{j\sigma} \rangle f^\dagger_{i\sigma} f_{i\sigma'} \\ &= \chi_{ij} f^\dagger_{j\sigma} f_{i\sigma} + \chi_{ji} f^\dagger_{i\sigma} f_{j\sigma} - \frac{1}{2}(f^\dagger_{i\sigma} f_{i\sigma} + f^\dagger_{j\sigma} f_{j\sigma}) \ , \end{aligned} \tag{2.44}$$

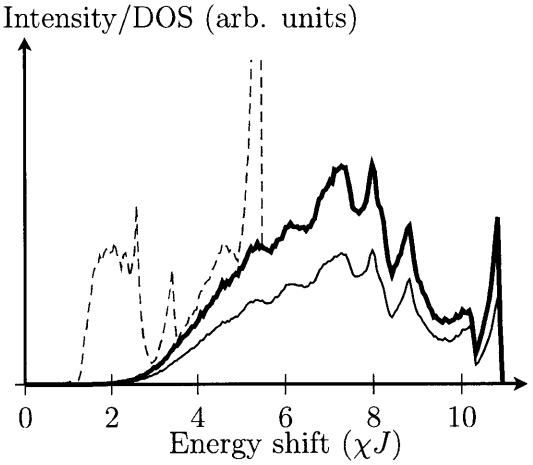

Figure 2-10: Plots of density of states (thin red curve) and E_g Raman intensity (thick blue curve) contributed by final states having two spinon-antispinon pairs, together with the overall E_g Raman intensity (broken gray curve), all computed with a bin size of $0.05\chi J$ in energy. Note that the relative scale between the intensity plots and the DOS plot is arbitrary and is set here such that both curves are visible.

where the spin indices σ, σ' are summed in the above. The mean-field parameter χ_{ij} here is the same as the one introduced in Sec. 1.2.

However, one should be mindful that while the constraint $\sum_\sigma f_{j\sigma}^\dagger f_{j\sigma} = 1$ is strictly enforced in the exact spin-liquid state, it is enforced only on average in the mean-field representation. Therefore, *while operators of the form $f_{j\sigma}^\dagger f_{j\sigma}$ should induce no transition between $|i\rangle$ and $|f\rangle$, the matrix element $\langle f|f_{j\sigma}^\dagger f_{j\sigma}|i\rangle$ may be non-zero at mean-field.* To avoid such problem, the $f_{j\sigma}^\dagger f_{j\sigma}$ terms in Eq. (2.44) are thrown away by hand.

With this precaution, I_{E_g} is recalculated by numerically sampling the final states, and is done so for the one-pair and two-pair contributions separately. The results are shown on Figs. 2-10 and 2-11. It has been verified that the sum of Raman intensities from the two figures (with the relative ratio determined by the details of the numerical calculations) produces an overall intensity profile that matches Fig. 2-9.

The density of states (DOS) for two-pair and one-pair excitations having zero total momenta have been plotted alongside with the respective Raman intensities in Figs. 2-10 and 2-11. From the figures, it can be seen that the DOS matches the Raman

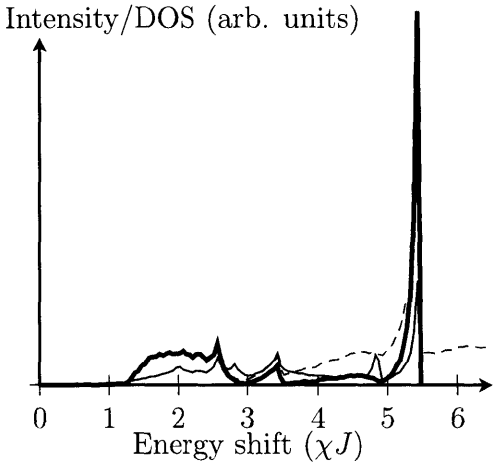

Figure 2-11: Plots of density of states (thin red curve) and E_g Raman intensity (thick blue curve) contributed by final states having one spinon-antispinon pair, together with the overall E_g Raman intensity (broken gray curve), all computed with a bin size of $0.05\chi J$ in energy. Note that the relative scale between the intensity plots and the DOS plot is arbitrary.

intensity profile very well for two-pair excitations, and less so (but still reasonably well) for one-pair excitations. This can be understood by rewriting the first line of Eq. (2.41) as $I_\alpha(\Delta\omega) = \overline{\left|\langle f|O_\alpha|i\rangle\right|^2}\mathcal{D}(\Delta\omega)$, in which $\mathcal{D}(\mathcal{E})$ denotes the density of state at energy $\mathcal{E}$ and $\overline{\left|\langle f|O_\alpha|i\rangle\right|^2}$ denotes the average matrix element squared at the same energy. From this, the DOS is expected to match the Raman intensity well as long as the average matrix element does not change drastically with energy—an assumption more valid for two-pair states as opposed to one-pair ones, because of the larger phase space available in the former case.

Moreover, the sharp peak appearing near $5.5\chi J$ in Fig. 2-9 can now be attributed to one-pair excitations, which can in turn be attributed to a peak in the one-pair DOS. From the band structure (Fig. 1-7), it can be checked that $\Delta\omega = 5.41\chi J$ *corresponds to the energy difference between the top flat band and the saddle point* $\boldsymbol{k} = \mathbf{0}$ *at the bottom band.* The enhanced phase space near this energy is thus the likely cause of this peak-like feature.

Next I shall consider the low-energy ($\Delta\omega < 2\chi J$) part the of Raman intensity more carefully, checking if the intensity profile is an exponential or a power law, and

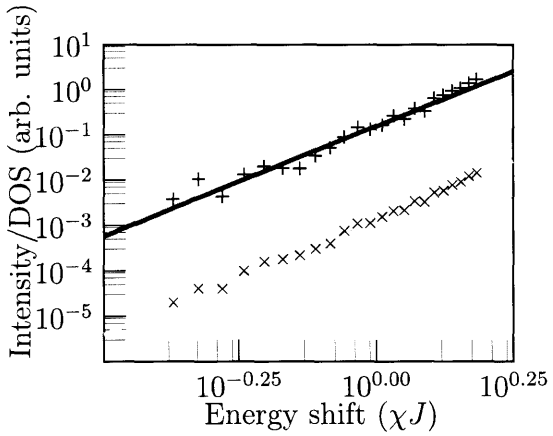

Figure 2-12: Log-log plot of the DOS (red × symbols) and Raman intensity in the E_g channel (blue + symbols) for two-pair excitations. Simple linear fits (straight lines in pink and cyan) give a slope of 5.1 for the DOS data and 4.9 for the Raman intensity data.

determining the exponent if the latter case holds. To enhance the quality of the data, and since only the low-energy behavior concerns us, the final states are resampled by restricting the antispinon to the highest occupied band $E_{+,-}$ and the spinon to the lowest unoccupied band $E_{+,+}$ (despite this, the two-pair data is consistently non-zero only above $\Delta\omega = 0.4\chi J$). The resulting data are shown in the log-log plots in Figs. 2-12 and 2-13. Since the smaller exponent dominates as $\Delta\omega \to 0$, the *overall Raman intensity in the E_g channel scales roughly as $I_{E_g} \propto (\Delta\omega)^3$ at low energy.*

From the plots, it is clear that the DOS and the Raman intensity both follow a power law, with a higher exponent for the two-pair excitations as compared to the one-pair ones. *Analytically, it is easy to check that $\mathcal{D}_{1\text{pair}} \propto \Delta\omega$ for the Dirac Hamiltonian Eq. (1.24)*, since the integral involves four components of momenta subjected to three constraints (energy and momentum conservation), and that $|\boldsymbol{q}|$ scales as energy. *Similarly, it is easy to check that $\mathcal{D}_{2\text{pair}} \propto (\Delta\omega)^5$ in the Dirac Hamiltonian.* Furthermore, since the eigenstates of the Dirac Hamiltonian depend only on $\theta = \tan^{-1}(q_y/q_x)$ but not on $|\boldsymbol{q}|$, *the average matrix element squared $\overline{|\langle f|O_\alpha|i\rangle|^2}$ must be constant in energy.* However, to the $t^2/(\omega_i - U)$ order in the E_g channel (Eqs. 2.11–2.12), the matrix element turns out to be exactly zero for all one-pair excitations in the Dirac Hamiltonian. Hence, at low energy, we expect $I_{2\text{pair}} \propto \mathcal{D}_{2\text{pair}} \propto (\Delta\omega)^5$ and

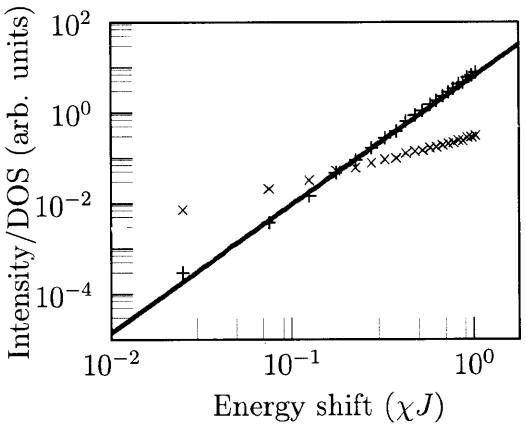

Figure 2-13: Log-log plot of the DOS (red × symbols) and Raman intensity in the E_g channel (blue + symbols) for one-pair excitations. Simple linear fits (straight lines in pink and cyan) give a slope of 1.0 for the DOS data and 2.8 for the Raman intensity data.

$I_{1\text{pair}} \propto (\Delta\omega)^\alpha$ with $\alpha > 1$, consistent with the numerical results in Figs. 2-12 and 2-13.

Since $\mathcal{D}_{1\text{pair}} \propto \Delta\omega$, it leaves open the possibility that $I_{E_g} \propto \Delta\omega$ at higher order in $t/(\omega_i - U)$. While this possibility cannot be ruled out in the present work, it is found that *the vanishing of matrix elements in the Dirac Hamiltonian for all one-pair excitations persist to the* $t^4/(\omega_i - U)^3$ *order.*[2] Hence, even if $I_{E_g} \propto \Delta\omega$ at some higher order, its effect will not be prominent unless the system is sufficiently near resonance.

In the data presented above the contributions arising from $O_{E_g^{(1)}}$ and $O_{E_g^{(2)}}$ have been summed. By computing the two contributions separately, it can be checked that each contribute equally. In fact, it has been checked that *the intensity profiles are essentially identical upon an arbitrary rotation in the kagome plane for the one-pair and two-pair excitations separately.* In other words, the quantity $I_{E_g}(\Delta\omega, \theta)$, defined

[2]To perform the analytic calculations, the expectation $\langle f_i^\dagger f_j \rangle$ for next- and next-next-nearest neighbors are needed. From the $U(1)$ DSL ansatz these must be real, equal in magnitude, but vary in signs. As a shortcut, the signs are determined from numerical calculations. It turns out that the cancellation holds separately for next-nearest neighbor terms and next-next-nearest ones. Thus the determination of signs is adequate for reaching the present conclusion.

by:

$$I_{E_g}(\Delta\omega,\theta) = \sum_f |\langle f|O_{E_g^{(1)}}\cos\theta + O_{E_g^{(2)}}\sin\theta|i\rangle|^2 \times \delta(\mathcal{E}_f^{(\mathrm{Hb})} - \mathcal{E}_i^{(\mathrm{Hb})} - \Delta\omega) \ , \quad (2.45)$$

is found to be independent of θ, and remain so even if the sum is restricted to one-pair or two-pair states. Our numerical results are thus consistent with the analytical arguments given by Cepas *et. al.*[78]

2.2.2 A_{1g} channel

Using $O_{A_{1g}}$ in Eg. 2.13 in place of $O_{E_g^{(1)}}$ and $O_{E_g^{(2)}}$, the calculation of the Raman intensity profile can be repeated for the A_{1g} channel. The results are shown in Fig. 2-14. From the figure, we see that the Raman intensity profile of the A_{1g} channel also has a broad continuum up to a cutoff near $11\chi J$. However, the sharp peak near $5.5\chi J$ that appears in the E_g channel is markedly missing.

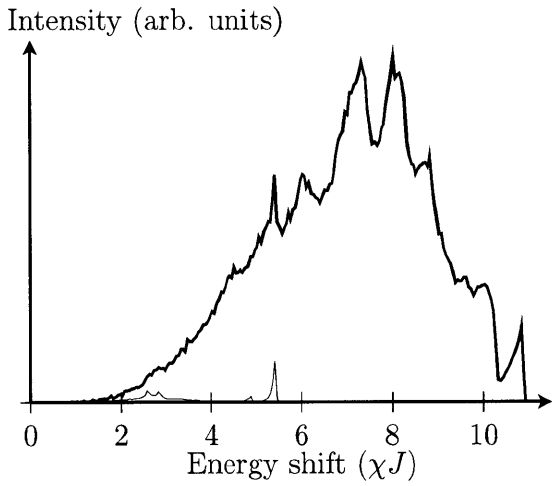

Figure 2-14: Plots of the overall Raman intensity (thick and blue) and its contribution by one-pair states (thin and red) in the A_{1g} channel, both with the same vertical scale and computed with a bin size of $0.05\chi J$ in energy.

Decomposing the Raman intensity into one-pair and two-pair contributions as in Sec. 2.2.1, it can be seen that *the overall Raman intensity profile in the A_{1g} channel is dominated by the two-pair states.* Since the sharp peak near $5.5\chi J$ is originated

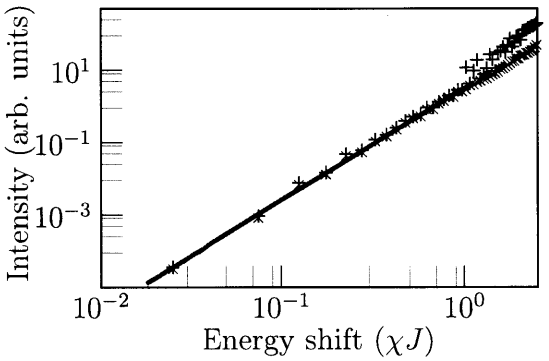

Figure 2-15: Log-log plot of the Raman intensity (blue + symbols) and its contribution by one-pair states (red × symbols) in the A_{1g} channel. Simple linear fit (straight line in cyan) for the one-pair data up to $\Delta\omega = \chi J$ gives a slope of 3.1.

from the one-pair contribution, this explains the absence of sharp peak in the A_{1g} channel.

However, at low energy ($\Delta\omega \lesssim 1.5\chi J$) the Raman intensity profile is still dominated by the one-pair contribution. And by plotting the Raman intensity profile in a log-log scale (Fig. 2-15), we see that the low-energy behavior is characterized by a power law with exponent $\alpha \approx 3$, similar to the value obtained in the E_g channel. Again, it can be checked on analytical ground[2] that the matrix element vanishes for all one-pair state in the Dirac Hamiltonian, consistent with the numerical results.

2.2.3 A_{2g} channel

For the A_{2g} channel, to the leading order in $t/(\omega_i - U)$, the Raman process receives contributions from excited states having one, two, and three pairs of spinon-antispinon. The overall Raman intensity coming from these spinon-antispinon pairs are plotted in Fig. 2-16. It can be seen that the continuum also appears in this channel, now ranging from $0\chi J$ up to approximately $16\chi J$, which corresponds to approximately three times the total spinon bandwidth. Moreover, sharp peaks not unlike the one in the E_g channel are observed at various energies. Again, it can be checked that these sharp peaks can be attributed to the various features of the $U(1)$ DSL bands, particularly to the flat-band-to-saddle and saddle-to-saddle transitions.

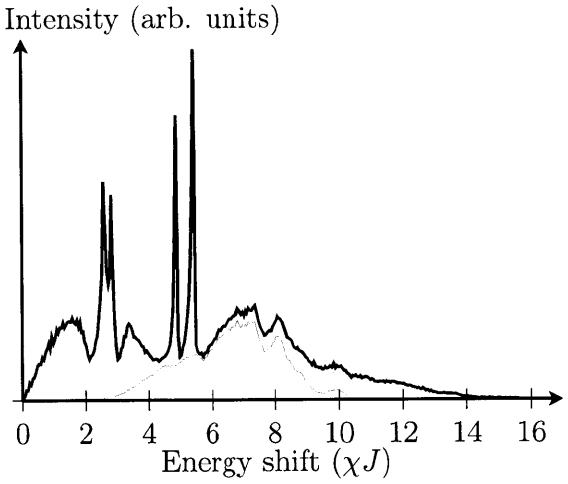

Figure 2-16: Raman intensity in the A_{2g} channel arising from spinon-antispinon pairs (thick and blue), and its contribution from two-pair (thin and red) and three-pair (thin and green) states. All computed with a bin size of $0.05\chi J$ in energy.

Note that *the low-energy Raman transition is much more prominent in the A_{2g} channel* than that in the E_g and A_{1g} channels. In particular, the Raman intensity in this channel has a broad peak near $\Delta\omega = 1.5\chi J$, below which it is visibly linear. From Fig. 2-16, the prominence of low-energy Raman transition trace back to the relatively large average matrix elements in the one-pair transitions. Moreover, the linear behavior suggests that $\overline{|\langle f|O_a|i\rangle|^2}$ no longer vanishes in the Dirac Hamiltonian, so that $I_{1\text{pair}} \propto \mathcal{D}_{1\text{pair}} \propto \Delta\omega$ at low energy.

The forgoing discussion neglected an important contribution to the A_{2g} Raman intensity. Recall that in computing the one-pair contribution, a mean-field factorization is performed (Eq. (2.44)), in which the Hubbard-Stratonovich variable χ_{ij} is treated as a constant. However, because of the emergent gauge structure in the U(1) spin-liquid theory, the dynamics of the phase of χ_{ij} cannot really be neglected. Fortunately, since the projection of the T-matrix onto the E_g and A_{1g} channel Eqs. 2.11–2.13 involves no non-trivial closed path, the results presented above should still be *qualitatively* correctly, even though quantitative corrections to the detailed predictions (such as the exponents of the power laws at low-energy) may be present.

The situation for the A_{2g} channel is different, as can be seen by considering the

full contraction of the spin-chirality term $\boldsymbol{S}_1 \cdot (\boldsymbol{S}_2 \times \boldsymbol{S}_3)$ into χ_{ij}:

$$\begin{aligned} i\boldsymbol{S}_1 \cdot (\boldsymbol{S}_2 \times \boldsymbol{S}_3) &= \frac{1}{4}\Big((f_1^\dagger f_3)(f_3^\dagger f_2)(f_2^\dagger f_1) - \text{h.c.}\Big) \\ &\mapsto \frac{1}{4}\Big(\chi_{13}^{(0)}\, e^{i\alpha_{13}} \chi_{32}^{(0)}\, e^{i\alpha_{32}} \chi_{21}^{(0)}\, e^{i\alpha_{21}} - \text{h.c.}\Big) + \dots \\ &= (C\, e^{i(\alpha_{13}+\alpha_{32}+\alpha_{21})} - \text{h.c.}) + \dots\,, \end{aligned} \tag{2.46}$$

where $\chi_{ij}^{(0)}$ denotes the part of χ_{ij} that can be treated as constant, and $C = \chi_{13}^{(0)}\chi_{32}^{(0)}\chi_{21}^{(0)}/4$. For convenience I shall denote $(C\, e^{i(\alpha_{ik}+\alpha_{kj}+\alpha_{ji})} - \text{h.c.})$ as Q_{ijk} henceforth.

Note that $e^{i(\alpha_{13}+\alpha_{32}+\alpha_{21})}$ is the emergent gauge flux enclosed by the loop $1 \to 3 \to 2 \to 1$. *Since the emergent gauge field is fluctuating, this gauge flux can lead to an excitation of the kagome system.* Physically, the excitations generated by Q can be thought of as a *collective* excitation in the system, which exists on top of the individual spinon-antispinon excitations. This is analogous to the situation in an ordinary Fermi liquid, where plasmon mode exists on top of the electron-hole continuum.

Since the fluctuation of α_{ij} can be considered as a collective excitation in the system, as an approximation the final states $|f_{\text{gauge}}\rangle$ connected to the ground state by Q can be assumed to be lying in a separate sector than the spinon-antispinon pairs previously considered. Then, the total Raman intensity in the A_{2g} channel can be obtained by adding the contributions by these collective states to the contributions by the spinon-antispinon pair states.

The contribution to the Raman intensity by $|f_{\text{gauge}}\rangle$ can be computed from the QQ correlator. To do so, we start with Eq. (2.46), take the continuum limit, and Taylor expand the exponential. Then, $\alpha_{13} + \alpha_{32} + \alpha_{21} \mapsto \oint_{\wp_{132}} \boldsymbol{\alpha} \cdot d\boldsymbol{x} = \iint_{\Omega_{132}} \mathscr{b}\, d^2\boldsymbol{x}$, where $\mathscr{b} = \partial_x \alpha_y - \partial_y \alpha_x$ is the emergent "magnetic" field. Here $\wp_{132}$ denotes the closed loop $1 \to 3 \to 2 \to 1$ and Ω_{132} denotes the area enclosed by this path. Thus, $Q_{ijk} \approx 2i|C|\left(\sin(\phi_0) + \cos(\phi_0) \iint_{\Omega_{ijk}} \mathscr{b}\, d^2\boldsymbol{x}\right) \approx 2i|C|\big(\sin(\phi_0) + \cos(\phi_0)\Omega_{ijk}\, \mathscr{b}(\boldsymbol{r}_{ijk})\big)$, where $C = |C|e^{i\phi_0}$ and $\boldsymbol{r}_{ijk}$ denotes the position of the three-site loop. [3] The QQ

[3] Since the photon momentum is small, we can ignore distances at the lattice scale. Thus, the precise definition of $\boldsymbol{r}_{ijk}$ do not concern us.

correlator is thus converted into a $\mathscr{b}\mathscr{b}$ correlator. Hence:

$$I_{A_{2g}}^{(\text{gauge})} \approx C' \int dt\, e^{i\Delta\omega t} \langle i | \Big(\sum_{\boldsymbol{R}} \sum_{\triangle\text{'s}} \mathscr{b}(\boldsymbol{r}_{ijk}, t) e^{-i\boldsymbol{q}\cdot\boldsymbol{r}_{ijk}} \Big)^\dagger \Big(\sum_{\boldsymbol{R}} \sum_{\triangle\text{'s}} \mathscr{b}(\boldsymbol{r}_{ijk}, 0) e^{-i\boldsymbol{q}\cdot\boldsymbol{r}_{ijk}} \Big) | i \rangle \ , \tag{2.47}$$

where C' is a numerical constant, and will not be kept track of below. Note that the photon momentum has been restored, which introduce the factor $e^{-i\boldsymbol{q}\cdot\boldsymbol{r}_{ijk}}$, with $\boldsymbol{q} = \boldsymbol{k}_i - \boldsymbol{k}_f$ the momentum transferred to the lattice. The $\sum_{\triangle\text{'s}}$ is a shorthand for summing over the different three-site geometries on a unit cell with the appropriate coefficients, as is shown in Eq. (2.14).

Since $\mathscr{b} = \partial_x \alpha_y - \partial_y \alpha_x$, $\mathscr{b}(\boldsymbol{x}) = \sum_k (i\boldsymbol{k} \times \boldsymbol{\epsilon}_k) \alpha_{\boldsymbol{k}} e^{i\boldsymbol{k}\cdot\boldsymbol{x}} - (i\boldsymbol{k} \times \boldsymbol{\epsilon}_k^*) \alpha_{\boldsymbol{k}}^\dagger e^{-i\boldsymbol{k}\cdot\boldsymbol{x}}$, where $\boldsymbol{\epsilon}_k$ is the polarization of the emergent gauge field at momentum $\boldsymbol{k}$. Moreover, $\alpha_k |i\rangle = 0$ and $\langle i | \alpha_k^\dagger = 0$. Hence, upon Fourier transform,

$$I_{A_{2g}}^{(\text{gauge})} \propto \langle i | (i\boldsymbol{q} \cdot \boldsymbol{\epsilon}_q) \alpha_{\boldsymbol{q}}(\Delta\omega) \alpha_{\boldsymbol{q}}^\dagger(0) (-i\boldsymbol{q} \cdot \boldsymbol{\epsilon}_q^*) | i \rangle \ . \tag{2.48}$$

The correlator that we need to compute is thus one of a gauge field in 2+1 dimensions coupled to relativistic fermions (i.e., fermions described by the Dirac Hamiltonian Eq. (1.24)). This situation has been considered by Ioffe and Larkin[83] under the context of high-T_c superconductivity, who found that:

$$\Pi_{\alpha\beta}(\boldsymbol{q}, \omega_E) = \frac{1}{8} \frac{\omega_E^2 \delta_{\alpha\beta} + v_F^2 q^2 \delta_{\alpha\beta} - v_F^2 q_\alpha q_\beta}{(\omega_E^2 + v_F^2 q^2)^{1/2}} \ , \tag{2.49}$$

where $\Pi_{\alpha\beta}(\boldsymbol{q}, \omega_E)$ is the polarization function of the gauge field in Euclidean spacetime, and $v_F = \chi J a / \sqrt{2}\hbar$ is the Fermi velocity at the Dirac node. Hence,

$$\begin{aligned} I_{A_{2g}}^{(\text{gauge})} &\propto -q^2 \operatorname{Im} \left\{ \frac{8}{(v_F^2 q^2 - \Delta\omega^2 + i\eta)^{1/2}} \right\} + \cdots \\ &\propto \frac{q^2 \Theta(\Delta\omega - v_F q)}{(\Delta\omega^2 - v_F^2 q^2)^{1/2}} + \cdots \ . \end{aligned} \tag{2.50}$$

For herbertsmithite, v_F is estimated[74] to be 5.0×10^3 m/s. Hence, even at back scattering and with optical light at wavelength $\lambda \approx 500$ nm, $v_F q$ corresponds to a frequency shift of approximately 4.0 cm^{-1} only, which is too small to be resolved by

current instruments. Therefore, the collective excitation associated with the gauge flux will appear as *a characteristic* $1/\omega$ *singularity* in experiments.

Physically, if the gauge boson is non-dissipative, the Green's function would have a simple pole, corresponding to a sharp delta-function-like signal. That we have a $1/\omega$ singularity in place of a delta function tells us that the gauge photon mode is strongly dissipative and is in fact overdamped. Following the analogy with the ordinary plasmon mode as stated above, this dissipative behavior of the emergent gauge boson can be thought of as the analog of the Landau damping.

2.2.4 Discussions

In this chapter I have presented calculations of Raman intensity profile based on the Shastry–Shraiman formalism, assuming the validity of the U(1) Dirac spin-liquid state. The results show a broad continuum in the Raman intensity profile in all symmetry channels, each displays a power-law behavior at low energy. Moreover, the profiles are found to be invariant under arbitrary rotations in the kagome plane. For the E_g and the A_{2g} channels, the continuum is accompanied by occasional sharp peaks that can be attributed to the various features of the $U(1)$ DSL bands. In addition, the Raman intensity profile in the A_{2g} channel also contains a characteristic $1/\omega$ singularity, which arose in our model from an excitation of the emergent U(1) gauge field.

However, several caveats in our theoretical predictions should be noted. First, in order to compare with experimental data, χJ must be converted to physical units. In Ref. [74], Hermele *et. al.* estimated χ by fitting the spectrum of projected one-particle excitations to the mean-field band structure, and found that $\chi \approx 0.40$. Together with $J \approx 190K$, this gives $\chi J \approx 56$ cm^{-1}. However, there is considerable uncertainty in this estimation, and so it may be a good idea to take χ as a fitting parameter when comparisons with experiments are made.

Second, when the contribution to the Raman intensity profile by spinon-antispinon pairs are calculated, the excited spinons and antispinons have essentially been treated as free fermions. However, they should really be regarded as complicated composite

fermions, which interact with each other through an effective gauge field. Consequently, the actual excitation spectrum of the quasiparticles will almost certainly look *quantitatively* different from the ones presented here. Specifically, there may be finite lifetime effects, particularly prominent at high-energy, that causes the Raman intensity profile to be "washed out" compared with the ones presented here. Because of this, the sharp peaks that appear in Figs. 2-9 and 2-16 may not be present in the actual data. Furthermore, while the low-energy power-law structure of the Raman intensity profile is expected to survive, the detailed exponent is almost certainly modified from their mean-field values. Similarly, the contribution of Raman intensity in the A_{2g} channel by the emergent gauge boson may scale as $I_{A_{2g}}^{(\text{gauge})} \propto (\Delta\omega)^{\alpha}$, with α modified from -1.

Third, in the derivation of the operators that correspond to the Raman transitions in the different channels, Eqs. 2.11–2.14, we stopped at the zeroth order in t/U and the leading order in $t/(\omega_i - U)$. While terms higher order in t/U can be safely neglected, the same cannot be said for $t/(\omega_i - U)$, particularly near resonance ($\omega_i \approx U$). Therefore, these higher-order contributions, which modify the Raman intensity profile from those presented in the previous sections, may show up in actual data. In particular, the Raman intensity profile may not exhibit the abrupt drops as in Figs. 2-9 and 2-14. Furthermore, since $\mathcal{D}_{\text{1-pair}} \propto \Delta\omega$, a power-law with exponent much closer to 1 may be found in the E_g and A_{1g} channels at low energy.

Fourth, while it is argued that a $1/\omega$ singularity should be present in the A_{2g} channel, we have lost track of the ratio between its contribution and that by the spinon–antispinon pairs. Since the intensity of this singularity is proportional $|\boldsymbol{q}|^2$, it may be difficult to detect in optical Raman spectroscopy, in which the momentum transfer $\boldsymbol{q}$ is much smaller than the inverse of lattice constant.

In the beginning of this chapter I have mentioned the proposal by Cepas *et. al.* to distinguish between the spin-liquid state and the VBS state by the angular dependence of the Raman intensity profile. In light of the results presented in this chapter, there is another feature in the Raman spectrum that can be used to distinguish between the two states. For *in general, in a VBS state the spin excitations is gapped, while*

in a spin-liquid state it is gapless. Consequently, the Raman intensity profile should show an exponential dependence in the former case, and a power-law dependence in the latter case.

Recently, Wulferding *et. al.*[84] have obtained Raman intensity data for herbertsmithite. Their data, extending from 30 to 1500 cm^{-1}, shows a broad background that persists beyond 500 cm^{-1}, in addition to a quasielastic line and several sharp peaks at finite frequency shifts. Furthermore, at low temperature (5 K) the quasielastic line is suppressed and the low-energy portion of their data shows a linear dependence with respect to the Raman shift. While their data are quantitatively different from the results of our theoretical calculations presented in Secs. 2.2.1–2.2.3, the existence of a broad continuum can be seen as consistent with the U(1) Dirac spin-liquid model, even though the appearances of the other features would require the consideration of extra contributions (e.g., from the Zn impurities[57, 61]) that are not present in our model.

2.3 Extension to RIXS

In the previous section I have discussed the possibility of detecting the emergent gauge boson in Raman scattering. From Eq. (2.50), it can be seen that the resulting signal will be suppressed by a factor of q^2. Moreover, since the threshold for the signal, $v_F q$, is expected to be small, one has to look at the scaling behavior of the signal at low frequency shifts, which may not produce as clear a signature as a well-defined peak at finite frequency shifts. Given that RIXS can in principle probe excitations that are at finite momenta, one may wonder if RIXS offers a better opportunity for detecting this emergent gauge boson.

Because of the exponential decay of atomic orbital wavefunction, and because the electromagnetic fields of the photons may complete many cycles of oscillation across the distance between two atomic sites, in most RIXS experiments the transitions that accompany the absorption or emission of photons are dominated by virtual states in which the core hole and the extra valence electron are located on the same

site [85, 86, 87]. Compared to the inter-site transitions in the Raman case, the polarizations of the incident and scattered photons in such intra-site transitions are not coupled to the chirality of the hopping pathways. Consequently, the spin-chirality terms from hopping pathways that carry opposite chiralities will cancel out each other.

However, intra-site transitions can in principle be suppressed if the photon frequency is tuned to a forbidden atomic transition (e.g., an $1s$–$3d$ transition in Cu^{2+}). Moreover, the issues of reduced wavefunction overlap for inter-site transition and rapid electromagnetic field oscillation can be partially alleviated by tuning to transitions to and from core electrons of higher principal quantum numbers, and the issue of rapid electromagnetic field oscillation can be further alleviated by arranging the photon momenta to be at large angle relative to the direction of the site-to-site bond. Unless the inter-site transitions are forbidden by symmetry reason, such setup offers a possibility in which effects of spin-chirality terms can be observed in polarization filtered signals.

In the specific case of herbertsmithite, the half-filled 3d orbital in Cu^{2+} are oriented such that the electron lopes are pointing roughly at the direction of the oxygen, which is tilted away from the kagome plane by an angle of approximately 30° and is making an angle with the Cu–Cu bond by approximately 15° (see Fig. 2-17(a)). While the orientation of the half-filled 3d orbital may not be optimal in maximizing the matrix element of the transition, there is no general symmetry reason for it to vanish either. Moreover, from the available data in cuprates, the transition energy of the $1s$–$3d$ (pre K-edge), $2s$–$3d$ (pre L-edge), and $3s$–$3d$ (pre M-edge) in Cu^{2+} are of the order of 10 keV, 1 keV, and 100 eV respectively [85, 88, 89]. Compared with the Coulomb repulsion U of the top 3d orbital in Cu^{2+}, which is less than 10 eV, the enhancement to the Raman signature of the emergent gauge boson from the q^2 factor in these transitions can be substantial. Furthermore, since the nearest-neighbor Cu–Cu distance in herbertsmithite is approximately 3.5 Å [26], in both the $2s$–$3d$ (wavenumber $\sim$ 0.5 Å) and $3s$–$3d$ (wavenumber $\sim$ 0.05 Å) transitions the photon electromagnetic field will be relatively in-phase across the Cu–Cu bond even without arranging photon momenta to be at large angle relative to the kagome plane. Thus,

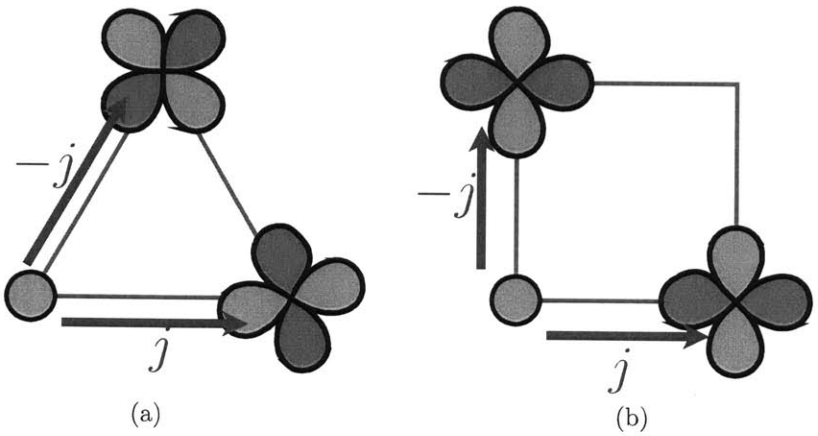

Figure 2-17: The orientation of the half-filled 3d orbitals of Cu^{2+} in (a) herbertsmithite and (b) cuprates. The Red and blue shading of the orbital indicates relative signs. For simplicity the tilt of the orbitals from the kagome plane in herbertsmithite is omitted.

even after the reduced matrix element in the photon-induced transitions are taken into account, the $2s$–$3d$ and $3s$–$3d$ may still be promising for detecting the emergent gauge boson of the $U(1)$ DSL state.

Focusing on RIXS processes that involves inter-site photon induced transitions, one can modify the Shastry–Shraiman formulation to obtain an effective T-matrix in terms of spin operators. The major changes are: First, the electron-photon coupling H_C now corresponds to photon-induced hopping in which a core hole and a valence 3d electron are created or annihilated. To describe such process, one of the valence electron operator in Eq. (2.2) should be replace by the respective operator for the core electron, and the constants t_{ij} in Eq. (2.2) must be replaced by the appropriate constant that take into account of the matrix element of the core-to-valence transition, whose magnitude I shall denote by j. Observe that from symmetry consideration the sign of j now depends whether the hop is clockwise or anticlockwise relative to the center of the triangle, as evident from Fig. 2-17(a). Similarly, for the case of cuprates, the sign of j depends on whether which crystal axes the hop is aligned to (c.f. Fig. 2-17(b)). Second, while both the doublon and holon can hop around in the Raman case, in RIXS it is more appropriate to assume that the core-hole is immobile.

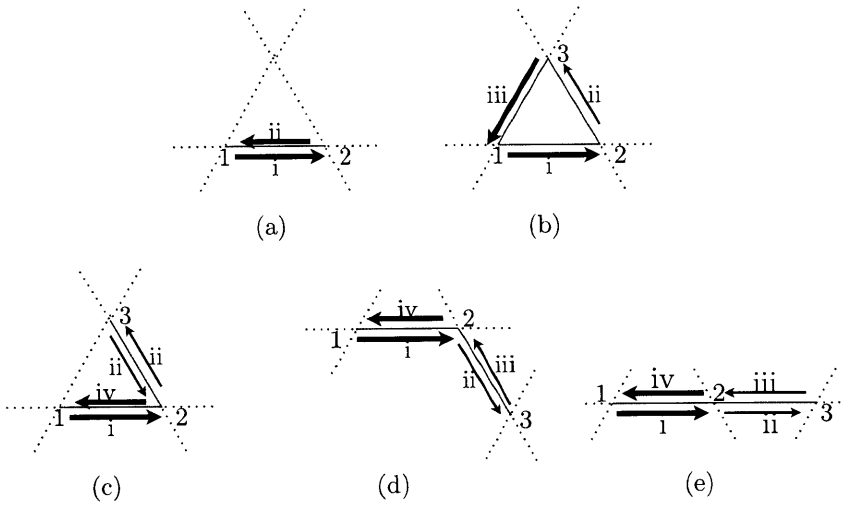

Figure 2-18: Pathways that contribute to RIXS to order $(t,j)^4/\mathcal{E}_1^3$.

Third, the energy denominator $U-\omega_i$ that appears in the original Shastry–Shraiman formulation must be replaced by the appropriate energy difference between the initial and virtual state, which I shall call $\mathcal{E}_1$. Note that the finite lifetime of the core hole can be incorporated in this formulation by adding an imaginary part $i\Gamma$ to $\mathcal{E}_1$. Finally, in the RIXS case the core hole and the valence doublon can co-exist on the same site. However, since the two interact with each other via (possibly screened) Coulomb interaction, the energy denominator must be modified from $\mathcal{E}_1$ to $\mathcal{E}_1 - U_c$ when they reside on the same site (numerically, U_c is estimated to be approximately 7 eV for cuprates, which is about 0.8 of U that appears in Hubbard model in that case [86]). Since it is assumed that we are near resonance ($t < \mathcal{E}_1 \ll U$) and that $t \ll U$, pathways that contains intermediate states in which core hole and valence doublons reside on the same site should be considered as contributions first order in the expansion in t/U.

With the above changes, one can repeat the derivation of transition matrix in the Shastry–Shraiman formulation. Up to the choice of the initial site and initial current, pathways that contribute up to the order $\mathcal{O}(t^2j^2/\mathcal{E}_1^3)$ are listed Fig. 2-18. Note that the contributions from the pathways in Fig. 2-18(d) and Fig. 2-18(e) are identical to that from Fig. 2-18(c) upon relabeling the third lattice site. The contributions from

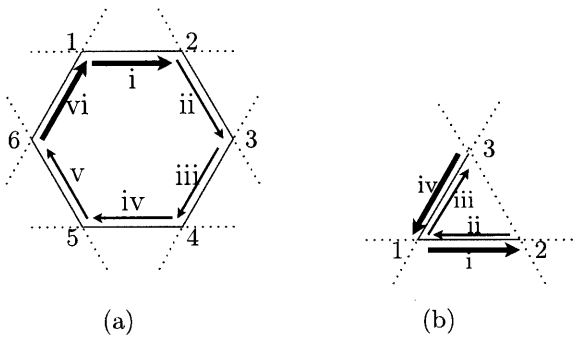

Figure 2-19: Pathways that contribute to the spin chirality term in RIXS.

the pathways in Fig. 2-18(a) – Fig. 2-18(c) are (recall that our convention of unit vectors have been defined in Fig. 2-6):

$$T_a = e_i^x(-\bar{e}_f^x)\frac{(ij)(-ij)}{\mathcal{E}_1}(c_c^\dagger c_2)(c_2^\dagger c_c) = -\frac{j^2}{\mathcal{E}_1}e_i^x\bar{e}_f^x\,\mathrm{tr}\{\chi_2\} = -(e_i^x\bar{e}_f^x)\frac{j^2}{\mathcal{E}_1}\ , \tag{2.51}$$

$$\begin{aligned} T_b &= e_i^x(\bar{e}_f^w)\frac{(ij)(-t)(-ij)}{\mathcal{E}_1^2}(c_c^\dagger c_3)(c_3^\dagger c_2)(c_2^\dagger c_c) = -\frac{tj^2}{\mathcal{E}_1^2}e_i^x\bar{e}_f^w\,\mathrm{tr}\{\chi_3\chi_2\} \\ &= -(e_i^x\bar{e}_f^w)\frac{tj^2}{\mathcal{E}_1^2}\left(\frac{1}{2}+2\boldsymbol{S}_2\cdot\boldsymbol{S}_3\right)\ , \end{aligned} \tag{2.52}$$

$$\begin{aligned} T_c &= e_i^x(-\bar{e}_f^z)\frac{(ij)(-t)^2(-ij)}{\mathcal{E}_1^3}(c_c^\dagger c_2)(c_2^\dagger c_3)(c_3^\dagger c_2)(c_2^\dagger c_c) = -\frac{t^2j^2}{\mathcal{E}_1^2}e_i^x\bar{e}_f^x\,\mathrm{tr}\{\chi_3\}\,\mathrm{tr}\{\chi_2\} \\ &= -(e_i^x\bar{e}_f^x)\frac{t^2j^2}{\mathcal{E}_1^3}\ , \end{aligned} \tag{2.53}$$

where c_c ($c_c^\dagger$) denotes the electron annihilation (creation) operator associated with the core hole.

Unfortunately, none of these pathways give rise to a spin-chirality term. In fact, it can be checked that the lowest-order terms that contribute to the spin-chirality terms are the ones in which the doublon hops through a hexagon, as depicted in

Fig. 2-19(a), which is of order $t^4j^2/\mathcal{E}_1^5$:

$$\begin{aligned} T_{\text{hex}} &= e_i^x(-\bar{e}_f^w)\frac{(ij)(-t)^4(-ij)}{\mathcal{E}_1^5}(c_c^\dagger c_6)(c_6^\dagger c_5)(c_5^\dagger c_4)(c_4^\dagger c_3)(c_3^\dagger c_2)(c_2^\dagger c_c) \\ &= -\frac{t^4j^2}{\mathcal{E}_1^5}e_i^x\bar{e}_f^w \operatorname{tr}\{\chi_6\chi_5\chi_4\chi_3\chi_2\} \\ &\doteq -(e_i^x\bar{e}_f^w)\frac{it^4j^2}{2\mathcal{E}_1^5}\sum_{2\le a<b<c\le 6}\boldsymbol{S}_a\cdot(\boldsymbol{S}_b\times\boldsymbol{S}_c)\ , \end{aligned} \tag{2.54}$$

where I retain only the spin-chirality contributions on the third line. As in the Raman case, one can then sum over all possible initial current and initial site to obtain a non-zero overall contribution to the spin-chirality term in the A_{2g} channel.

Alternatively, if one counts also the pathways that are first order in the expansion in t/U, the process in which the doublon hops through the core-hole site to the third site of the triangle (Fig. 2-19(b)) also contribute to the spin chirality term:

$$\begin{aligned} T_{U_c} &= e_i^x(\bar{e}_f^w)\frac{(ij)(-t)^2(-ij)}{\mathcal{E}_1^2(\mathcal{E}_1-U_c)}(c_c^\dagger c_3)(c_3^\dagger c_1)(c_1^\dagger c_2)(c_2^\dagger c_c) = \frac{t^2j^2}{\mathcal{E}_1^2(\mathcal{E}_1-U_c)}e_i^x\bar{e}_f^w \operatorname{tr}\{\chi_3\chi_1\chi_2\} \\ &\doteq (e_i^x\bar{e}_f^w)\frac{2it^2j^2}{\mathcal{E}_1^2(\mathcal{E}_1-U_c)}\boldsymbol{S}_3\cdot(\boldsymbol{S}_1\times\boldsymbol{S}_2)\ , \end{aligned} \tag{2.55}$$

If we assume that $\mathcal{E}_1$ in RIXS and $(\omega_i - U)$ in Raman spectroscopy are of the same order, we see that the coefficients of spin-chirality term in the RIXS T-matrix is down by a factor of $j^2/(t^2U)$ or $j^2/\mathcal{E}_1^2$ when compared to the Raman case. While this counts as a disadvantage to RIXS, one should also remember that the coupling between the emergent gauge boson and the spin-chirality term is enhanced by a factor of q. Thus, when both effects is accounted for, RIXS may still holds hopes for observing the emergent gauge boson in the $U(1)$ DSL state. In addition, because of the finite momentum transfer in RIXS, the signal from the emergent gauge boson will now have a threshold at $\Delta\omega = v_Fq$ in addition to the $1/(\Delta\omega^2 - v_F^2q^2)^{1/2}$ decay, which may help to distinguish the emergent gauge boson from other signals.

It is also interesting to remark that the dichotomy of the square lattice versus kagome lattice is essentially reversed here: While contribution to the spin-chirality term vanishes at the $t^2j^2/\mathcal{E}_1^3$ order in the kagome lattice, it is non-vanishing for the

square lattice at this order. Specifically, the only legitimate pathway that remains from Fig. 2-1 is the one in Fig. 2-1(a), which contributes:

$$\begin{aligned} T_a^{\square} &= e_i^x(-\bar{e}_f^y)\frac{(ij)(-t)^2(-ij)}{\mathcal{E}_1^3}(c_c^\dagger c_3)(c_3^\dagger c_4)(c_4^\dagger c_2)(c_2^\dagger c_c) = -\frac{t^2j^2}{\mathcal{E}_1^3}e_i^x\bar{e}_f^y\,\mathrm{tr}\{\chi_3\chi_4\chi_2\} \\ &\doteq -(e_i^x\bar{e}_f^y)\frac{2it^2j^2}{\mathcal{E}_1^3}\boldsymbol{S}_3\cdot(\boldsymbol{S}_4\times\boldsymbol{S}_2)\ . \end{aligned} \tag{2.56}$$

It can then be easily check that sum over different directions of initial current produces a non-vanishing contribution to the spin-chirality term. Consequently, the effect of spin-chirality term in RIXS may be much more prominent in the cuprates as compared to herbertsmithite.

Chapter 3

The $U(1)$ DSL state in B-field

In this chapter I shall consider the effect of weak magnetic field on the $U(1)$ DSL state. As explained in the introduction, the $U(1)$ DSL state can be considered as a quantum critical phase with many competing orders. The application of an external magnetic field as a perturbation is thus likely to tilt the delicate balance between the various orders and thus lead to new behaviors of the system. What I will show is that at the mean-field level, the Landau level (LL) state obtained by adding a uniform emergent gauge flux on top of the $U(1)$ DSL ansatz will produce a lower energy than the Fermi pocket state in which the background emergent gauge flux pattern is unmodified. Unlike in the familiar case of quantum Hall systems, the LL state obtained this way contains a gapless mode, which turns out to carry $S_z = 1$. Importantly, the existence of this gapless S_z fluctuation implies that the XY-symmetry is broken in the system. In other words, in addition to the tilting of spins along the direction of the applied B-field, the component of spins perpendicular to the applied B-field will also be ordered in this phase.

3.1 Landau level state vs. Fermi pocket state

Recall that the charge degree of freedom is frozen in a Mott insulator. Consequently, the only effect of an external magnetic field is to add a Zeeman term $\Delta H_{\mathrm{Z}} = -g\mu_B \sum_i \boldsymbol{B} \cdot \boldsymbol{S}_i$ to the Heisenberg Hamiltonian Eq. (1.3). For convenience

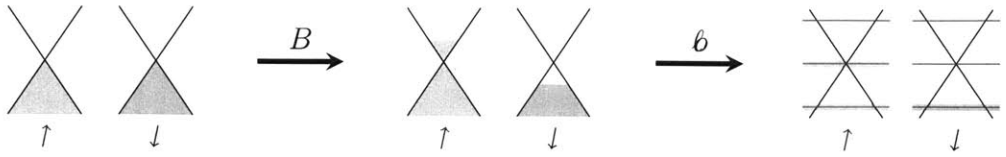

Figure 3-1: The formation of Landau levels in the spin-1/2 kagome system when an external B-field is applied.

we shall choose our spin quantization axis such that the B-field is along the $+\hat{z}$ direction (note that the spin quantization axis and the axes of the kagome lattice need not be related). Then, if we assume that the mean-field state is still described by the $U(1)$ DSL ansatz of having 0 flux through the triangles and π flux through the hexagons, then in the mean-field picture the only change from the zero-field case is that the filling fraction of the up and down spins are modified, which results in spinon Fermi pockets for the up-spins antispinon Fermi pocket in the down-spins. For future reference, such state will be referred to as the "Fermi pocket" (FP) state.

However, it is possible that other mean-field ansatzes will produce lower energies. Recall that in the zero-field case the $U(1)$ DSL has been argued to be a global minimum in energy. Thus, if the external B-field is sufficiently small, the new global minimum should be related to the $U(1)$ DSL state by small perturbation in the mean-field parameters.

In particular, one can imagine perturbing the $U(1)$ DSL ansatz such that an additional amount of uniform background emergent gauge flux is introduced. In such case, from the Dirac node structure of the spinon bands at low energies and from elementary quantum mechanics, it is easy to see that the spinon energy spectrum will then be described by Landau levels (LLs) having energy $\mathcal{E}_n = \pm\nu\sqrt{2n\flat}$ and degeneracy $N_n = \flat\mathsf{A}/2\pi$, where $\flat = \partial_x\alpha_y - \partial_y\alpha_x$ is the "magnetic field" associated with the emergent gauge field α and A is the area of the lattice, both taken in an appropriate continuum limit.

Observe that the Landau level spectrum has zero energy states, in which there is no energy cost to occupy a spinon. As a result, in the spinon sector it would be energetically favorable to have Landau levels opened. To be precise, if we set aside

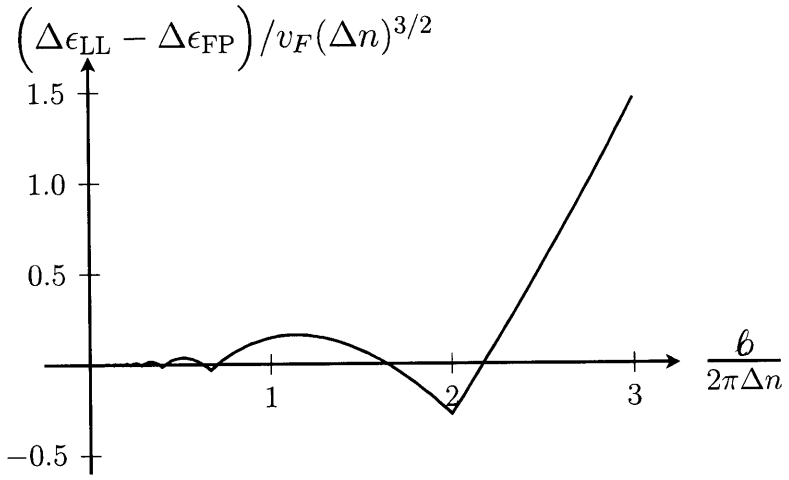

Figure 3-2: Energy difference between the FP state and the LL state for a single direct cone when Δn is held fixed while $\mathscr{b}$ varies.

the Zeeman energy (which is common to both the FP state and the LL state) and define the Dirac cone filled to the Dirac point as the zero-energy reference point, then for a single Dirac cone, the energy density of the FP state with excess spinon density of $\Delta n > 0$ is given by:

$$\Delta\epsilon_{\rm FP} = \int_{|\boldsymbol{k}|\le k_F} v_F|\boldsymbol{k}|\frac{d^2\boldsymbol{k}}{(2\pi)^2} = v_F\int_0^{\sqrt{4\pi\Delta n}}\frac{k^2dk}{2\pi} = \frac{2\sqrt{\pi}}{3}(\Delta n)^{3/2}\,, \tag{3.1}$$

while under a uniform emergent "magnetic" field $\mathscr{b}$, the energy of the corresponding LL state is given by:

$$\Delta\epsilon_{\rm LL} = \frac{\mathscr{b}v_F}{2\pi}\left(\sum_{n=-\infty}^{\lfloor\lambda-1/2\rfloor}\mathrm{sgn}(n)\sqrt{2|n|\mathscr{b}} + \left[\!\left[\lambda-\frac{1}{2}\right]\!\right]\sqrt{2\mathscr{b}\left\lceil\lambda-\frac{1}{2}\right\rceil} - \int_{-\infty}^{0}\frac{k^2dk}{2\pi}\right)\,, \tag{3.2}$$

where $\lambda = 2\pi\Delta n/\mathscr{b}$, and which $\mathrm{sgn}(x)$, $\lfloor x\rfloor$, $\lceil x\rceil$, and $[\![x]\!]$ denotes the sign, floor, ceiling, and fractional part of x, respectively. Note that the lower limit of the sum and the integral in Eq. (3.2) has to be taken together in a consistent manner, since each expression is by itself divergent.

In Fig. 3-2 the energy difference between the FP state and the LL state is plotted

as a function of the emergent "magnetic" field ϕ at a fixed Δn (note that by particle-hole symmetry of the Dirac cone the energy difference between the FP state and the LL state is independent of the sign of Δn). From the plot, it is clear that the spinon energy is minimized for a LL state in which there are two flux quanta of the emergent gauge flux per Dirac cone spinon, which corresponds to the case where the zeroth LL is exactly filled (or, when $\Delta n < 0$, exactly emptied). In such case the energy of the LL state is known to have the closed form expression [90, 91]:

$$\Delta\epsilon^*_{\mathrm{LL}} = \frac{\zeta(3/2)(\Delta n)^{3/2}}{\sqrt{2\pi}} , \tag{3.3}$$

where $\zeta(x)$ is the Riemann zeta function.

Since at the mean-field level the fluctuation of the emergent gauge field costs no additional energy, from the above argument we see that if $(N_\uparrow - N_\downarrow)/\mathsf{A} = x$, then the ansatz in which $\phi = x/2$ uniformly on top of the $U(1)$ DSL flux pattern will be the most energetically favorable state at the mean-field level. In the following we shall focus on the physical property of this particular LL state.

3.2 Chern–Simons theory, gapless mode, and XY order

To describe the low-energy properties of this LL state, it is useful to adopt a *hydrodynamic* approach well-known in the quantum Hall literature[92, 93, 94]. In this approach, a duality transformation is applied, in which a gauge field is introduced to describe the current associated with a matter field, and which the two are related by:

$$J^\mu = \frac{1}{2\pi}\epsilon^{\mu\nu\lambda}\partial_\nu a_\lambda , \tag{3.4}$$

where J^μ is the current of the matter field and a_λ is the associated gauge field. Here μ, ν, and λ are spacetime indices that run from 0 to 2, and $\epsilon^{\mu\nu\lambda}$ is the totally antisymmetric Levi-Civita symbol.

In this formalism, a single-layer quantum Hall system of filling fraction (a.k.a. Hall number) $\nu = 1/m$ is described by the following effective Lagrangian:

$$\mathcal{L} = -\frac{m}{4\pi}\epsilon^{\mu\nu\lambda}a_\mu\partial_\nu a_\lambda - \frac{e}{2\pi}\epsilon^{\mu\nu\lambda}a_\mu\partial_\nu A_\lambda + \dots \tag{3.5}$$

where A^μ is the external electromagnetic field and "..." represents terms with higher derivatives, and hence unimportant at low energies. In particular, at the lowest order in derivatives among the terms dropped is the "Maxwell term":

$$\mathcal{L}_{\text{Maxwell}} = -\frac{1}{2g^2}(\partial_\mu a_\nu - \partial_\nu a_\mu)(\partial^\mu a^\nu - \partial^\nu a^\mu)\,. \tag{3.6}$$

The effective Lagrangian Eq. (3.5) can be understood by considering the equation of motion (EOM) with respect to the dual gauge field a^μ, which in the time-component gives $\nu = 2\pi J^0/(-eB)$, in agreement with the LL picture and the interpretation of ν as the filling fraction.

For an N-layer quantum Hall system, Eq. (3.5) generalizes to:

$$\begin{aligned}\mathcal{L} &= -\frac{1}{4\pi}\epsilon^{\mu\nu\lambda}a_{I\mu}K_{IJ}\partial_\nu a_{J\lambda} - \frac{e}{2\pi}\epsilon^{\mu\nu\lambda}q_I a_{I\mu}\partial_\nu A_\lambda + \dots \\ &= -\frac{1}{4\pi}\epsilon^{\mu\nu\lambda}\boldsymbol{a}_\mu K\partial_\nu\boldsymbol{a}_\lambda - \frac{e}{2\pi}\epsilon^{\mu\nu\lambda}(\boldsymbol{q}\cdot\boldsymbol{a}_\mu)\partial_\nu A_\lambda + \dots\end{aligned} \tag{3.7}$$

here a_I^μ is the dual gauge field that corresponds to the matter field in the I-th layer, $\boldsymbol{a}_\mu = (a_1^\mu, \dots, a_N^\mu)^T$ and $\boldsymbol{q} = (q_1, \dots, q_N)^T$ are N-by-1 vectors, and $K = [K_{IJ}]$ is an N-by-N real symmetric matrix.

Except that external EM field A^μ is replace by an emergent gauge field α^μ here (recall that the external electro-magnetic field appears only in the Zeeman term, and has no implication on orbital motion), the LL state discussed in the previous section is completely analogous to a multi-layer quantum Hall system. In particular, recall there there is one flux quanta of emergent gauge field per excess up-spin (and for each excess up-spin there is one deficient down-spin). Thus, if we treat the up-spin and down-spin as separate species, then the up-spin has Hall conductance $+1$ while the down-spin has Hall conductance -1. The low-energy effective theory that describes

the LL state is thus given by the following Chern–Simons theory:[1]

$$\begin{aligned}\mathcal{L} &= -\frac{1}{4\pi}\epsilon^{\mu\nu\lambda}a_{\uparrow\mu}\partial_\nu a_{\uparrow\lambda} + \frac{1}{4\pi}\epsilon^{\mu\nu\lambda}a_{\downarrow\mu}\partial_\nu a_{\downarrow\lambda} + \frac{1}{2\pi}\epsilon^{\mu\nu\lambda}\left(a_{\uparrow\mu}+a_{\downarrow\mu}\right)\partial_\nu\alpha_\lambda + \dots \\ &= -\frac{1}{4\pi}\epsilon^{\mu\nu\lambda}\boldsymbol{c}_\mu^T K\partial_\nu\boldsymbol{c}_\lambda + \dots\ ,\end{aligned} \tag{3.8}$$

where the K-matrix is given by:

$$K = \begin{pmatrix} 0 & -1 & -1 \\ -1 & 1 & 0 \\ -1 & 0 & -1 \end{pmatrix}\ . \tag{3.9}$$

As before, the "..." denotes terms higher in derivatives, including first and foremost the Maxwell term analogous to Eq. (3.6). In the second line, we have combined the three gauge fields internal to the system into a column vector $\boldsymbol{c}^\mu = (\alpha^\mu; a_\uparrow^\mu, a_\downarrow^\mu)^T$. For brevity, henceforth we shall omit spacetime indices that are internally contracted, e.g., writing $\epsilon a\partial b$ instead of $\epsilon^{\mu\nu\lambda}a_\mu\partial_\nu b_\lambda$ and $(\epsilon\partial a)^\mu$ instead of $\epsilon^{\mu\nu\lambda}\partial_\nu a_\lambda$. In a similar spirit, we shall write $\partial a\partial a$ instead of $(\partial_\mu a_\nu - \partial_\nu a_\mu)(\partial_\mu a_\nu - \partial_\nu a_\mu)$ for the Maxwell term.

Note that unlike Eq. (3.7), we have included the emergent gauge field α^μ in $\boldsymbol{c}^\mu$. This is because α^μ is internal to the system and can be spontaneously generated while the EM field in the usual quantum Hall case is external and fixed. This distinction is crucial when considering the compressibility of the system. Usually, the formation of LLs implies that all excitations (single-particle or collective) are gapped, which in turn implies that the state is incompressible. However, this is true only if the gauge field that couples to the matter fields is external. Since the α field is internal to the system, it can fluctuate smoothly in space while keeping the LL structure intact and the overall spin imbalance unchanged. Intuitively, if the α field varies across space at a sufficiently long wavelength, then the spinons in each local spatial region can still be described by the LL picture, but the LLs will have a larger (smaller) spacing

[1] In a more detailed treatment each *Dirac nodes* can be treated as a separate species. This, however, will introduce an unnecessary complication for the present purpose. For more details, see Sec. 4.2

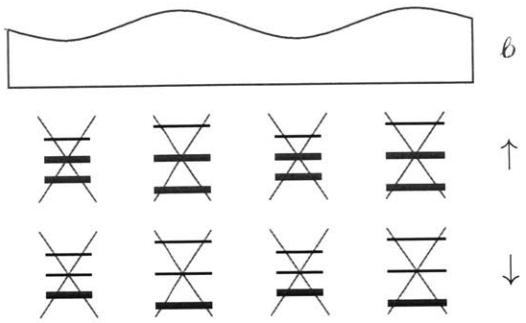

Figure 3-3: The physical picture of the breathing mode when external magnetic field is applied. The filled LL states are indicated by thick horizontal lines while the unfilled LL states are indicated by the thin (black) horizontal lines. The original band structure for spinon when no additional α flux is introduced is also indicated in the background (gray).

in regions where the α field is stronger (weaker). Since the LL structure is intact and the wavelength of this variation can be made arbitrarily long, the energy cost of such "breathing mode" can be made arbitrarily small. This breathing mode is thus a gapless density mode of the system. See Fig. 3-3 for illustration. Note that all species of spinons co-fluctuate with the α field in this density mode.

The other excitations of the system can be grouped into two general types. The first type consists of smooth density fluctuations in which the fluctuations of spinons, and α field are mismatched. The second type consists of quasiparticle excitations that involve spinons excited from one LL to another. Both types of excitations are gapped.

In terms of the Chern–Simons formulation, it is easy to check that the K-matrix in Eq. (3.9) contains *exactly one zero eigenvalue*, with eigenvector $\boldsymbol{p}_0 = (1; 1-1)^T$. Let λ_i be the eigenvalues of K, with $\boldsymbol{p}_i$ the corresponding eigenvectors, let $P = [\boldsymbol{p}_0, \boldsymbol{p}_1, \boldsymbol{p}_2]$ be the orthogonal matrix form by the eigenvectors of K, and let $\boldsymbol{c}' = (c'_0, c'_1, c'_2)^T = P^\dagger \boldsymbol{c}$. Then, Eq. (3.8) can be rewritten in terms of $\boldsymbol{c}'$ as:

$$\mathcal{L} = -\frac{1}{4\pi} \sum_{j>0} \lambda_j \epsilon c'_j \partial c'_j + g \partial c'_0 \partial c'_0 + \dots \tag{3.10}$$

The Maxwell term $g\partial c'_0 \partial c'_0$ for c'_0 in Eq. (3.10) originates from the terms in "..." of

Eq. (3.8), which is ordinarily suppressed by the Chern–Simons terms. However, since the Chern–Simons term $\epsilon c\partial c$ vanishes for c'_0, the *Maxwell terms term becomes the dominant term* for c'_0 at low-energy. Note that although at the mean-field level the α field itself does not have a Maxwell term, the zero-mode c'_0 does have a Maxwell term originated from the matter-field components.

The existence of this gapless mode is in fact a rather general consequence of zero total Hall number (i.e., $\sum_{\text{all species}} \nu = 0$). See Ref. [93]. Since the Maxwell term has a gapless linearly-dispersing spectrum, we see that the c'_0 indeed corresponds to a gapless excitation. Moreover, since all other gauge-field components have non-zero Chern–Simons terms, excitations in these gauge-field components are gapped (these excitations corresponds to the "mismatched" density fluctuation mentioned earlier), verifying the earlier assertion that there is only one gapless density mode.

From the physical picture depicted in Fig. 3-3, it is evident that the fluctuation of the gapless mode is tied (via the variation of LL degeneracy across space) to the fluctuation in S_z. More specifically, since each quanta of α flux is tied to one excess up-spin and one deficient down-spin in the gapless mode, and since the two spin species carry $S_z = \pm 1/2$ quantum numbers, it follows that each flux quanta of the gauge field ${c'_0}^{\mu}$ that corresponds to the gapless mode carries $S_z = 1$ quantum number. In the Chern–Simons formulation this is manifested by the fact that $\boldsymbol{s} \cdot \boldsymbol{p}_0 = 1$, in which $\boldsymbol{s} = (0; 1/2, -1/2)^T$ is the "spin vector" that marked the S_z quantum number carried by the different matter field species.

Recall that the S_z quantum number of the system is conserved at a fixed external magnetic field B. The existence of a linearly-dispersing gapless mode of this conserved density as the only gapless excitation of the system is, amazingly, an indication that corresponding symmetry is spontaneously broken in the ground state [95, 96]. The more familiar example is that of superfluidity, where the phonon mode is the signature of Bose condensation. The argument relies on the duality between the compact $U(1)$ gauge theory $\mathcal{L} = \frac{1}{2g^2}(\boldsymbol{e}^2 - b^2)$ and the XY model $\mathcal{L} = \sum_{\mu}(\partial_\mu \theta)^2$ in $2+1$ dimensions [35, 97], in which the magnetic field b corresponds to $\dot{\theta}$ and the electric field $\mathbf{e}$ corresponds to a vector normal to $\nabla\theta$ (to be precise, $e_i = \epsilon_{ij}\partial_j\theta$). The latter

relation implies that electric charge which is the source of $1/r$ electric field in the gauge theory corresponds to a vortex in the XY ordered phase. In the deconfined (Coulomb) phase, the photon is the only gapless excitation. It corresponds to the Goldstone mode of the ordered XY model.

By definition the insertion of a monopole at time τ creates an additional flux quanta, which in our case is tied to the addition of $S_z = 1$. Since the total spin is conserved, the appearance of free monopoles and anti-monopoles is strictly forbidden and we are in the Coulomb phase. On the other hand we can insert by hand a monopole at position i and remove it at position j. The action of the monopole–anti-monopole pair in $2+1$ dimensions is the same as the Coulomb energy between charges in 3 spatial dimensions and goes as $1/r$. Hence $\langle V(r)^\dagger V(r')\rangle \sim \exp(-|r-r'|^{-1})$ has long range correlation. Since the slowly varying field operator $V^\dagger$ increases S_z by 1, it is related to the lattice-scale spin operator S_i^+, but with a possible staggering pattern. i.e., we may write $V^\dagger \sim \sum_i e^{i\theta_i} S_i^+$, where the sum is restricted to the lattice sites in the vicinity of where the flux is inserted. The above reasoning thus indicates that the spin is ordered in the XY plane (i.e., the plane perpendicular to the applied field).

Note from the above argument that the monopole operator $V^\dagger$ in the effective QED_3 description of the $U(1)$ DSL state is essentially the staggered magnetization operator of the XY order. Moreover, since the B-field is coupled to conserved quantities, it has scaling dimension 1 in the QED_3 description. From these, it follows that the staggered magnetization M in the XY plane must scale as $M \sim B^z$, where z is scaling dimension of the monopole operator in the $U(1)$ DSL state.

3.3 Discussions

While the mean-field arguments given in the above sections suggest that an XY order will develop when the spin-1/2 kagome system is subjected to an external magnetic field, there are some loose ends that need to be addressed. First, since the above arguments are made at the mean-field level, one may doubt if the preference of the

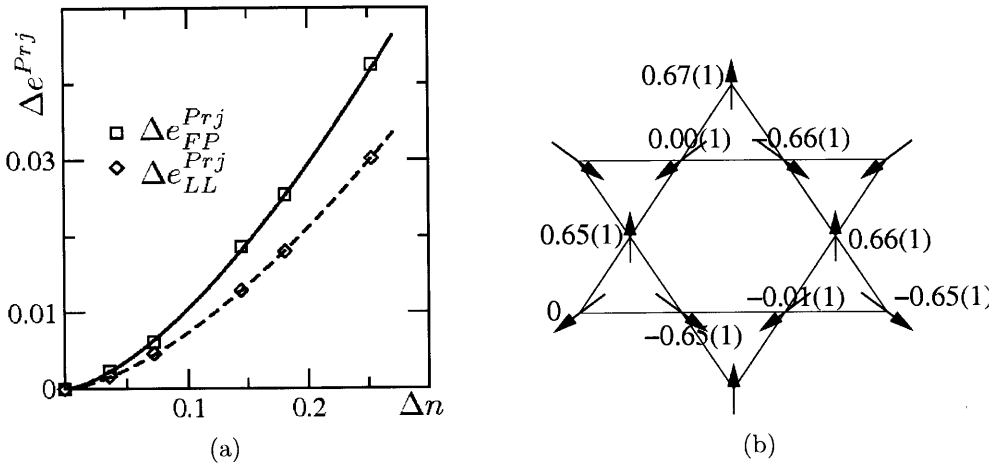

Figure 3-4: VMC results for the $U(1)$ DSL state under external B-field: (a) Energy density Δe of the LL state and the FP state as a function of spin imbalance density Δn. The solid and dotted lines are obtained by fitting the data to the scaling form $\Delta e = a\Delta n^{3/2} + b\Delta n^2$. (b) The XY spin order in the LL state, in which the number besides each spin is the relative phase of S_i^+ operator computed by projected LL state in units of π Note that the relative phase of the spin at the left-bottom corner is set as zero. Both figures are taken from Ref. [98]

LL state over the FP state will remain unchanged when the fluctuation of the emergent gauge field is taken into account. Second, while the above argument suggests that the system will be XY ordered, the precise ordering pattern has not been determined. Since the ordering pattern of a spin system can be measured in neutron scattering, it is particularly desirable to obtain this information for the LL state.

Fortunately, the two issues mentioned above can be resolved by preforming variational Monte Carlo calculations on the projected wavefunction (c.f. Sec. 1.2.2), which has been carried out by Ying Ran in the paper that we published on this subject [98]. From the results, it is indeed confirmed that the projected LL state has a lower energy than the projected FP state (Fig. 3-4(a)). Moreover, the ordering pattern is found to be the $q = 0$ state in the literature of classical kagome spin system (Fig. 3-4(b)).

In addition, one may also wonder how the picture may have changed if further interactions, in particular the Dzyaloshinskii-Moriya term, is added to the system. Interestingly, it turns out that if the DM is treated as a perturbation to the $U(1)$ DSL state, then the effect it has in the low-energy effective theory is completely

analogous to the effect of the Zeeman term [74]. Thus the presence of the DM term is likely to enhance the XY order that have appeared in this chapter.

As mentioned in Sec. 1.3.2, the question of whether the ground state of the spin-1/2 kagome system is a valence bond solid or a spin liquid has not be settled conclusively. If the spin-1/2 kagome system is a VBS, it will surely not break S_z symmetry in a small magnetic field because the VBS phases are fully gapped. The S_z symmetry can be broken at an external magnetic field larger than the spin gap due to the triplon condensation. However the XY magnetic order generated in this fashion is unlikely to be the $q = 0$ pattern because the VBS orders itself breaks translation symmetries and thus the corresponding XY orders are also likely to break translation symmetries and result in a large unit cell. Therefore the spontaneous spin ordering presented in this chapter can be used to differentiate the $U(1)$ DSL from VBS states experimentally.

Furthermore, since the LL state breaks the parity and S_z rotation symmetry, it is separated from the high temperature paramagnetic phase by at least one *finite* temperature phase transition. This transition can be first order or continuous. If the transition is a continuous one that restores the S_z-$U(1)$ symmetry, it is expected to be in the Kosterlitz-Thouless universality, and the transition temperature can be estimated as $T_c \sim \frac{\mu_B B}{k_B}$ when $\mu_B B \lesssim \chi J$. This is because the external magnetic field B is the only energy scale if it is much smaller than the spinon bandwidth. Since these are intrinsic properties of the $U(1)$ DSL state in magnetic field, they can be used to experimentally detect the possible DSL ground state in Herbertsmithite and other materials where a $U(1)$ DSL state may be realized.

Chapter 4

Doping the $U(1)$ DSL state

So far much of the theoretical and experimental efforts of the kagome system has been focused in the half-filled (i.e., spin-1/2) case, including the works I presented in the two previous chapters. However, given Anderson's proposal that the pseudo-gap phase of the cuprates can be considered as a spin liquid [21], it would be interesting to consider what may happen to the spin-liquid state when the system is doped. Experimentally, doping in herbertsmithite can be achieved by substituting the chlorine with sulfur in herbertsmithite. And as explained in the Sec. 1.2.3, a theoretical description of the doped case can be obtained by extending the Schwinger fermion representation Eqs. (1.6)–(1.8) to the slave-boson representation Eq. (1.17).

In this chapter I shall present my work on the theoretical study of doping the $U(1)$ DSL state. In light of Anderson's proposal [21] and the phase diagram of the cuprate, one may expect that the system becomes superconducting once it has been doped. This is indeed what we shall find. However, the superconducting state thus obtained turns out to be more interesting than usual. In particular, I shall argue that the superconductor contains minimal vortices of flux $hc/4e$, and may contain fractionalized quasiparticles having semionic mutual statistics. As the the case of external magnetic field studied in Chapter 3, the emergent gauge field and the possibility of a Landau level structure will play important roles in producing these properties of the doped system.

4.1 Landau-level picture of the doped state

If we assume that the doped kagomé system is described by the $U(1)$ DSL ansatz as in the undoped case, and that the doping is x per site, then each doubled unit cell will contain $6x$ holons and $3-3x$ spinons per spin. By Fermi statistics, the spinons will fill the lowest $3-3x$ bands and thus can be described by anti-spinon pockets at each Dirac node. Similarly, by Bose statistics the holons will condense at each quadratic band bottom. As in Chapter 3, such state shall be referred to as the Fermi-pocket (FP) state.

However, as in Chapter 3, one may consider an ansatz in which an additional amount of uniform α flux is included, whose effect would be to produce Landau levels (LLs) in both the holon and spinon sector. As before, such state shall be referred to as the LL state. Recall that in the absence of holons, both mean-field calculation and projection wavefunction study indicate that the LL state is energetically favored over the FP state. Since the spinon bands are linear near half-filling while the lowest holon band is quadratic near its bottoms, at the mean-field level the energy gain from the spinon sector (which scales as 3/2 power of the b field) will be larger than the energy cost in the holon sector (which scales as square of the b field) at low doping. Therefore, even after the holons are taken into account, the LL state is expected to have a lower energy than the FP state.

Furthermore, from mean-field it can be seen that the energy gain will be maximal when the α field is adjusted such that the zeroth spinon LLs are exactly empty. Since each flux quanta of the α field corresponds to one state in each LL, and that each anti-spinon pocket contains $3x/2$ states for a doping of x per site, the flux must be $3x$ flux quanta per doubled unit cell for this to happen.

As for the holon sector, there are $6x$ holons per doubled unit cell or equivalently $3x/2$ holons per band bottom. Since the holon carries the electric charge and are hence are mutually repulsive, one may expect them to fill the four band bottoms symmetrically. In such case the first LL of each of the holon band bottom would be exactly *half-filled*, which implies that the holons would form four Laughlin $\nu = 1/2$

quantum Hall states. Since the Laughlin $\nu = 1/2$ state is gapped and incompressible, this symmetric scenario should be energetically favorable.[1]

4.2 Chern–Simons theory of the doped state

From the physical arguments given above, it can be seen that the effective description of the doped system is again analogous to that of a mulit-layered quantum Hall system, and thus may contain non-trivial topological orders, manifesting in, e.g., fractional quasiparticles with non-trivial statistics. As in Chapter 3, a *hydrodynamic approach*, in which a gauge field is introduced to describe the current associated with a matter field as in Eq. (3.4), will be adopted to describe the system.

For the holon sector, we can represent the holons at each of the four band bottoms by a dual gauge field b_J^μ $(J = 1, 2, 3, 4)$. Since the holons at each band bottom form a Laughlin $\nu = 1/2$ state, the total Hall number for the holon sector is $\sum_J \nu_J = 2$. For the spinon sector the situation is more subtle. Since the zeroth LL is empty and all the LLs below it are fully filled at each Dirac node, we may represent the spinons near each of the four Dirac nodes by a dual gauge field a_I^μ $(I = 1, 2, 3, 4)$ having Hall number $\nu = -1$. However, since α is internal to the system, the combined system of holons and spinons must be α neutral, which requires $\sum_{\text{all species}} \nu = 0$ and hence in the spinon sector $\sum_I \nu_I = -2$. To circumvent this problem, we introduce two additional dual gauge fields a_5^μ and a_6^μ, each having Hall number $\nu = +1$. The two fields a_5^μ and a_6^μ can be thought of as arising from the physics of spinons near the band bottoms of the two spin species. In this setting, $a_1^\mu, \ldots, a_4^\mu$ are expected to carry good spin and $\boldsymbol{k}$ quantum numbers,[2] while a_5^μ and a_6^μ are expected to carry good spin quantum number only. Note also that $a_1^\mu, \ldots, a_4^\mu$ possess an emergent $SU(4)$ symmetry of spin and pseudo-spin (i.e., $\boldsymbol{k}$-points).

[1] The stability of the Laughlin $\nu = 1/2$ state of boson can be seen by flux attachment argument. Since there are two flux quanta per boson, attaching one flux quanta to each boson maps the Laughlin $\nu = 1/2$ state of boson to an integer quantum Hall state of fermion, which is gapped and incompressible. In contrast, a $\nu = 1$ quantum Hall state for boson is mapped to a free fermion gas upon attaching one flux quanta to each boson, and hence is unstable.

[2] The $\boldsymbol{k}$ quantum numbers should be regarded as center-of-mass crystal momentum of the Hall condensate.

In the present case we will be interested in the vortices and the quasiparticles in the system, which can be included in the Chern–Simons formulation by adding a "charge" term to the Chern–Simons Lagrangian. In particular, for a single vortex or quasiparticle, the Lagrangian of the single-layer quantum Hall system, Eq. (3.5), is modified to:

$$\mathcal{L} = -\frac{m}{4\pi}\epsilon^{\mu\nu\lambda}a_\mu\partial_\nu a_\lambda - \frac{e}{2\pi}\epsilon^{\mu\nu\lambda}a_\mu\partial_\nu A_\lambda + \ell a_\mu j_V^\mu + \dots \tag{4.1}$$

where j_V^μ is the current density associated with vortices or quasiparticles. Note that from the duality transformation Eq. (3.4), the charge term $\Delta\mathcal{L} = \ell a_\mu j_V^\mu$ in the dual Lagrangian Eq. (4.1) can alternatively be viewed as a source of vortex in the matter field current J^μ, in agreement with the interpretation of this term as a physical vortex. To see that the charge term can also be interpreted as a quasiparticle, one can consider the equation of motion with respect to the dual gauge fields. With a stationary quasiparticle at x_0 such that $j_V^\mu = (\delta(x - x_0), 0, 0)$, the EOM reads, in the time-component:

$$J^0 = -\frac{e\nu}{2\pi}B + \ell\nu\delta(x - x_0) + \dots \tag{4.2}$$

which confirms that $j_V^\mu = (\delta(x - x_0), 0, 0)$ is a source term for a quasiparticle having charge $\ell\nu$. In particular, a physical electron at x_0 can be associated with $j_V^\mu = (\delta(x - x_0), 0, 0)$ and $\ell = \nu^{-1}$.

The statistics of the quasiparticles can be deduced by integrating out the dual gauge field a^μ in Eq. (4.1), from which we obtained the well-known Hopf term:

$$\mathcal{L}' = \pi\widetilde{j}^\mu\nu\left(\frac{\epsilon_{\mu\nu\lambda}\partial^\nu}{\partial^2}\right)\widetilde{j}^\lambda + \dots, \tag{4.3}$$

where $\widetilde{j}^\mu = -(e/2\pi)\epsilon^{\mu\nu\lambda}\partial^\nu A^\lambda + \ell j_V^\mu$ is the sum of terms that couple linearly to a^μ.

The statistical phase θ when one quasiparticle described by $\ell = \ell_1$ winds around another with $\ell = \ell_2$ can then be computed by evaluating the quantum phase $e^{iS} = e^{i\int\mathcal{L}'}$, with $\widetilde{j}^\mu = \ell_1 j_{V1}^\mu + \ell_2 j_{V2}^\mu$ being the total current produced by both quasiparticles. Performing the calculation, this yields [94] $\theta = 2\pi\nu\,\ell_1\ell_2$.

In particular, for the statistical phase accumulated when an electron winds around a quasiparticle of charge $\ell = \nu^{-1}$ to be a multiple of 2π, ℓ must be an integer. This provides a quantization condition for the possible values of ℓ.

In the multi-layer case, vortices and quasiparticles can similarly be included by adding a charge term:

$$\Delta\mathcal{L} = \left(\sum\nolimits_I \ell_I a_{I\mu}\right) j_V^\mu = (\boldsymbol{\ell}\cdot\boldsymbol{a}_\mu) j_V^\mu \tag{4.4}$$

where $\boldsymbol{\ell} = (\ell_1, \ldots, \ell_N)^T$ is an N-by-1 *integer* vector.

Assuming that $\det K \neq 0$, the procedure for integrating out the dual gauge fields can similarly be carried out, which yields:

$$\mathcal{L}' = \pi(\widetilde{\boldsymbol{j}}^T)^\mu K^{-1}\left(\frac{\epsilon_{\mu\nu\lambda}\partial^\nu}{\partial^2}\right)\widetilde{\boldsymbol{j}}^\lambda + \ldots . \tag{4.5}$$

where $\widetilde{\boldsymbol{j}}^\mu = -\boldsymbol{q}(e/2\pi)\epsilon^{\mu\nu\lambda}\partial^\nu A^\lambda + \boldsymbol{\ell} j_V^\mu$. The statistical phase θ when one quasiparticle described by $\boldsymbol{\ell} = \boldsymbol{\ell}_1$ winds around another with $\boldsymbol{\ell} = \boldsymbol{\ell}_2$ can then be computed in a similar way as in the single-layer case, which yields $\theta = 2\pi\,\boldsymbol{\ell}_1^T K^{-1}\boldsymbol{\ell}_2$. The information of quasiparticle statistics is thus contained entirely in K^{-1}.

Assembling dual gauge fields of the different species of holons and spinons as described above, the low-energy effective theory for the doped kagomé system is thus given by the following Chern–Simons theory:

$$\begin{aligned}\mathcal{L} = {} & \frac{1}{4\pi}\sum_{I=1}^{4}\epsilon^{\mu\nu\lambda}a_{I\mu}\partial_\nu a_{I\lambda} - \frac{1}{4\pi}\sum_{I=5}^{6}\epsilon^{\mu\nu\lambda}a_{I\mu}\partial_\nu a_{I\lambda} - \frac{2}{4\pi}\sum_J \epsilon^{\mu\nu\lambda}b_{J\mu}\partial_\nu b_{J\lambda} \\ & + \frac{1}{2\pi}\epsilon^{\mu\nu\lambda}\left(\sum_I a_{I\mu} + \sum_J b_{J\mu}\right)\partial_\nu\alpha_\lambda + \frac{e}{2\pi}\sum_J \epsilon^{\mu\nu\lambda}b_{I\mu}\partial_\nu A_\lambda \\ & + \left(\sum_I \ell_I a_{I\mu} + \sum_J \ell_J b_{J\mu}\right) j_V^\mu + \ldots \qquad (4.6) \\ = {} & -\frac{1}{4\pi}\epsilon^{\mu\nu\lambda}\boldsymbol{c}_\mu^T K\partial_\nu\boldsymbol{c}_\lambda + \frac{e}{2\pi}\epsilon^{\mu\nu\lambda}(\boldsymbol{q}\cdot\boldsymbol{c}_\mu)\partial_\nu A_\lambda + (\boldsymbol{\ell}\cdot\boldsymbol{c}_\mu) j_V^\mu + \ldots . \qquad (4.7)\end{aligned}$$

As before, the "..." denotes terms higher in derivatives, including first and foremost

the Maxwell term analogous to Eq. (3.6). Similar to the previous chapter, the eleven gauge fields internal to the system, including the emergent gauge field α^μ, are combined into a column vector $\boldsymbol{c}^\mu = (\alpha^\mu; a_1^\mu, \ldots, a_6^\mu; b_1^\mu, \ldots, b_4^\mu)^T$ in the second line. The "charge vector" $\boldsymbol{q}$ in this case is $\boldsymbol{q} = (0; 0,0,0,0,0,0; 1,1,1,1)^T$, and the K-matrix K takes the block form:

$$K = \left(\begin{array}{c|cccc|cc|cccc} 0 & -1 & -1 & -1 & -1 & -1 & -1 & -1 & -1 & -1 & -1 \\ \hline -1 & -1 & 0 & 0 & 0 & 0 & 0 & 0 & 0 & 0 & 0 \\ -1 & 0 & -1 & 0 & 0 & 0 & 0 & 0 & 0 & 0 & 0 \\ -1 & 0 & 0 & -1 & 0 & 0 & 0 & 0 & 0 & 0 & 0 \\ -1 & 0 & 0 & 0 & -1 & 0 & 0 & 0 & 0 & 0 & 0 \\ \hline -1 & 0 & 0 & 0 & 0 & 1 & 0 & 0 & 0 & 0 & 0 \\ -1 & 0 & 0 & 0 & 0 & 0 & 1 & 0 & 0 & 0 & 0 \\ \hline -1 & 0 & 0 & 0 & 0 & 0 & 0 & 2 & 0 & 0 & 0 \\ -1 & 0 & 0 & 0 & 0 & 0 & 0 & 0 & 2 & 0 & 0 \\ -1 & 0 & 0 & 0 & 0 & 0 & 0 & 0 & 0 & 2 & 0 \\ -1 & 0 & 0 & 0 & 0 & 0 & 0 & 0 & 0 & 0 & 2 \end{array}\right). \tag{4.8}$$

Note that the three terms in Eq. (4.7) can be understood as follows: the first term describes smooth internal dynamics of the system; the second term describes its response under an external EM field; and the third term describes the topological excitations of the system, which can be thought of as combinations of vortices in various matter-field components. As explained above, $\boldsymbol{\ell}$ must be an integer vector. Furthermore, since the α field is not a dual gauge field and contains no topological excitation (otherwise the local constraint Eq. (1.18) will be violated), the α-component of $\boldsymbol{\ell}$ for a physical topological excitation must be zero.

As in the original quantum Hall case, The coefficients that appear in K and $\boldsymbol{q}$ can be understood by considering the EOMs resulting from it. Upon variations with

respect to a_I^μ, b_J^μ, and α^μ, we get:

$$J_{aI}^\mu = -\frac{1}{2\pi}\epsilon^{\mu\nu\lambda}\partial_\nu\alpha_\lambda \qquad (\mathrm{I} = 1,2,3,4)\,, \tag{4.9}$$

$$J_{aI}^\mu = \frac{1}{2\pi}\epsilon^{\mu\nu\lambda}\partial_\nu\alpha_\lambda \qquad (\mathrm{I} = 5,6)\,, \tag{4.10}$$

$$J_{bJ}^\mu = \frac{1}{2}\cdot\frac{1}{2\pi}\epsilon^{\mu\nu\lambda}\partial_\nu\alpha_\lambda + \frac{e}{2\pi}\epsilon^{\mu\nu\lambda}\partial_\nu A_\lambda\,, \tag{4.11}$$

$$0 = \sum_I J_{aI}^\mu + \sum_J J_{bJ}^\mu\,. \tag{4.12}$$

The first three equations are in agreement with the picture that spinons form integer quantum Hall states while holons form Laughlin $\nu = 1/2$ states under the presence of α flux, and that spinons carry no EM charge while holons carry EM charge e. Moreover, the fourth equation can be seen as a restatement of the occupation constraint Eq. (1.18).

As in the previous chapter I shall omit spacetime indices that are internally contracted for brevity. In addition, I shall write vectors and matrices in block form whenever appropriate, which will be abbreviated by using $\mathbb{I}_n$ to denote an n-by-n identity matrix, $\mathbb{O}_{m,n}$ to denote an m-by-n zero matrix, and $\mathbb{E}_{m,n}$ to denote an m-by-n matrix with all entries equal to 1 (such that $c\mathbb{E}_{m,n}$ denotes an m-by-n matrix with all entries equal to c). In this notation, the $\boldsymbol{q}$-vector becomes $\boldsymbol{q} = (0; \mathbb{O}_{1,4}, \mathbb{O}_{1,2}, \mathbb{E}_{1,4})^T$ and the K-matrix in Eq. (4.8) becomes:

$$K = \begin{pmatrix} 0 & -\mathbb{E}_{1,4} & -\mathbb{E}_{1,2} & -\mathbb{E}_{1,4} \\ -\mathbb{E}_{4,1} & -\mathbb{I}_4 & \mathbb{O}_{4,2} & \mathbb{O}_{4,4} \\ -\mathbb{E}_{2,1} & \mathbb{O}_{2,4} & \mathbb{I}_2 & \mathbb{O}_{2,4} \\ -\mathbb{E}_{4,1} & \mathbb{O}_{4,4} & \mathbb{O}_{4,2} & 2\mathbb{I}_4 \end{pmatrix}. \tag{4.13}$$

4.3 Superconductivity and physical vortices

Neglecting the external electromagnetic field for the moment, it can be seen that the quantum Hall system described by Eq. (4.6) is again compressible, i.e., the system contains a gapless linearly-dispersing density mode, in which the fluctuation of the α

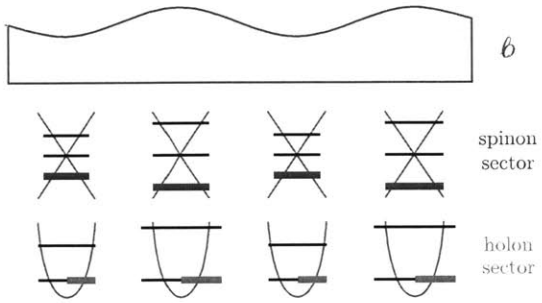

Figure 4-1: The physical picture of the breathing mode in the doped case. The filled LL states are indicated by thick horizontal lines while the unfilled LL states are indicated by the thin (black) horizontal lines. The original band structure for spinon and holon when no additional α flux is also indicated in the background (gray).

field, the spinon densities, and the holon densities are tied together, keeping the local constraint Eq. (1.18) and the LL structure intact. See Fig. 4-1 for illustration. Since the holon carries charge $+e$, the gapless mode in this case is a charge-density mode.

As before, the other excitations of the system can be grouped into two general types. The first type consists of smooth density fluctuations in which the fluctuations of holons, spinons, and α field are mismatched. The second type consists of quasiparticle excitations that involve holons or spinons excited from one LL to another. Both types of excitations are gapped. *Since the breathing mode is the only gapless mode, it is non-dissipative, and hence the system is a superfluid when the coupling to EM fields are absent. Moreover, since the breathing mode is charged under the EM field, the system will be a superconductor when the coupling to EM field are included.* Alternatively, as in the previous chapter we can treat the gapless mode as the Goldstone mode associated with a spontaneous symmetry broken ground state. With this association, the superconductivity can be seen as arising from the usual Anderson–Higgs mechanism in which this Goldstone mode is "eaten up" by the electromagnetic field. It should be noted that a similar superconducting mechanism has been proposed in the context of cuprates [99].

Note that this superconductor described above *spontaneously* breaks the time-reversal symmetry, since the sign of the additional amount of α flux is flipped under time reversal. Furthermore, since all four species of holons are binded together in the

breathing mode, each carrying charge $+e$, a minimal vortex in this superconductor is expected to carry a flux of $hc/4e$. We shall now show these claims more vigorously from the Chern–Simons theory Lagrangian we derived in Eq. (4.7).

It is easy to check that the K-matrix K in Eq. (4.8) contains *exactly one zero eigenvalue*, with eigenvector $\boldsymbol{p}_0 = (2; -2\mathbb{E}_{1,4}, 2\mathbb{E}_{1,2}; \mathbb{E}_{1,4})^T$. Let λ_i be the eigenvalues of K, with $\boldsymbol{p}_i$ the corresponding eigenvectors, let $P = [\boldsymbol{p}_0, \boldsymbol{p}_1, \ldots, \boldsymbol{p}_{10}]$ be the orthogonal matrix form by the eigenvectors of K, and let $\boldsymbol{c}' = (c'_0, \ldots, c'_{10})^T = P^\dagger \boldsymbol{c}$. Then, Eq. (4.7) can be rewritten in terms of $\boldsymbol{c}'$ as:

$$\begin{aligned}\mathcal{L} &= -\frac{1}{4\pi}\sum_{j>0}\lambda_j \epsilon c'_j \partial c'_j + \frac{e}{2\pi}\epsilon(\boldsymbol{q}\cdot P\boldsymbol{c}')\partial A + (\boldsymbol{\ell}\cdot P\boldsymbol{c}')_\mu j_V^\mu \\ &\quad + g\partial c'_0 \partial c'_0 + \ldots \\ &= \frac{e}{2\pi}(\boldsymbol{q}\cdot\boldsymbol{p}_0)\epsilon c'_0 \partial A + (\boldsymbol{\ell}\cdot\boldsymbol{p}_0) c'_{0\mu} j_V^\mu + g\partial c'_0\partial c'_0 + \ldots \\ &\quad + (\text{terms without } c'_0)\ ,\end{aligned} \tag{4.14}$$

where, as in the previous chapter, the Maxwell term $g\partial c'_0\partial c'_0$ for c'_0 in Eq. (4.14) originates from the terms in "..." of Eq. (4.7), which is ordinarily suppressed by the Chern–Simons terms. Since the Maxwell term has a gapless spectrum, we see that the zero-mode c'_0 indeed corresponds to a gapless excitation. Again, the existence of the zero-mode can be seen as a rather general consequence of zero total Hall number [93].

Note that the eigenvector $\boldsymbol{p}_i$ can be interpreted as the ratio of density fluctuations between the different field components in the mode c'_i. Thus the zero-mode indeed involves the fluctuations of all species of spinons and holons, tied together by the internal α field.

Moreover, since all other gauge-field components have non-zero Chern–Simons terms, excitations in these gauge-field components are gapped (these excitations corresponds to the "mismatched" density fluctuation mentioned earlier), verifying the earlier assertion that there is only one gapless density mode. Moreover, since $\boldsymbol{q}\cdot\boldsymbol{p}_0 \neq 0$, we see that the zero-mode is indeed charged under the external EM field. Hence, as

argued above, the doped system is a superconductor.

Since the system is a superconductor, when a sufficiently large external B field is applied, physical vortices, with the amount of flux through each vortex quantized, are expected to form. In the Chern–Simons formulation, these physical vortices manifest in the topological term $(\boldsymbol{\ell}\cdot\boldsymbol{c}_\mu)j_V^\mu$ in Eq. (4.6). Taking an isolated topological excitation with $(j_V^0, j_V^1, j_V^2) = (\delta(x-x_0), 0, 0)$, considering the EOM associated with c_0' as resulted from Eq. (4.14), and remembering that $(\epsilon\partial A)^0 = \epsilon^{0\mu\nu}\partial_\mu A_\nu = B$ is the physical magnetic field, we obtain (in units which $\hbar = c = 1$):

$$B = -\frac{2\pi}{e}\frac{\boldsymbol{\ell}\cdot\boldsymbol{p}_0}{\boldsymbol{q}\cdot\boldsymbol{p}_0}\delta(x-x_0) + \ldots . \tag{4.15}$$

This is the *Meissner effect*, which again confirms that the system is a superconductor. Moreover, it is easy to check that non-zero $|(\boldsymbol{\ell}\cdot\boldsymbol{p}_0)/(\boldsymbol{q}\cdot\boldsymbol{p}_0)|$ has a minimum of 1/4 (attained by, e.g., an $\boldsymbol{\ell}$-vector having a single "+1" in one of its b_J components and "0" in all its other components). From this we conclude that the magnetic flux through a minimal vortex is $hc/4e$, justifying the intuitive claim given above.

4.4 Quasiparticles—Statistics

It is important to note that not all topological excitations are EM-charged. The structure of these EM-neutral topological excitations highlights the differences between this system and a conventional superconductor, and hence qualify the adjective "exotic." We shall call these EM-neutral topological excitations "quasiparticles," to distinguish them from the EM-charged "physical vortices" considered in the previous section.

From Eq. (4.15), a topological excitation carries a non-zero magnetic flux if and only if $\boldsymbol{\ell}\cdot\boldsymbol{p}_0 \neq 0$. In other words, a topological excitation is EM-neutral if and only if it does not couple to the zero-mode. Note that the quantity $\boldsymbol{\ell}\cdot\boldsymbol{p}_0$ can be regarded as the zero-mode "charge" carried by the topological excitation. A topological excitation with $\boldsymbol{\ell}\cdot\boldsymbol{p}_0 \neq 0$ couples to the zero-mode and carries its "charge," which induces an $1/r$ "electric" field of the zero-mode and gives rise to a diverging energy gap $\Delta \sim \ln L$,

where L is the system size. In comparison, a topological excitation that satisfies $\boldsymbol{\ell}\cdot\boldsymbol{p}_0 = 0$ is decoupled from the zero-mode and hence has a finite energy gap and short ranged interactions. These EM-neutral topological excitations are thus analogous to the (possibly fractionalized) quasiparticles in quantum Hall systems, and it is sensible to consider the (mutual) statistics between them.

Recall that the set of $\boldsymbol{\ell}$-vectors (which may have non-zero α-component) form an eleven dimensional vector space. The set of $\boldsymbol{\ell}$-vectors satisfying $\boldsymbol{\ell}\cdot\boldsymbol{p}_0 = 0$ forms a ten dimensional subspace of this eleven dimensional space. The K-matrix restricted to this subspace, K_r, is invertible. Hence we can integrate out the gauge fields associated with this subspace (i.e., the gauge fields $c'_1, \ldots, c'_{10}$ in Eq. (4.14)). This will convert the terms we omitted in Eq. (4.14) under the texts "terms without c'_0" into a Hopf term. Explicitly, upon integrating out $c'_1, \ldots, c'_{10}$ the Lagrangian takes the form:

$$\begin{aligned}\mathcal{L}'' &= \frac{e}{2\pi}(\boldsymbol{q}\cdot\boldsymbol{p}_0)\epsilon c'_0\partial A + (\boldsymbol{\ell}\cdot\boldsymbol{p}_0)c'_{0\mu}j_V^\mu + g\partial c'_0\partial c'_0 + \ldots \\ &\quad + \pi(\widetilde{\boldsymbol{j}}^T)^\mu K_r^{-1}\left(\frac{\epsilon_{\mu\nu\lambda}\partial^\nu}{\partial^2}\right)\widetilde{\boldsymbol{j}}^\lambda + \ldots \\ &= (\text{terms with } c'_0) + \pi(\widetilde{\boldsymbol{j}}^T)^\mu K_r^{-1}\left(\frac{\epsilon_{\mu\nu\lambda}\partial^\nu}{\partial^2}\right)\widetilde{\boldsymbol{j}}^\lambda + \ldots,\end{aligned} \tag{4.16}$$

(c.f. Eq. (4.5)), where $\widetilde{\boldsymbol{j}}^\mu = j_V^\mu\boldsymbol{\ell} + (e/2\pi)(\epsilon\partial A)^\mu\boldsymbol{q}$.

As in the quantum Hall case, from Eq. (4.16) the statistical phase θ when one quasiparticle described by $j_V^\mu\boldsymbol{\ell}$ winds around another described by $j'_V{}^\mu\boldsymbol{\ell}'$ can be read off as $\theta = 2\pi\boldsymbol{\ell}^T K_r^{-1}\boldsymbol{\ell}'$. For identical quasiparticles, $\theta/2$ gives the statistical phase when two such quasiparticles are exchanged.

For explicit computation a basis for $\boldsymbol{\ell}$-vectors for this ten-dimensional subspace must be specified. Naively one may simply choose this basis to be the set of eigenvectors of K having non-zero eigenvalues. This choice turns out to be inconvenient as some of the eigenvectors of K are non-integer while the quantization condition requires all $\boldsymbol{\ell}$ to be integer vectors. Hence, instead we shall use the following basis:

$$
\begin{aligned}
\boldsymbol{\ell}_1 &= (0;-1,1,0,0,\mathbb{O}_{1,2};\mathbb{O}_{1,4})^T\,,\\
\boldsymbol{\ell}_2 &= (0;-1,0,1,0,\mathbb{O}_{1,2};\mathbb{O}_{1,4})^T\,,\\
\boldsymbol{\ell}_3 &= (0;-1,0,0,1,\mathbb{O}_{1,2};\mathbb{O}_{1,4})^T\,,\\
\boldsymbol{\ell}_4 &= (0;\mathbb{O}_{1,4},\mathbb{O}_{1,2};0,0,1,-1)^T\,,\\
\boldsymbol{\ell}_5 &= (0;\mathbb{O}_{1,4},\mathbb{O}_{1,2};0,1,0,-1)^T\,,\\
\boldsymbol{\ell}_6 &= (0;\mathbb{O}_{1,4},\mathbb{O}_{1,2};1,0,0,-1)^T\,,\\
\boldsymbol{\ell}_7 &= (0;0,1,0,0,\mathbb{O}_{1,2};0,1,1,0)^T\,,\\
\boldsymbol{\ell}_8 &= (0;1,0,0,0,1,0;\mathbb{O}_{1,4})^T\,,\\
\boldsymbol{\ell}_9 &= (0;\mathbb{E}_{1,4},\mathbb{E}_{1,2};\mathbb{E}_{1,4})^T\,,\\
\boldsymbol{\ell}_{10} &= (-1;\mathbb{O}_{1,4},0,1;\mathbb{O}_{1,4})^T\,.
\end{aligned}
\tag{4.17}
$$

It can be shown that all integer $\boldsymbol{\ell}$-vectors satisfying $\boldsymbol{\ell}\cdot\boldsymbol{p}_0 = 0$ can be written as *integer* combinations of the above basis vectors. It should be remarked that $\boldsymbol{\ell}_1$ through $\boldsymbol{\ell}_6$ are indeed eigenvectors of K, with $\boldsymbol{\ell}_1$ through $\boldsymbol{\ell}_3$ having eigenvalue -1 and $\boldsymbol{\ell}_4$ through $\boldsymbol{\ell}_6$ having eigenvalue 2. However, $\boldsymbol{\ell}_7$ through $\boldsymbol{\ell}_{10}$ are not eigenvectors of K.

In this basis, K_r^{-1} takes the form:

$$
K_r^{-1} = \left(\begin{array}{ccc|cccc|ccc}
-2 & -1 & -1 & & & & -1 & 1 & & \\
-1 & -2 & -1 & & \mathbb{O}_{3,3} & & 0 & 1 & \mathbb{O}_{3,2} & \\
-1 & -1 & -2 & & & & 0 & 1 & & \\
 & & & 1 & 1/2 & 1/2 & 1/2 & 0 & & \\
 & \mathbb{O}_{3,3} & & 1/2 & 1 & 1/2 & 1/2 & 0 & \mathbb{O}_{3,2} & \\
 & & & 1/2 & 1/2 & 1 & 0 & 0 & & \\
-1 & 0 & 0 & 1/2 & 1/2 & 0 & 0 & 0 & 0 & 0 \\
\hline
1 & 1 & 1 & 0 & 0 & 0 & 0 & 0 & 0 & 0 \\
 & & & & & & 0 & 0 & 0 & 1 \\
 & \mathbb{O}_{2,3} & & & \mathbb{O}_{2,3} & & 0 & 0 & 1 & 1
\end{array}\right)\,.
\tag{4.18}
$$

Note that $\boldsymbol{\ell}_{10}$ contains a non-zero α-component and is thus unphysical. Moreover,

from our interpretation of a_5 and a_6 as arising from the physics of band bottoms, we expect a topological excitation in these two components to be much more energetically costly than those of the other matter fields. Hence we can also neglect $\boldsymbol{\ell}_8$ and $\boldsymbol{\ell}_9$. Thus only the top-left block of K_r^{-1} is relevant for the statistics of low-lying physical quasiparticle excitations. Henceforth we shall restrict the meaning "quasiparticle" to those whose $\boldsymbol{\ell}$-vector is an integer combination of $\boldsymbol{\ell}_1$ through $\boldsymbol{\ell}_7$.

From K_r^{-1} it can be seen that the system contains quasiparticles with non-trivial mutual statistics. In particular, *there there are fermions having semionic mutual statistics* (i.e., a phase factor of π when one quasiparticle winds around another), manifesting in, e.g., quasiparticles described by $\boldsymbol{\ell}_4$ and $\boldsymbol{\ell}_5$.

The self-statistics and mutual statistics of different quasiparticles can be understood intuitively. Recall that our system is constructed by coupling integer and fractional quantum Hall states via a common constraint gauge field α. If we assume that the different quantum Hall states are independent of each other, i.e., a "charge" in one matter-field component has trivial bosonic statistics with a "charge" in a different matter-field component, then *the statistics of these quasiparticles can be read off by considering their underlying constituents.* For example, since $\boldsymbol{\ell}_4$ and $\boldsymbol{\ell}_5$ overlaps in one $\nu = 1/2$ component, their mutual statistics is semionic. Similarly, since $\boldsymbol{\ell}_4$ overlaps with itself in two $\nu = 1/2$ components, its self-statistics is fermionic.[3] From this intuitive picture, it is evident that a "+1" in a spinon component in the $\boldsymbol{\ell}$-vector should be identified with a spinon excitation on top of the integer quantum Hall state that formed near the corresponding Dirac node, while a "+1" in a holon component in the $\boldsymbol{\ell}$-vector should be identified with *half-holon* excitation on top of the $\nu = 1/2$ quantum Hall state that formed near the corresponding band bottom. Similarly, a "−1" in a spinon (holon) component in the $\boldsymbol{\ell}$-vector should be identified as an anti-spinon (anti-half-holon). See Fig. 4-2 for illustration.

To discuss these quasiparticles further, it is useful to divide them into three classes. The first class consists of quasiparticles with spinon components only and will be re-

[3]For this intuitive picture to be accurate, the sign of the component must also be taken into account.

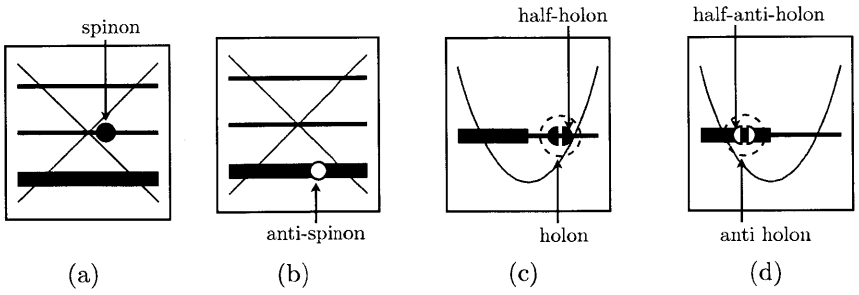

Figure 4-2: Physical interpretation of $\boldsymbol{\ell}$-vector: (a) a single "+1" in a spinon component identified as spinon; (b) a single "−1" in a spinon component identified as anti-spinon; (c) a single "+1" ("+2") in a holon component identified as half-holon (holon); and (d) a single "−1" ("−2") in a holon component identified as anti-half-holon (anti-holon). The thick (red) horizontal lines indicate filled LLs that forms the ground state of the system, while the thin (black) horizontal lines indicate unfilled LLs.

ferred to as "spinon quasiparticles" (SQP). The second class consists of quasiparticles with holon components only and will be referred to as "holon quasiparticles" (HQP). The remaining class consists of quasiparticles that have both spinon and holon components, and will be referred to as "mixed quasiparticles" (MQP). The first two classes can be constructed by compounding "elementary" quasiparticles of the same type. For SQP, the "elementary" quasiparticles are described by $\boldsymbol{\ell}$-vectors having exactly one "+1" component and one "−1" component in the spinon sector (e.g., the $\boldsymbol{\ell}_1, \boldsymbol{\ell}_2$, and $\boldsymbol{\ell}_3$ in Eq. (4.17)). For HQP, the "elementary" quasiparticles are described by $\boldsymbol{\ell}$-vectors having exactly one "+1" component and one "−1" component in the holon sector (e.g., the $\boldsymbol{\ell}_4, \boldsymbol{\ell}_5$, and $\boldsymbol{\ell}_6$ in Eq. (4.17)). As for the MQP, one can start with "minimal" quasiparticles with exactly one "+1" component in the spinon sector and one "+2" components in the holon sector, and build all MQP by compounding at least one such "minimal" quasiparticles together with zero or more "elementary" SQP and HQP. Alternatively, one may start with a second type of "minimal" quasiparticle in the MQP sector, which has exactly one "+1" component in the spinon sector and two "+1" components in the holon sector, and build all MQP by compounding at least one such "minimal" quasiparticles together with zero or more "elementary" SQP and HQP (note that the second-type of "minimal" MQP is simply a "minimal"

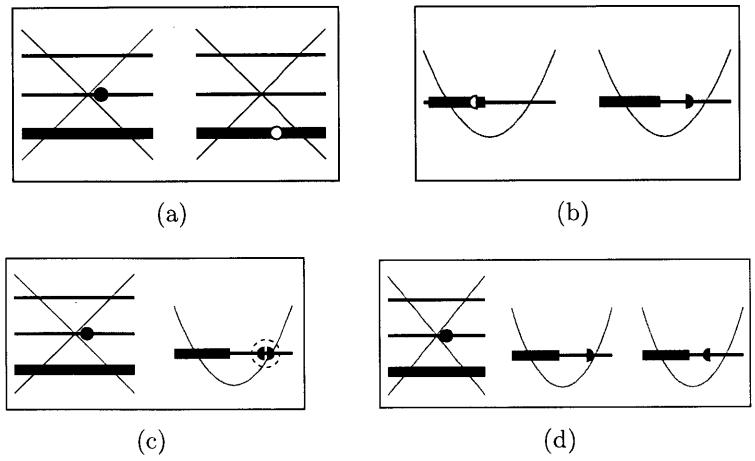

Figure 4-3: Visualization of the (a) "elementary" SQP; (b) "elementary" HQP; (c) "minimal" MQP of the first type; and (d) "minimal" MQP of the second type.

MQP of the first type compounded with an "elementary" HQP. The introduction of two different types of "minimal" MQP will be clear in the following).

These "elementary" and "minimal" quasiparticle excitations can be visualized in the following way: The "elementary" SQP can be visualized as a particle-hole excitation in the spinon quantum Hall levels, in which a spinon is removed from one Dirac node and added in another. The elementary HQP can be visualized as a particle-hole excitation in the holon quantum Hall levels, in which a *half* holon is transferred from one band bottom to another. The minimal MQP can be visualized as adding both spinon and (half) holons into the original system. See Fig. 4-3 for illustrations.

With this classification, the information on the self- and mutual- statistics of the quasiparticles contained in K_r^{-1} can be summarized more transparently in terms of the self- and mutual- statistics of the "elementary" SQP, "elementary" HQP, and "minimal" MQP. The result is presented in Table 4.1.

Table 4.1: Self- and mutual- statistics of the "elementary" and "minimal" quasiparticles in the doped kagomé system. The adjective "elementary" or "minimal" are omitted but assumed in the table entries. The subscript I and II indicates the type of "minimal" MQP considered (see the main text for their definitions). When an entry contain multiple cases, both cases are possible but are realized by different quasiparticles in the respective sectors.

Type	Self-Statistics[1]	Mutual Statistical Phase[2]			
		SPH	HPH	MQP_I	MQP_{II}
SQP	b	2π	2π	2π	2π
HQP	f	2π	π or 2π	2π	π or 2π
MQP_I	f	2π	2π	2π	2π
MQP_{II}	b	2π	π or 2π	2π	π or 2π

[1] b=bosonic, f=fermionic, s=semionic

[2] Phase angle accumulated when one quasiparticle winds around another, modulo 2π.

4.5 Quasiparticles—Quantum Numbers

Since the quasiparticles have finite energy gaps and short-ranged interactions, they may carry well-defined quantum numbers. In particular, it is sensible to consider the $\boldsymbol{k}$ quantum numbers for these quasiparticles, since they arise from LLs that form near Dirac points or band bottoms with well-defined crystal momentum $\boldsymbol{k}$. Similarly, it is sensible to consider the S_z quantum numbers for quasiparticles with spinon components. We shall see that this program can be carried out for "elementary" spinon quasiparticles and for the "minimal" mixed quasiparticles of first type, but not easily for the "elementary" holon quasiparticles and the "minimal" mixed quasiparticles of the second type.

Recall from Sec. 1.3.3 that the unit cell is doubled in the tight-binding model of the $U(1)$ DSL state, because a flux of π is enclosed within the original unit cell, which causes the translation operators that correspond to different lattice vectors fail to commute (c.f. Eq. (1.21)). Consequently, let T_{a_1} and T_{a_2} to be the translation operator that corresponds to the lattice vectors $\boldsymbol{a}_1$ and $\boldsymbol{a}_2$ as defined in Fig. 1-4, the single-spinon and single-holon states in the $U(1)$ DSL ansatz generally form multi-dimensional irreducible representations under the joint action of T_{a_1} and T_{a_2} (i.e.,

T_{a_1} and T_{a_2} manifest as multi-dimensional matrices that cannot be simultaneously diagonalized when acting on these states), and cannot be labeled simply by a pair of numbers (c_1, c_2) as in the ordinary case[4]. Furthermore, the matrices for T_{a_1} and T_{a_2} will in general be *α-gauge-dependent.* However, when an even number of spinon and holon excitations are considered as a whole, the total phase accumulated when the particles circle around the original unit cell becomes a multiple of 2π, and thus $[T_{a_1}, T_{a_2}] = 0$ *in such subspace.* Hence it is possible to reconstruct the crystal momentum in the original Brillouin zone via projective symmetry group if our attention is restricted to such states. Physically, the gauge dependence of single-spinon and single-holon states indicate that they cannot be created *alone.*

It can be checked that all SQP are composed of an even number of spinons and anti-spinons. The above discussion then implies that they carry well-defined $\boldsymbol{k}$ quantum numbers in the original Brillouin zone. To derive the transformational properties under T_{a_1} and T_{a_2}, we compute the transformation properties of the original spinon matter fields. The procedures for doing so have been described in details in Ref. [74], here we shall just state the results.

Let $\eta_1, \ldots, \eta_4$ denote the topological excitations near the four (two $\boldsymbol{k}$-vectors and two spins) Dirac nodes as indicated in Fig. 4-4(a). Then, assuming that they have the same transformational properties as the underlying spinon fields at the same Dirac nodes,

$$\begin{aligned}
T_{a_1}[\eta_1] &= e^{i\pi/12}\eta_2\,, \quad & T_{a_2}[\eta_1] &= e^{i\pi/2}\eta_1\,,\\
T_{a_1}[\eta_2] &= e^{11i\pi/12}\eta_1\,, \quad & T_{a_2}[\eta_2] &= e^{-i\pi/2}\eta_2\,,\\
T_{a_1}[\eta_3] &= e^{i\pi/12}\eta_4\,, \quad & T_{a_2}[\eta_3] &= e^{i\pi/2}\eta_3\,,\\
T_{a_1}[\eta_4] &= e^{11i\pi/12}\eta_3\,, \quad & T_{a_2}[\eta_4] &= e^{-i\pi/2}\eta_4\,.
\end{aligned} \tag{4.19}$$

Furthermore, we assume that T_{a_1} and T_{a_2} satisfy the generic conjugation and composition laws:

$$T[\psi^*] = (T[\psi])^*\,, \quad T[\psi\cdot\psi'] = T[\psi]\cdot T[\psi']\,. \tag{4.20}$$

[4]In the ordinary case, (c_1, c_2) are simply eigenvalues of T_{a_1} and T_{a_2}, respectively, and are related to the crystal momentum $\boldsymbol{k}$ in the *original* Brillouin zone via $\exp(i\boldsymbol{k}\cdot\hat{x}) = c_1$ and $\exp(i\boldsymbol{k}\cdot\boldsymbol{r}_2) = c_2$.

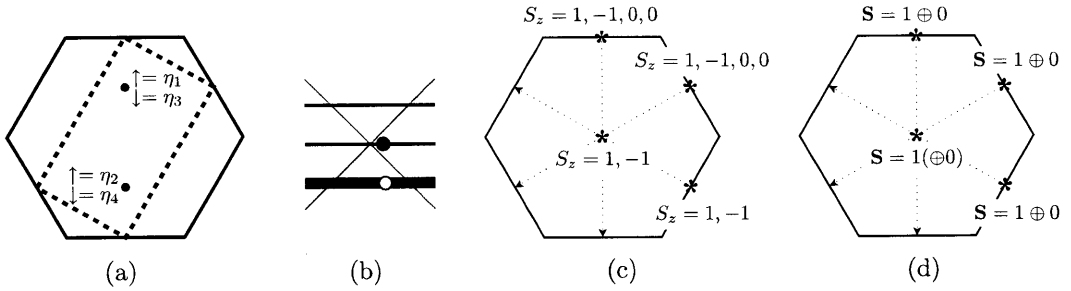

Figure 4-4: (a) The labels for the four spinon topological excitations. (b) Physical interpretation of the "missing states" in the fixed S_z quantization and doubled unit cell Chern–Simons formulation. (c) Spectrum of "elementary" SQP, with $\boldsymbol{k}$ and S_z quantum number indicated, before restoring full symmetry. (d) Spectrum of "elementary" SQP after restoring the SU(2) symmetry by adding extra quasiparticles. The dotted arrows indicate equivalent $\boldsymbol{k}$-point upon translation by the *original* reciprocal lattice vectors (spanned by $2\boldsymbol{k}_1$ and $\boldsymbol{k}_2$ in Fig. 1-6(b)). For dimension of the Brillouin zone, c.f. Fig. 1-6(b).

where ψ, ψ' denotes generic quasiparticle states, ψ^* denotes an anti-particle of ψ, and $\psi \cdot \psi'$ denotes a bound state composed of ψ and ψ'.

A general basis for "elementary" SQP is spanned by $\eta_i \eta_j^*$ with $i \neq j$. There are twelve distinct "elementary" SQP, which form six *reducible* representations under T_{a_1} and T_{a_2}. Upon diagonalization, the resulting "elementary" SQP in the new basis each carry distinct S_z and $\boldsymbol{k}$ (in the original Brillouin zone) quantum numbers. These are summarized in Fig. 4-4(c).

Notice that Fig. 4-4(c) is somewhat unsettling. First, even though we have not performed a PSG study on rotation operators, intuition on rotation symmetry suggests that there should be four states (with $S_z = 1, -1, 0,$ and 0) located at $\boldsymbol{k} = (\pi, -\pi/\sqrt{3})$. Second, although our Chern–Simons theory is formulated with a fixed quantization axis for spin, the $SU(2)$ spin-rotation symmetry should remain unbroken. Therefore, the S_z eigenvalues should organize into $SU(2)$ representations for each $\boldsymbol{k}$ value. While this is true for $\boldsymbol{k} = (\pi, \pi/\sqrt{3})$ and $\boldsymbol{k} = (0, 2\pi/\sqrt{3})$, where the "elementary" SQP form $1 \oplus 0$ representations, the same does not hold for $\boldsymbol{k} = (\pi, -\pi/\sqrt{3})$ and $\boldsymbol{k} = (0, 0)$.

The two issues mentioned above indicate that some topological excitations are

lost in our formulation. In other words, *there are topological excitations that have trivial S_z quantum numbers but non-trivial $\boldsymbol{S}$ quantum numbers. Similarly, there are topological excitations that have trivial $\boldsymbol{k}$ quantum numbers in the reduced Brillouin zone but non-trivial $\boldsymbol{k}$ quantum numbers in the original Brillouin zone.* Physically, the original of these missing excitations can be understood as follows: in the hydrodynamic approach, an $\boldsymbol{\ell}$-vector with a single "+1" in a spinon component represent a spinon at a Dirac node, while $\boldsymbol{\ell}$-vector with a single "−1" in a spinon component represent an anti-spinon at a Dirac node. The previously defined set of $\boldsymbol{\ell}$-vectors that characterized the "elementary" SQP fail to captured an excitonic state in which a spinon is excited from a filled LL to an empty LL, thus leaving an anti-spinon behind (see Fig. 4-4(b) for an illustration), which precisely carry trivial S_z quantum numbers and transform trivially under T_{r1} and T_{a_2}. Note that there are four possible excitonic states of this form, hence we expect four states to be added. In our Chern–Simons formulation, these excitations may be disguised as combinations of density operators ($\sim \partial \boldsymbol{c}$).

From Fig. 4-4(c) and the forgoing discussions, it is evident that extra states should be added at $\boldsymbol{k} = (\pi, \pi/\sqrt{3})$ and $\boldsymbol{k} = (0,0)$, so that the states at $\boldsymbol{k} = (0,0)$ and $\boldsymbol{k} = (\pi, \pi/\sqrt{3})$ each form a $1 \oplus 0$ representation of $SU(2)$. The final result after making this reparation is shown in Fig. 4-4(c). Formally, the same result can be reached if we allow objects of the form $\eta_i \eta_i^*$ to be counted as elementary SQP, then apply Eq. (4.19) and the procedure of diagonalization as before in this extended basis.

Observe that the "elementary" spinon SQP (and hence the entire SQP sector) all carry integer spins. However, we also know that a conventional superconductor contains spin-1/2 fermionic excitations (i.e., the Bogoliubov quasiparticles). From our assignment of S_z quantum number and from the table of quasiparticle statistics Table 4.1, it is evident that the "minimal" MQP of the first type play the role the these Bogoliubov quasiparticles in the doped kagomé system. In contrast, minimal MQP of the second type are *spin-1/2 quasiparticles that carry bosonic statistics* and hence is another distinctive signatures of this exotic superconductor.

Since a "minimal" MQP of the first type can be treated as a bound state of a

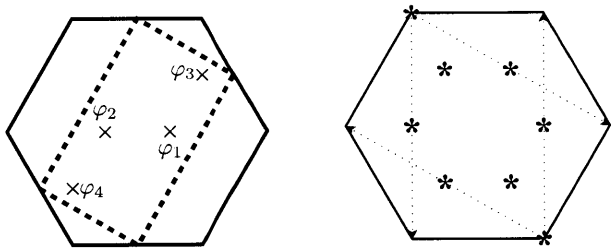

Figure 4-5: (a) The labels for the four holon excitations. (b) Spectrum of "elementary" MQP of the first type, with $\boldsymbol{k}$ quantum number indicated. Each point in $\boldsymbol{k}$ space forms a $\boldsymbol{S} = 1/2$ representation in spin. The dotted arrows indicate equivalent $\boldsymbol{k}$-point upon translation by the *original* reciprocal lattice vectors.

spinon and a holon (c.f. Fig. 4-3(c)), the $\boldsymbol{k}$ quantum number in the original Brillouin zone are again well-defined for them. To construct their quantum numbers, we need to know how holons transform under T_{a_1} and T_{a_2}. Let $\varphi_1, \ldots, \varphi_4$ denotes the *half-holon* excitations near the four holon band bottom as indicated in Fig. 4-4(a), such that $\varphi_1^2, \ldots, \varphi_4^2$ denotes the corresponding *holon* excitations (c.f. Fig. 4-2(c)). Following the same procedure that produces Eq. (4.19), we obtain the transformation laws:

$$\begin{aligned}
T_{a_1}[\varphi_1^2] &= \varphi_4^2\,, & T_{a_2}[\varphi_1^2] &= e^{i\pi/6}\varphi_1^2\,,\\
T_{a_1}[\varphi_2^2] &= \varphi_3^2\,, & T_{a_2}[\varphi_2^2] &= e^{-i\pi/6}\varphi_2^2\,,\\
T_{a_1}[\varphi_3^2] &= e^{-i\pi/3}\varphi_2^2\,, & T_{a_2}[\varphi_3^2] &= e^{5i\pi/6}\varphi_3^2\,,\\
T_{a_1}[\varphi_4^2] &= e^{i\pi/3}\varphi_1^2\,, & T_{a_2}[\varphi_4^2] &= e^{-5i\pi/6}\varphi_4^2\,.
\end{aligned} \tag{4.21}$$

A general basis for "minimal" MQP of the first type is spanned by $\eta_i\varphi_j^2$. There are sixteen distinct first-type "minimal" MQP, which form eight *reducible* representations under T_{a_1} and T_{a_2}. Upon diagonalization, the resulting first-type "minimal" MQP in the new basis each carry distinct S_z and $\boldsymbol{k}$ (in the original Brillouin zone) quantum numbers, and the full $SU(2)$ representation in spin can be recovered trivially by combining spin-up and spin-down states. The final results are summarized in Fig. 4-5(b).

Having considered the SQP sector and the "minimal" MQP of the first type, one

may attempt to carry out similar analysis for the HQP sector and for the "minimal" MQP of the second type. However, in doing so, issues arise from the fractionalization of holons into half-holons. Recall that in deriving the transformational rules of the quasiparticles, we identify the components of $\boldsymbol{\ell}$ as being spinon and holon excitations, and assume that these excitations carry the same quantum numbers as the underlying spinons and holons that form the LLs in the first place. However, the HQP sector and the "minimal" MQP of the second type are bound states that involve *half-holons*, whose quantum numbers cannot be directly inferred from the underlying spinons and holons. More concretely, we need to know the transformation laws $T[\varphi_i\varphi_j^*]$ for half-holon–anti-half-holon pairs $\varphi_i\varphi_j^*$ in order to construct their quantum numbers, but we only have information about transformation laws $T[\varphi_j^2]$ of holon excitation φ_j^2.

It is far from clear how $T[\varphi_i\varphi_j^*]$ can be related to $T[\varphi_j^2]$. The answer for such question may even be non-unique. We have already seen an analogous situation in the forgoing discussion: while the spinon–anti-spinon pairs $\eta_i\eta_j^*$ have well-defined gauge-invariant $\boldsymbol{k}$ quantum numbers in the original Brillouin zone, the single spinons η_i form gauge-dependent two-dimensional representations under T_{a_1}.

The possible ambiguity in the transformation law $T[\varphi_i\varphi_j^*]$ of half-holon–anti-half-holon pairs $\varphi_i\varphi_j^*$ signifies that it may not be possible to produce these quasiparticles *alone*. Although a half-holon–anti-half-holon pair can be thought of as resulted from removing a half-holon from one band bottom and adding one in another, it is not clear that the process can be done in via single half-holon tunneling. This is analogous to the case when two fractional quantum Hall system are separated by a constriction, where it is only possible to tunnel physical electrons.[100]

Combining the results from Sect. 4.4 and 4.5, we see that there are two very different class of quasiparticle excitations in the doped kagome system—which can be termed as "conventional" and "exotic," respectively. The "conventional" class consists of quasiparticles that can be created alone, which carry well-defined crystal momentum $\boldsymbol{k}$ in the original Brillouin zone and possess conventional (fermionic or bosonic) statistics. These include the spinon particle-holes, the holon (but not half-holon) particle-holes, the "minimal" mixed quasiparticles of the first type (a.k.a. the

"Bogoliubov quasiparticles"), and their composites. It should be noted that these "conventional" quasiparticles can all be considered as descendants of the "Bogoliubov quasiparticles." Indeed, it can be checked that the spinon particle-holes shown in Fig. 4-4(d) can be obtained by compounding the appropriate "Bogoliubov quasiparticles" (and their antiparticles) that appears in Fig. 4-5(b).

In contrast, the "exotic" class consists of quasiparticle that cannot be created alone, whose crystal momentum may not be well-defined, and whose statistics may be fractional. These include the half-holon particle-holes and the "minimal" mixed quasiparticles of the second type (which are "Bogoliubov quasiparticles" dressed with a half-holon particle-hole). In terms of the *underlying electronic system*, the former class are excitations that are *local* in terms of the *underlying* electron operators c and $c^\dagger$, while the latter class are excitations that are *non-local* in terms of c and $c^\dagger$.

It should be warned that questions regarding the energetics (and hence stability) of the quasiparticles have not been touched in Sect. 4.4 and 4.5. In particular, it is not clear whether the bosonic or the fermionic spin-1/2 excitation has a lower energy. Though this information is in principle contained in the Maxwell term Eq. (3.6), to obtain it requires a detailed consideration of the short-distance physics in the t–J model, and is beyond the scope of this thesis.

4.6 An alternative derivation by eliminating the auxiliary field

It is a curious result that in Eq. (4.18), once the unphysical $\boldsymbol{\ell}_{10}$ is removed from the spectrum, the quasiparticle represented by $\boldsymbol{\ell}_9$ becomes purely bosonic (i.e., having trivial bosonic mutual statistics with all other quasiparticles and trivial bosonic self-statistics). This suggests that $\boldsymbol{\ell}_9$ corresponds to some local density excitation of the system and thus should not be regarded as topological. Moreover, the procedure of first treating $\boldsymbol{\ell}_{10}$ as part of the spectrum in computing K_r^{-1} and then removing this degree of freedom at the very end of the calculation seems somewhat dubious. Recall

that the gauge field α^μ is introduced to enforce the occupation constraint Eq. (1.18). This gauge field is thus an *auxiliary* field that is void of self-dynamics (i.e., the term $\epsilon\alpha\partial\alpha$ vanishes) and topologically trivial (i.e., the α-component of $\boldsymbol{\ell}$ must be zero). Therefore, one may attempt to *re-derive the previous results by eliminating this α field right at the beginning by enforcing the constraint directly.* This can indeed be done, as we shall show in the following.

Recall that the EOM with respect to α^μ leads to the constraint equation Eq. (4.12) in the Chern–Simons formulation. From this, one may argue that *the effect of introducing the α field can alternatively be produced by setting $\sum_I a_I^\mu + \sum_J b_J^\mu = 0$ directly.* To do so, we perform a two-step transformation on the Lagrangian Eq. (4.7). First, we set:

$$a_6'^{\,\mu} = \sum_I a_I^\mu \qquad \text{and} \qquad a_I'^{\,\mu} = a_I^\mu \text{ for } I \neq 6\,; \tag{4.22}$$

$$b_1'^{\,\mu} = \sum_J a_J^\mu \qquad \text{and} \qquad b_J'^{\,\mu} = b_J^\mu \text{ for } J \neq 1\,. \tag{4.23}$$

Then the constraint becomes $a_6'^{\,\mu} + b_1'^{\,\mu} = 0$, which we enforce directly by setting:

$$\rho^\mu = -a_6'^{\,\mu} = b_1'^{\,\mu}\,, \tag{4.24}$$

thus eliminating one variable.

Note that since the α field appears in Eq. (4.7) only through the term $\epsilon(\sum_I a_I + \sum_J b_J)\partial\alpha$, it got dropped out of the transformed Chern–Simons Lagrangian. Letting $\tilde{\boldsymbol{c}} = (\rho; a_1', \ldots, a_5'; b_2', \ldots, b_4')$, which is a column vector of only nine (as opposed to eleven) gauge fields, Eq. (4.7) becomes:

$$\mathcal{L} = \frac{1}{4\pi}\epsilon\tilde{\boldsymbol{c}}^T\tilde{K}\partial\tilde{\boldsymbol{c}} - \frac{e}{2\pi}\epsilon(\tilde{\boldsymbol{q}}\cdot\tilde{\boldsymbol{c}})\partial A + (\tilde{\boldsymbol{\ell}}\cdot\tilde{\boldsymbol{c}})_\mu j_V^\mu + \ldots\,, \tag{4.25}$$

where $\tilde{\boldsymbol{q}} = (1; \mathbb{O}_{1,5}; \mathbb{O}_{1,3})^T$ is the transformed charge vector, and $\tilde{K}$ is the transformed

K-matrix:

$$\tilde{K} = \left(\begin{array}{c|ccccc|ccc} 3 & 1 & 1 & 1 & 1 & 1 & -2 & -2 & -2 \\ \hline 1 & 0 & 1 & 1 & 1 & 1 & & & \\ 1 & 1 & 0 & 1 & 1 & 1 & & & \\ 1 & 1 & 1 & 0 & 1 & 1 & \multicolumn{3}{c}{\mathbb{O}_{5,3}} \\ 1 & 1 & 1 & 1 & 0 & 1 & & & \\ 1 & 1 & 1 & 1 & 1 & 2 & & & \\ \hline -2 & & & & & & 4 & 2 & 2 \\ -2 & \multicolumn{5}{c}{\mathbb{O}_{3,5}} & 2 & 4 & 2 \\ -2 & & & & & & 2 & 2 & 4 \end{array}\right) \tag{4.26}$$

As for topological excitations, from the transformation between $\boldsymbol{c}$ and $\tilde{\boldsymbol{c}}$, it can be seen that the correspondence between $\boldsymbol{\ell}$ and $\tilde{\boldsymbol{\ell}}$ reads:

$$\begin{aligned} \boldsymbol{\ell} &= (0; n_{a1}, \ldots n_{a6}; n_{b1}, \ldots n_{b4})^T \\ &\Updownarrow \\ \tilde{\boldsymbol{\ell}} &= (n_{b1} - n_{a6}; n_{a1} - n_{a6}, \ldots, n_{a5} - n_{a6}; \\ &\quad n_{b2} - n_{b1}, \ldots, n_{b4} - n_{b1})^T \end{aligned} \tag{4.27}$$

Hence, $\boldsymbol{\ell}$ is an integer vector if and only if $\tilde{\boldsymbol{\ell}}$ is also an integer vector. Moreover, from Eq. (4.27) it can be seen that $\boldsymbol{\ell}_9$ is mapped to $\tilde{\boldsymbol{\ell}} = \mathbf{0}$, which is consistent with our previous argument that the quasiparticle corresponding to $\boldsymbol{\ell}_9$ is purely bosonic and hence should be considered as non-topological.[5]

Although K and $\tilde{K}$ look rather different superficially,[6] all the major conclusions from Sect. 4.3–4.5 can be reproduced with $\tilde{K}$. In particular, we shall check that the existence of a single gapless mode, the $hc/4e$ flux through a minimal vortex, and the semionic quasiparticle statistics can all be obtained from $\tilde{K}$.

It is easy to check that $\tilde{K}$ has exactly one zero eigenvalue, with $\tilde{\boldsymbol{p}}_0 = (4; -2\mathbb{E}_{1,4}, 2; \mathbb{E}_{1,3})^T$ its eigenvector. Using the transformation equations Eqs. (4.22)–(4.24), we see that

[5]More generally, given $\tilde{\boldsymbol{\ell}}$ in the transformed basis, the corresponding $\boldsymbol{\ell}$ is determined up to multiples of $\boldsymbol{\ell}_9$.

[6]It can even be checked that K contains irrational eigenvalues that are *not* eigenvalues of $\tilde{K}$.

this eigenvector corresponds precisely to the eigenvector $\boldsymbol{p}_0$ we found in Sect. 4.3. Thus, again we conclude that the system contains a gapless mode associated with superconductivity, and that this gapless mode can be interpreted as fluctuations of all spinons and holons species whose ratio is matched (through their common coupling to the gauge field α^μ).

Moreover, the amount of magnetic flux that passes through a physical vortex is still described by Eq. (4.15) upon the obvious modifications. Since $\tilde{\boldsymbol{q}} \cdot \tilde{\boldsymbol{p}}_0 = 4$, we recover the conclusion that a minimal physical vortex carries a flux of $hc/4e$. Furthermore, it can be checked that $\boldsymbol{\ell} \cdot \boldsymbol{p}_0 = \tilde{\boldsymbol{\ell}} \cdot \tilde{\boldsymbol{p}}_0$ for $\boldsymbol{\ell}$, $\tilde{\boldsymbol{\ell}}$ satisfying the correspondence Eq. (4.27). Hence the flux carried by a vortex calculated from $\tilde{K}$ agrees with the value calculated from K.

As before, the quasiparticle excitations (which are EM-neutral, short-ranged interacting, and have finite energy gaps) are characterized by the condition that $\tilde{\boldsymbol{\ell}} \cdot \tilde{\boldsymbol{p}}_0 = 0$, which defines an eight-dimensional subspace of the nine-dimensional space in this case. The K-matrix restricted to this subspace, $\tilde{K}_r$, is invertible. We may choose a basis for this subspace that corresponds to the basis choice Eq. (4.17) in the original representation. Explicitly,

$$\begin{aligned}
\tilde{\boldsymbol{\ell}}_1 &= (0; 0, -1, 1, 0, 0; \mathbb{O}_{1,3})^T \\
\tilde{\boldsymbol{\ell}}_2 &= (0; 0, -1, 0, 1, 0; \mathbb{O}_{1,3})^T \\
\tilde{\boldsymbol{\ell}}_3 &= (0; 0, -1, 0, 0, 1; \mathbb{O}_{1,3})^T \\
\tilde{\boldsymbol{\ell}}_4 &= (0; 0, \mathbb{O}_{1,4}; 0, 1, -1)^T \\
\tilde{\boldsymbol{\ell}}_5 &= (0; 0, \mathbb{O}_{1,4}; 1, 0, -1)^T \\
\tilde{\boldsymbol{\ell}}_6 &= (1; 0, \mathbb{O}_{1,4}; -1, -1, -2)^T \\
\tilde{\boldsymbol{\ell}}_7 &= (0; 0, 0, 1, 0, 0; 1, 1, 0)^T \\
\tilde{\boldsymbol{\ell}}_8 &= (0; 1, 1, 0, 0, 0; \mathbb{O}_{1,3})^T
\end{aligned} \tag{4.28}$$

Then, it can be checked that:

$$\tilde{K}_r^{-1} = \begin{pmatrix} -2 & -1 & -1 & & & & -1 & 1 \\ -1 & -2 & -1 & & \mathbb{O}_{3,3} & & 0 & 1 \\ -1 & -1 & -2 & & & & 0 & 1 \\ & & & 1 & 1/2 & 1/2 & 1/2 & 0 \\ & \mathbb{O}_{3,3} & & 1/2 & 1 & 1/2 & 1/2 & 0 \\ & & & 1/2 & 1/2 & 1 & 0 & 0 \\ -1 & 0 & 0 & 1/2 & 1/2 & 0 & 0 & 0 \\ 1 & 1 & 1 & 0 & 0 & 0 & 0 & 0 \end{pmatrix} \tag{4.29}$$

in agreement with the results in Sect. 4.4.

4.7 Discussions

In this chapter we have considered the theory of a doped spin-1/2 kagomé lattice described by the t–J model. We start with the slave-boson theory and the assumption that the undoped system is described by the $U(1)$ Dirac spin liquid, from which we argued that the doped system is analogous to a coupled quantum Hall system, with the role of the external magnetic field in the usual case taken up by an emergent gauge field α. The analogy with quantum Hall systems compels us to introduce the Chern–Simons theory as an effective description of the low-energy physics of the system. This allows us to describe the superconductivity, the physical vortices, and the electromagnetically neutral quasiparticles in a unified mathematical framework. We show that there are two alternative Chern–Simons theories that produce identical results—one with the auxiliary field α kept until the end, and the other with the auxiliary field and a redundant dual matter field eliminated at the beginning.

In our scenario, the coupled quantum Hall system consists of four species of spinons and four species of holons at low energy. We show that such system exhibit superconductivity and that the flux carried by a minimal vortex is $hc/4e$. The system also contains fermionic quasiparticles with semionic mutual statistics, and bosonic spin-1/2

quasiparticle. As for the quantum numbers carried by the quasiparticles, we analyzed the spinon sector in details and found that it is possible to recover the full $SU(2)$ and (un-enlarged) lattice symmetry of the "elementary" quasiparticles in this sector, upon the inclusion of quasiparticles that are not easily represented in the original fixed-spin-quantization-axis, enlarged-unit-cell description. The same classification of quantum numbers are also carried out for the spin-1/2 fermionic quasiparticles, which are the analog of Bogoliubov quasiparticles in our exotic superconductor.

In this chapter we have argued that the doped spin-1/2 kagomé system may exhibit exotic superconductivity that is higher unconventional. However, it should be remarked we have presented only one possible scenario for the doped kagomé system. For example, it is possible that the ground state of the undoped system is a valence bond solid and hence invalidate our analysis. Furthermore, experimentally realizing the idealized system considered considered in this chapter may involve considerable difficulties. For instance, in the case of Herbertsmithite, it is known that the substitution between Cu and Zn atoms can be as big as 5%. It is our hope that this chapter will generate further interests in the doped spin-1/2 kagomé system, as well as other systems that may exhibit analogous exotic superconducting mechanisms, both experimentally and theoretically.

Chapter 5

Conclusions

While the works presented in this thesis focus specifically on the $U(1)$ Dirac spin liquid state in the spin-1/2 kagome lattice and its descendants, they do illustrate the great potential offered by geometrically frustrated low-dimensional systems in realizing exotic phases of condensed matter that are accessible to experimental studies.

It is important to note that much of the unusual properties of the $U(1)$ DSL state arise from the exotic elementary excitations that it carries—these include the spinons, the holons, and most important the emergent gauge field. In Raman scattering, the spinons (and their antiparticles) are responsible for the broad continua that vanish as power laws at low energies, while the emergent gauge field is responsible for a characteristic $1/\omega$ singularity. In the cases where an external magnetic field is applied or where the system is doped, the emergent gauge field causes Landau levels to open up in the spinon spectrum, and lead to an XY-ordered state and an exotic superconductor, respectively.

Given the interesting physics that may manifest in the $U(1)$ DSL state, it may be a worthwhile pursue to consider other situations in which the emergent gauge field may play a predominant role. And as my works on the effects of external magnetic field and doping on the $U(1)$ DSL state illustrates, the emergent gauge field may continue to dictate the physical behavior of the system even if it is perturbed away from a spin liquid state. Consequently, it may be fruitful to extend our investigation to phases that are derived from the spin liquid state. As in the case where the

$U(1)$ DSL state is doped, such phases can exhibit exotic behaviors (e.g., semionic quasiparticles) that are hidden under conventional ones (e.g., superconductivity). It is the hope of the author of the present thesis that such investigations will eventually lead to the discovery of other theoretical models with interesting physical properties that would, with the increasing sophistication of experimental techniques, be realized in actual materials.

Bibliography

[1] P. Hohenberg and W. Kohn, "Inhomogeneous electron gas," Phys. Rev., **136**, B864 (1964).

[2] W. Kohn and L. J. Sham, "Self-consistent equations including exchange and correlation effects," Phys. Rev., **140**, A1133 (1965).

[3] Richard M. Martin, "Electronic Structure: Basic Theory and Practical Methods," (Cambridge University Press, 2004) Chap. 6–9.

[4] Thierry Giamarchi, "Quantum Physics in One Dimension," (Oxford University Press, 2003).

[5] Sin itiro Tomonaga, "Remarks on Bloch's method of sound waves applied to many-fermion problems," Prog. Theor. Phys., **5**, 544 (1950).

[6] F. D. M. Haldane, " 'Luttinger liquid theory' of one-dimensional quantum fluids," J. Phys. C, **14**, 2585 (1981).

[7] K Schönhammer, "The Luttinger liquid concept for interacting electrons in one dimension," J. Phys. C, **14**, 12783 (2002).

[8] Steven R. White, "Density matrix formulation for quantum renormalization groups," Phys. Rev. Lett., **69**, 2863 (1992).

[9] U. Schollwock, "The density-matrix renormalization group," Rev. Mod. Phys., **77**, 259 (2005).

[10] N. F. Mott, "The basis of the electron theory of metals, with special reference to the transition metals," Proc. R. Soc. Lond. A, **62**, 416 (1949).

[11] Assa Auerbach, "Interacting Electrons and Quantum Magnetism," (Springer-Verlag New York, 1994) Chap. 3.

[12] Robert M. White, "Quantum Theory of Magnetism: Magnetic Properties of Materials," (Springer-Verlag Berlin Heidelberg, 2007) Chap. 2, 3rd ed.

[13] Assa Auerbach, "Interacting Electrons and Quantum Magnetism," Springer-Verlag New York, 1994) Chap. 11.

[14] Charles Kittel, "Introduction to Solid State Physics," chapter 15, table 3. (John Wiley and Sons, 1996) Chap. 15, table 3, 7th ed.

[15] C. G. Shull, W. A. Strauser, and E. O. Wollan, "Neutron diffraction by paramagnetic and antiferromagnetic substances," Phys. Rev., **83**, 333 (1951).

[16] Harden M. McConnell and Ruth Lynden-Bell, "Paramagnetic excitons in solid free radicals," J. Chem. Phys., **36**, 2393 (1962).

[17] D. D. Thomas, H. Keller, and H. M. McConnell, "Exciton magnetic resonance in wurster's blue perchlorate," J. Chem. Phys., **39**, 2321 (1963).

[18] P. W. Anderson, "Resonating valence bonds: A new kind of insulator?" Materials Research Bulletin, **8**, 153 (1973).

[19] G. Baskaran, Z. Zou, and P. W. Anderson, "The resonating valence bond state and high-T_c superconductivity—a mean field theory," Solid State Commun., **63**, 973 (1987).

[20] Luca Capriotti, Adolfo E. Trumper, and Sandro Sorella, "Long-range Néel order in the triangular Heisenberg model." Phys. Rev. Lett., **82**, 3899 (1999).

[21] P. W. Anderson, "The resonating valence bond state in La_2CuO_4 and superconductivity," Science, **235**, 1196 (1987).

[22] Y. Kurosaki, Y. Shimizu, K. Miyagawa, K. Kanoda, and G. Saito, "Mott transition from a spin liquid to a Fermi liquid in the spin-frustrated organic conductor κ-$(ET)_2Cu_2(CN)_3$," Phys. Rev. Lett., **95**, 177001 (2005).

[23] Satoshi Yamashita, Yasuhiro Nakazawa, Masaharu Oguni, Yugo Oshima, Hiroyuki Nojiri, Yasuhiro Shimizu, Kazuya Miyagawa, and Kazushi Kanoda, "Thermodynamic properties of a spin-1/2 spin-liquid state in a κ-type organic salt," Nat. Phys., **4**, 459 (2008).

[24] T. Itou, A. Oyamada, S. Maegawa, M. Tamura, and R. Kato, "Quantum spin liquid in the spin-1/2 triangular antiferromagnet $EtMe_3Sb[Pd(dmit)_2]_2$," Phys. Rev. B, **77**, 104413 (2008).

[25] Yoshihiko Okamoto, Minoru Nohara, Hiroko Aruga-Katori, and Hidenori Takagi, Spin-liquid state in the $S = 1/2$ hyperkagome antiferromagnet $Na_4\ Ir_3O_8$," Phys. Rev. Lett., **99**, 137207 (2007).

[26] Matthew P. Shores, Emily A. Nytko, Bart M. Bartlett, and Daniel G. Nocera, "A structurally perfect $S = 1/2$ kagome antiferromagnet," J. Am. Chem. Soc., **127**, 13462 (2005).

[27] J. S. Helton, K. Matan, M. P. Shores, E. A. Nytko, B. M. Bartlett, Y. Yoshida, Y.and Takano, A. Suslov, Y. Qiu, J.-H. Chung, D. G. Nocera, and Y. S. Lee, "Spin dynamics of the spin-1/2 kagome lattice antiferromagnet $ZnCu_3(OH)_6Cl_2$," Phys. Rev. Lett., **98**, 107204 (2007).

[28] Yoshihiko Okamoto, Hiroyuki Yoshida, and Zenji Hiroi, "Vesignieite $BaCu_3V_2O_8(OH)_2$ as a candidate spin-1/2 kagome antiferromagnet," J. Phys. Soc. Jpn., **78**, 033701 (2009).

[29] Olexei I. Motrunich, "Orbital magnetic field effects in spin liquid with spinon Fermi sea: Possible application to κ-$(ET)_2Cu_2(CN)_3$," Phys. Rev. B, **73**, 155115 (2006).

[30] Olexei I. Motrunich, "Variational study of triangular lattice spin-1/2 model with ring exchanges and spin liquid state in κ-$(ET)_2Cu_2(CN)_3$," Phys. Rev. B, **72**, 045105 (2005).

[31] Tarun Grover, N. Trivedi, T. Senthil, and Patrick A. Lee, "Weak mott insulators on the triangular lattice: Possibility of a gapless nematic quantum spin liquid," Phys. Rev. B, **81**, 245121 (2010).

[32] Assa Auerbach, "Interacting Electrons and Quantum Magnetism," (Springer-Verlag New York, 1994) Chap 7.

[33] Xiao-Gang Wen, "Quantum Field Theory of Many-body System: From the Origin of Sound to an Origin of Light and Electrons," (Oxford University Press, 2004) Chap 9.

[34] G. Baskaran and P. W. Anderson, "Gauge theory of high-temperature superconductors and strongly correlated Fermi systems," Phys. Rev. B, **37**, 580 (1988).

[35] A. M. Polyakov, "Quark confinement and topology of gauge theories," Nucl. Phys. B, **120**, 429 (1977).

[36] Michael Hermele, T. Senthil, Matthew P. A. Fisher, Patrick A. Lee, Naoto Nagaosa, and Xiao-Gang Wen, "Stability of $U(1)$ spin liquids in two dimensions," Phys. Rev. B, **70**, 214437 (2004).

[37] Martin C. Gutzwiller, "Effect of correlation on the ferromagnetism of transition metals," Phys. Rev. Lett., **10**, 159 (1963).

[38] Claudius Gros, "Physics of projected wavefunctions," Ann. Phys. (NY), **189**, 53 (1989).

[39] Piers Coleman, "New approach to the mixed-valence problem," Phys. Rev. B, **29**, 3035 (1984).

[40] Patrick A. Lee, Naoto Nagaosa, and Xiao-Gang Wen, "Doping a Mott insulator: Physics of high-temperature superconductivity," Rev. Mod. Phys., **78**, 17 (2006).

[41] David A. Huse and Andrew D. Rutenberg, "Classical antiferromagnets on the kagome lattice," Phys. Rev. B, **45**, 7536 (1992).

[42] R. J. Baxter, "Colorings of a hexagonal lattice," J. Math. Phys., **11**, 784 (1970).

[43] J. T. Chalker, P. C. W. Holdsworth, and E. F. Shender, "Hidden order in a frustrated system: Properties of the heisenberg kagome antiferromagnet," Phys. Rev. Lett., **68**, 855 (1992).

[44] J. Villain, R. Bidaux, J.-P. Carton, and R. Conte, "Order as an effect of disorder," J. Phys. France, **41**, 1263 (1980).

[45] Jan N. Reimers and A. J. Berlinsky, "Order by disorder in the classical heisenberg kagome antiferromagnet," Phys. Rev. B, **49**, 9539 (1993).

[46] C. L. Henley and E. P. Chan, "Ground state selection in a kagome antiferromagnet," J. Magn. Magn. Mater., **140**, 1693 (1995).

[47] X. Obradors, A. Labarta, A. Isalgué, J. Tejada, J. Rodriguez, and M. Pernet, "Magnetic frustration and lattice dimensionality in $SrCr_8Ga_4O_{19}$," Solid State Commun., **65**, 189 (1988).

[48] A. P. Ramirez, G. P. Espinosa, and A. S. Cooper, "Elementary excitations in a diluted antiferromagnetic kagomé lattice," Phys. Rev. B, **45**, 2505 (1992).

[49] Mikio Takano, Teruya Shinjo, and Toshio Takada, "On the spin arrangement in 'kagome' lattice of antiferromagnetic $KFe_3(OH)_6(SO_4)_2$," J. Phys. Soc. Jpn., **30**, 1049 (1970).

[50] T. Inami, M. Nishiyama, S. Maegawa, and Y. Oka, "Magnetic structure of the kagome lattice antiferromagnet potassium jarosite $KFe_3(OH)_6(SO_4)_2$," Phys. Rev. B, **61**, 12181 (2000).

[51] A. Keren, K. Kojima, L. P. Le, G. M. Luke, W. D. Wu, Y. J. Uemura, M. Takano, H. Dabkowska, and M. J. P. Gingras, "Muon-spin-rotation measurements in the kagome lattice systems: Cr-jarosite and Fe-jarosite," Phys. Rev. B, **53**, 6451 (1996).

[52] S.-H. Lee, C. Broholm, M. F. Collins, L. Heller, A. P. Ramirez, Ch. Kloc, E. Bucher, R. W. Erwin, and N. Lacevic, "Less than 50% sublattice polarization in an insulating $S = 3/2$ kagome antiferromagnet at $T \approx 0$," Phys. Rev. B, **56**, 8091 (1997).

[53] Zenji Hiroi, Masafumi Hanawa, Naoya Kobayashi, Minoru Nohara, Hidenori Takagi, Yoshitomo Kato, and Masashi Takigawa, "Spin-1/2 kagome-like lattice in volborthite $Cu_3V_2O_7(OH)_2 \cdot 2H_2O$," J. Phys. Soc. Jpn., **70**, 3377 (2001).

[54] M. Yoshida, M. Takigawa, H. Yoshida, Y. Okamoto, and Z. Hiroi, "Phase diagram and spin dynamics in volborthite with a distorted kagome lattice," Phys. Rev. Lett., **103**, 077207 (2009).

[55] Z Hiroi, H Yoshida, Y Okamoto, and M Takigawa, "Spin-1/2 kagome compounds: Volborthite vs herbertsmithite," J. Phys.: Conf. Ser., **145**, 012002 (2009).

[56] Marcos Rigol and Rajiv R. P. Singh, "Kagome lattice antiferromagnets and Dzyaloshinsky-Moriya interactions," Phys. Rev. B, **76**, 184403 (2007).

[57] M. A. de Vries, K. V. Kamenev, W. A. Kockelmann, J. Sanchez-Benitez, and A. Harrison, "Magnetic ground state of an experimental $S = 1/2$ kagome antiferromagnet," Phys. Rev. Lett., **100**, 157205 (2008).

[58] Oren Ofer, Amit Keren, Emily A. Nytko, Matthew P. Shores, Bart M. Bartlett, Daniel G. Nocera, and Alex Baines, Chrisand Amato, "Ground state and excitation properties of the quantum kagome system $ZnCu_3(OH)_6Cl_2$ investigated by local probes" (2006), arXiv:cond-mat/0610540.

[59] P. Mendels, F. Bert, M. A. de Vries, A. Olariu, A. Harrison, F. Duc, J. C. Trombe, J. S. Lord, A. Amato, and C. Baines, "Quantum magnetism in the paratacamite family: Towards an ideal kagome lattice," Phys. Rev. Lett., **98**, 077204 (2007).

[60] F. Bert, S. Nakamae, F. Ladieu, D. L'Hôte, P. Bonville, F. Duc, J.-C. Trombe, and P. Mendels, "Low temperature magnetization of the $S = 1/2$ kagome antiferromagnet $ZnCu_3(OH)_6Cl_2$," Phys. Rev. B, **76**, 132411 (2007).

[61] F Bert, A Olariu, A Zorko, P Mendels, J C Trombe, F Duc, M A de Vries, A Harrison, A D Hillier, J Lord, A Amato, and C Baines, "Frustrated magnetism in the quantum kagome herbertsmithite $ZnCu_3(OH)_6Cl_2$ antiferromagnet," J. Phys.: Conf. Ser., **145**, 012004 (2009).

[62] Chen Zeng and Veit Elser, "Numerical studies of antiferromagnetism on a kagome net," Phys. Rev. B, **42**, 8436 (1990).

[63] Rajiv R. P. Singh and David A. Huse, "Three-sublattice order in triangular- and kagome-lattice spin-half antiferromagnets," Phys. Rev. Lett., **68**, 1766 (1992).

[64] P. W. Leung and Veit Elser, "Numerical studies of a 36-site kagome antiferromagnet," Phys. Rev. B, **47**, 5459 (1993).

[65] J. B. Marston and C. Zeng, "Spin-peierls and spin-liquid phases of kagome quantum antiferromagnets," J. Appl. Phys., **69**, 5962 (1991).

[66] P. Nikolic and T. Senthil, "Physics of low-energy singlet states of the kagome lattice quantum heisenberg antiferromagnet," Phys. Rev. B, **68**, 214415 (2003).

[67] G. Evenbly and G. Vidal, "Frustrated antiferromagnets with entanglement renormalization: Ground state of the spin-1/2 heisenberg model on a kagome lattice," Phys. Rev. Lett., **104**, 187203 (2010).

[68] Rajiv R. P. Singh and David A. Huse, "Ground state of the spin-1/2 kagome-lattice Heisenberg antiferromagnet," Phys. Rev. B, **76**, 180407 (2007).

[69] H. C. Jiang, Z. Y. Weng, and D. N. Sheng, "Density matrix renormalization group numerical study of the kagome antiferromagnet," Phys. Rev. Lett., **101**, 117203 (2008).

[70] C. Waldtmann, H.-U. Everts, B. Bernu, C. Lhuillier, P. Sindzingre, P. Lecheminant, and L. Pierre, "First excitations of the spin 1/2 Heisenberg antiferromagnet on the kagome lattice," Eur. Phys. J. B, **2**, 501 (1998).

[71] Philippe Sindzingre and Claire Lhuillier, "Low energy excitations of the kagome antiferromagnet and the spin gap issue" (2009) arXiv:0907.4164 [cond-mat].

[72] M. B. Hastings, "Dirac structure, RVB, and Goldstone modes in the kagome antiferromagnet," Phys. Rev. B, **63**, 014413 (2000).

[73] Ying Ran, Michael Hermele, Patrick A. Lee, and Xiao-Gang Wen, "Projected-wave-function study of the spin-1/2 heisenberg model on the kagome lattice," Phys. Rev. Lett., **98**, 117205 (2007).

[74] Michael Hermele, Ying Ran, Patrick A. Lee, and Xiao-Gang Wen, "Properties of an algebraic spin liquid on the kagome lattice," Phys. Rev. B, **77**, 224413 (2008).

[75] Xiao-Gang Wen, "Quantum orders and symmetric spin liquids," Phys. Rev. B, **65**, 165113 (2002).

[76] Thomas P. Devereaux and Rudi Hackl, "Inelastic light scattering from correlated electrons," Rev. Mod. Phys., **79**, 175 (2007).

[77] Akio Kotani and Shik Shin, "Resonant inelastic X-ray scattering spectra for electrons in solids," Rev. Mod. Phys., **73**, 203 (2001).

[78] O. Cepas, J. O. Haerter, and C. Lhuillier, "Detection of weak emergent broken-symmetries of the kagome antiferromagnet by Raman spectroscopy," Phys. Rev. B, **77**, 172406 (2008).

[79] B. Sriram Shastry and Boris I. Shraiman, "Theory of Raman scattering in Mott-Hubbard systems," Phys. Rev. Lett., **65**, 1068 (1990).

[80] B. S. Shastry and B. I. Shraiman, "Raman-scattering in Mott-Hubbard systems," Int. J. Mod. Phys. B, **5**, 365 (1991).

[81] P. A. Fleury and R. Loudon, "Scattering of light by one- and two-magnon excitations," Phys. Rev., **166**, 514 (1968).

[82] P. E. Sulewski, P. A. Fleury, K. B. Lyons, and S-W. Cheong, "Observation of chiral spin fluctuations in insulating planar cuprates," Phys. Rev. Lett., **67**, 3864 (1991).

[83] L. B. Ioffe and A. I. Larkin, "Gapless fermions and gauge fields in dielectrics," Phys. Rev. B, **39**, 8988 (1989).

[84] Dirk Wulferding, Peter Lemmens, Patric Scheib, Jens Roeder, Philippe Mendels, Mark A. de Vries, Shaoyan Chu, Tianheng Han, and Young S. Lee, "Interplay of thermal and quantum spin fluctuations on the kagome lattice" (2010), arXiv:1005.4831 [cond-mat].

[85] P. Abbamonte, C. A. Burns, E. D. Isaacs, P. M. Platzman, L. L. Miller, S. W. Cheong, and M. V. Klein, "Resonant inelastic X-ray scattering from valence excitations in insulating copper oxides," Phys. Rev. Lett., **83**, 860 (1999).

[86] Filomena Forte, Luuk J. P. Ament, and Jeroen van den Brink, "Magnetic excitations in La_2CuO_4 probed by indirect resonant inelastic X-ray scattering," Phys. Rev. B, **77**, 134428 (2008).

[87] J. P. Hill, G. Blumberg, Young-June Kim, D. S. Ellis, S. Wakimoto, R. J. Birgeneau, Seiki Komiya, Yoichi Ando, B. Liang, R. L. Greene, D. Casa, and T. Gog, "Observation of a 500 meV collective mode in $La_{2-x}Sr_xCuO_4$ and Nd_2CuO_4 using resonant inelastic X-ray scattering," Phys. Rev. Lett., **100**, 097001 (2008).

[88] G. Ghiringhelli, N. B. Brookes, E. Annese, H. Berger, C. Dallera, M. Grioni, L. Perfetti, A. Tagliaferri, and L. Braicovich, "Low energy electronic excitations in the layered cuprates studied by copper L_3 resonant inelastic X-ray scattering," Phys. Rev. Lett., **92**, 117406 (2004).

[89] Pieter Kuiper, J.-H. Guo, Conny Såthe, L.-C. Duda, Joseph Nordgren, J. J. M. Pothuizen, F. M. F. de Groot, and G. A. Sawatzky, "Resonant X-ray raman spectra of Cu *dd* excitations in $Sr_2CuO_2Cl_2$," Phys. Rev. Lett., **80**, 5204 (1998).

[90] A. N. Redlich, "Parity violation and gauge noninvariance of the effective gauge field action in three dimensions," Phys. Rev. D, **29**, 2366 (1984).

[91] J. B. Marston, "Instantons and massless fermions in (2+1)-dimensional lattice QED and antiferromagnets," Phys. Rev. Lett., **64**, 1166 (1990).

[92] Matthew P. A. Fisher and Dung-Hai Lee, "Correspondence between two-dimensional bosons and a bulk superconductor in a magnetic field," Phys. Rev. B, **39**, 2756 (1989).

[93] Xiao-Gang Wen and Anthony Zee, "Topological structures, universality classes, and statistics screening in the anyon superfluid," Phys. Rev. B, **44**, 274 (1991).

[94] A. Zee, "Quantum Field Theory in a Nutshell," (Princeton University Press, 2003) Chap. VI.1-3.

[95] X. G. Wen and A. Zee, "Compressibility and superfluidity in the fractional-statistics liquid," Phys. Rev. B, **41**, 240 (1990).

[96] Xiao-Gang Wen and A. Zee, "Neutral superfluid modes and 'magnetic' monopoles in multilayered quantum Hall systems," Phys. Rev. Lett., **69**, 1811 (1992).

[97] Xiao-Gang Wen, "Quantum Field Theory of Many-body Systems," (Oxford University Press, 2004) Chap. 6.

[98] Ying Ran, Wing-Ho Ko, Patrick A. Lee, and Xiao-Gang Wen, "Spontaneous spin ordering of a Dirac spin liquid in a magnetic field." Phys. Rev. Lett., **102**, 047205 (2009).

[99] Dung-Hai Lee, "Pairing via index theorem," Phys. Rev. B, **60**, 12429 (1999).

[100] Xiao-Gang Wen, "Topological orders and edge excitations in fractional quantum Hall states," Adv. Phys., **44**, 405 (1995).